Hydrate Formation and CH_4 Production from Natural Gas Hydrates

-

Emphasis on Boundary Conditions and Production Methods

Master Thesis in Reservoir Physics

by

Knut Arne Birkedal

Department of Physics and Technology
University of Bergen
Norway

May 2009

Summary

Natural gas hydrate is a solid state of gas and water at low temperature and high pressure. Gas hydrates are known to form hydrate plugs in production line, and has thus generally been considered a problem to the oil industry. However, the energy stored in gas hydrates is vast, and as the global energy demand increases, focus is shifted on gas hydrates as a potential energy resource.

The work presented in this thesis is a series of experimental studies of hydrate formation and dissociation kinetics in porous sandstone. The overall objective was to provide an improved basic understanding of processes involved with formation and production of methane (CH_4) gas hydrates within porous media and to obtain data for numerical modelling and scaling. CH_4 hydrate has been formed repeatedly in Bentheim sandstone rocks to study hydrate formation patterns as function of initial water and gas saturations and salinity, and to prepare for subsequent lab-scale gas production tests using two different production schemes: 1) CH_4 production by carbon dioxide replacement, and 2) CH_4 production by dissociation of hydrates through depressurization.

Salinity impacts on induction time and hydrate growth pattern has been investigated through six different experiments, looking at the effect of salinities ranging between 1 wt% and 10 wt%. Salts are well known hydrate inhibitors and may affect both induction time for nucleation and hydrate growth pattern. These results show that salinities below 4 wt% NaCl do not seem to affect the hydrate formation rate significantly. However, at higher salinities (4.5-10 wt% NaCl) the inhibition is evident. The results show a reduction of the amount of water converted to gas hydrates and an increase in induction time with increasing salinity.

Depressurization is by many considered the most promising production method, and is the only successful production method to date on field scale (The Messoyaka field located in the eastern Siberian permafrost). This production method is based on dissociation of gas hydrate by bringing the reservoir below the hydration pressure. In this work CH_4 was produced from Bentheim sandstone partly saturated with gas hydrate by reducing the pressure stepwise until dissociation commenced. The production was monitored both by *in situ* magnetic resonance imaging (MRI), and by material balance calculations from PVT data. Results were consistent with previous results (Husebø et al., 2008b), which indicates reproducibility of the experiment, and showed full recovery after 280 hours. Production of associated water was detected.

The second production scheme investigated was CH_4 production by exchange with carbon dioxide. When CH_4 hydrate is exposed to CO_2 an exchange of gas molecules will occur spontaneously, as CO_2-hydrate is the thermodynamic preferred hydrate. The molecular exchange process release CH_4 which can be made accessible for production. In this thesis experiments take advantage of MRI technology to monitor the *in situ* CH_4 release. Significant gas production was observed and corroborated previous reported experiments with recovery estimates between 50-85%. No hydrate dissociation was detected, and consequently no production of associated water was observed.

In the experiments conducted as part of this thesis, most of the water was converted into gas hydrates when the system was pressurized and brought below hydrate formation temperature. The exception was the last experiment, where CH_4 hydrate formation was stopped prior to completion, and CO_2 was injected into the porous sample with free water present. This

experiment was conducted to simulate a production scenario in a reservoir saturated with both free water and gas hydrate. The excess water formed CO_2 hydrates when CO_2 was introduced. Some production of CH_4 was observed; however, the time frame was limited and the amount of CH_4 was therefore not well quantified. Permeability measurements were made at two different stages of the process and revealed communication through the gas hydrate, but the results may have been compromised by presence of water and gas hydrates in injection and production lines.

Salinity impact on hydrate growth and induction time has been identified in this study. In addition, two production schemes have been investigated and compared, and show promising results.

Acknowledgements

First of all I would like to thank my supervisor Professor Arne Graue for providing such an interesting and challenging subject for my thesis. Thank you for time, support and guidance.

Thanks to Jim Stevens and James J. Howard at ConocoPhillips' Research Center in Bartlesville for letting me work in your lab and educating me along the way. A special thanks to Keith Hester for inspiring conversations and good coffee.

Thanks to Professor Bjørn Kvamme for teaching me about gas hydrates in your classes and for guidance on theoretical issues.

Thanks to Kåre Slettebakken and all the other people at the workshop for helping me build the necessary experimental setups. I appreciate your time and good advices.

Thanks to Rachid Maad for developing a Labview-based software for PVT logging.

Thanks to all my fellow students at 5th floor for your friendship and support. A special thanks to Jarle Husebø and Geir Ersland for the cooperation and numerous conversations and discussions on gas hydrates over the least two years.

Thanks to all the people at nuclear physics for social (and some technical) inputs. A special thanks to Kristian Ytre-Hauge for your friendship.

Thanks to Kristent Fellesskap for providing an indispensable fellowship. A special thanks to Petter Olav Kirkeholmen and Maria Grønner for the great work you do. You are an inspiration to others!

Thanks to all my friends. You may put your name here …….

A special thanks to my family for always motivating and encouraging me in the work I have been doing during the last years. Thanks to my parents, Tove Rusten Birkedal and Magne Birkedal, and to all my siblings: Mariann, Ole Andreas and Synnøve. I would also like to thank my in-laws.

Finally I would like to thank the person I love above all else – Marie Grindland Birkedal. Without your support, encouraging words, affectionate love and patience I would not have been able to complete this degree. You have kept me sane and relaxed during times of hard work.

Bergen, May 12, 2009

Knut Arne Birkedal

Table of Contents

PART III – ATTACHMENTS

Introduction

Natural gas hydrates are solid crystalline inclusion compounds which belong to the clathrate group due to its ability to encapsulate gas molecules in structural cages of water molecules at high pressure and low temperature. The gas hydrate looks quite similar to ice, but the chemical compound and some of its properties are different. Water molecules are connected through hydrogen bonds and form a lattice or crystalline structure, where a hydrophobic gas molecule is enclosed in the cavity of the structure. The encaged gas molecule is often referred to as a guest molecule, and typical guest molecules are methane (CH_4), ethane, propane or carbon dioxide. CH_4 is the most common guest molecule found in natural gas hydrates, and is therefore the main hydrate former in this work.

The formation of gas hydrate plugs in production pipelines has for a long time been a large challenge for the oil industry (Hammerschmidt, 1934). Removal of such plugs is time consuming, and certain risks are involved. By adding inhibitors such as methanol, these plugs can be removed. Hydrate dissociation will first start along the pipe wall, and thus the plug may become a high velocity projectile due to the differential pressure. Such plugs may cause severe damages on infrastructure and cause large safety issues. Initial industrial interest on gas hydrates was in effort to avoid such hydrate plugging of pipelines. Natural gas hydrates also represent a vast energy resource distributed in regions of permafrost and in sub-marine environments. The amount of *in situ* gas hydrates is still uncertain, but even conservative estimates suggests that if only a small fraction is recoverable it should still be considered a possible energy source due to its sheer size. It is estimated that energy stored in gas hydrates is twice the energy stored in other fossil energy sources like oil, conventional gas and coal (Kvenvolden, 1988). Estimates of gas stored in hydrates vary between 1-120 x 10^{15} m^3 (Sloan and Koh, 2008). The uncertainty in these estimates is rather significant, but even for the less optimistic estimate the gas hydrates represent a vast energy source. In comparison, estimated recoverable gas left in conventional reservoirs is approximately 4.4 x 10^{14} m^3. For the more optimistic estimates, the amount of energy stored in hydrates exceeds all fossil fuels combined by several multiples (Grace et al., 2008).The gas stored in gas hydrates provides cleaner energy upon combustion compared to oil and has – as concerns are raised on environmental issues – gained increased attention in industrial and scientific communities.

The Intergovernmental Panel on Climate Change (IPCC) reports severe climate consequences due to anthropogenic interference (IPCC, 2007). Sequestration of CO_2 into natural gas hydrates is one suggested hydrate production scenario, where CO_2 may swap place with the natural gas stored inside the cavities of the hydrate and thereby creating a new hydrate with CO_2 as a guest molecule (Ebinuma, 1993). Not only does this represent an environmentally friendly production scheme by sequestrating CO_2, it also offers increased thermodynamic stability of the gas hydrate (Graue et al., 2006a). Increased stability of metastable hydrate deposits situated at the sea floor may reduce gas-seeping. Hansen (2004) predicts that reduction in CH_4 seeping and emissions could outweigh the negative influences of CO_2 emissions.

Recently, promising gas production tests have started from selected hydrate reservoirs. However, new technology is needed to make correct assessments of the size and character of the gas hydrate accumulation (Thomas, 2001). In addition to new technology, basic understanding of the nature of natural gas hydrate accumulations in porous media is needed. The work presented here aims at contributing to the latter by core-scale studies in controlled laboratory experiments.

Several gas hydrate experiments have previously been conducted at the University of Bergen and at ConocoPhillips' Research Center (Bartlesville, OK, USA) in a collaboration between ConocoPhillips and the University of Bergen (Ersland, 2008, Husebø, 2008). Accordingly, an experimental gas hydrate setup was available for the work presented in this study. The existing experimental setup was modified to allow for extended gas hydrate research, and two additional gas hydrate experimental setups were designed and built as a part of this work. This was done due to repeated problems with the first experimental setup. In addition, one of the new experimental setups was equipped with a resistivity core holder to allow for *in situ* water saturation measurements and subsequent gas hydrate saturation determination. Resistivity measurements may also provide additional information that may corroborate permeability measurements.

The purpose of this study was to form CH_4 hydrates in Bentheim sandstone to study hydrate formation patterns as function of initial saturation and salinity. Salt is a hydrate inhibitor and will affect the thermodynamic stability of gas hydrate. It is therefore an important parameter to consider when estimating size and occurrences of natural gas hydrates. Hydrate growth is expected to decrease with increasing salinity, while the induction time is expected to increase.

The energy potential in natural gas hydrates is vast, and several different production schemes are referred to as possible production schemes in the literature. Two production methods will be investigated and compared in this study. Depressurization induced gas production from gas hydrates is by many considered the most cost efficient gas production method. This study will investigate gas recovery by pressure depletion from hydrate deposits in Bentheim sandstone. Production of associated water is considered a major disadvantage with this production scheme, and is expected to be observed during this experiment. High CH_4 production is expected through pressure depletion.

Injection of CO_2 into gas hydrates is predicted to induce an exchange process, upon which CH_4 is released and CO_2 maintains stability of the hydrate. This is a result of favorable thermodynamic stability offered by CO_2. This production method has the additional benefit of sequestrating a greenhouse gas. In this study, the effect of CO_2 injection into a Bentheim sandstone will be investigated. The core has been fractured along the longitudinal direction of the core to increase the contact area between CH_4 hydrate and injected CO_2. This is expected to increase the gas recovery.

Relative gas permeability will be measured in a Bentheim core partly saturated with free water and partly saturated with gas hydrates. CO_2 will then be injected at constant rate to observe how the free water responds to presence of an additional guest molecule. CO_2 hydrate formation in the free water is expected, with simultaneous exchange process between the established CH_4 hydrate. Endpoint gas permeability will be measured once all the free water has been converted into gas hydrates.

The content of this thesis is divided into two parts. Part I (Chapter 1 and 2) introduces some theory and basic concepts of gas hydrates. MRI was used to monitor *in situ* gas hydrate progression in some experiments and a basic introduction of this imaging method is provided in Chapter 2. Part II (Chapter 3, 4 and 5) focuses on experimental descriptions, where the experimental setups are described in detail in Chapter 3. Experimental results and discussion are presented in Chapter 4, while main conclusions are provided in Chapter 5.

Part I

Theory

Chapter 1

Fundamental Principles

1.1 Gas Hydrates

Gas hydrates consist of water molecules that interconnect in an open structural lattice, which encapsulates a hydrophobic guest molecule in order to provide stability to the clathrate structure. Water molecules are the main component in gas hydrates, and in order to interpret the properties of liquid water, ice and gas hydrates, it is essential to have some basic knowledge about the water molecule.

1.1.1 The water molecule

Water is the most abundant liquid found on earth and because no enzyme would be functional without water, it is the very foundation for existence of life. The water molecule consists of one oxygen atom and two hydrogen atoms. The oxygen atom has electronic configuration $1s^2 2s^2 2p^4$ with a total of eight electrons and is missing two electrons to complete its valence shell. These are provided through covalent bonding with two hydrogen atoms that are separated by a 104.45º angle and thus the valence shell is completed for all components. However, due to differences in *electronegativity*, which is defined as the ability of an atom in a molecule to attract shared electrons (Zumdahl, 2005), this covalent bond becomes a polar covalent bond, where the oxygen has a stronger affinity for the electrons. The oxygen atom has an electronegativity of 3.44, while the hydrogen atom has an electronegativity of 2.20 on the Pauling scale. This causes the water molecule to act as a dipole, with a negative charge close to the oxygen ($\delta-$), while the hydrogen becomes slightly positively charged ($\delta+$). Because of dipole-dipole attraction, or so called *hydrogen bonding*, each water molecule is attracted to other water molecules as well, as illustrated in Figure 1.1. This bond, which is a result of the *van der Waals-Keesom force*, is weaker than the covalent bond, but is still strong enough to keep the molecules together. The van der Waals-Keesom force influences some of the important properties of water, including its relatively high enthalpy of fusion and vaporization, because more energy is needed to break the hydrogen bonds between the molecules.

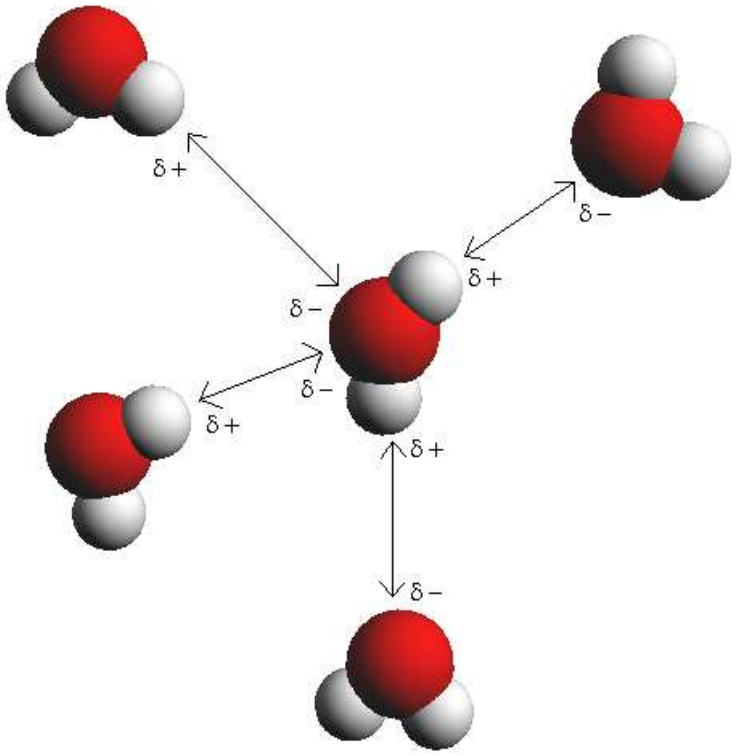

Figure 1.1 – Water molecules attracting each other and attaching through hydrogen bonding. The centre molecule has two positively charged hydrogen atoms. These attract two negatively charged oxygen atoms, and at the same time the negatively charged oxygen atom at the centre attracts two positively charged hydrogen atoms.

Water can be present as gas, liquid or solid, depending on temperature and pressure, as shown in Figure 1.2. Each solid line represents a phase boundary, and a slight temperature or pressure change may cause abrupt change between two physical states. The three phase boundaries converge into a unified triple point where small changes in pressure or temperature could result in any of the phases. Chapter 1.1.3 focuses on ice and its similarities to hydrate, due to the fact that this state of water closely resembles hydrate and its structures.

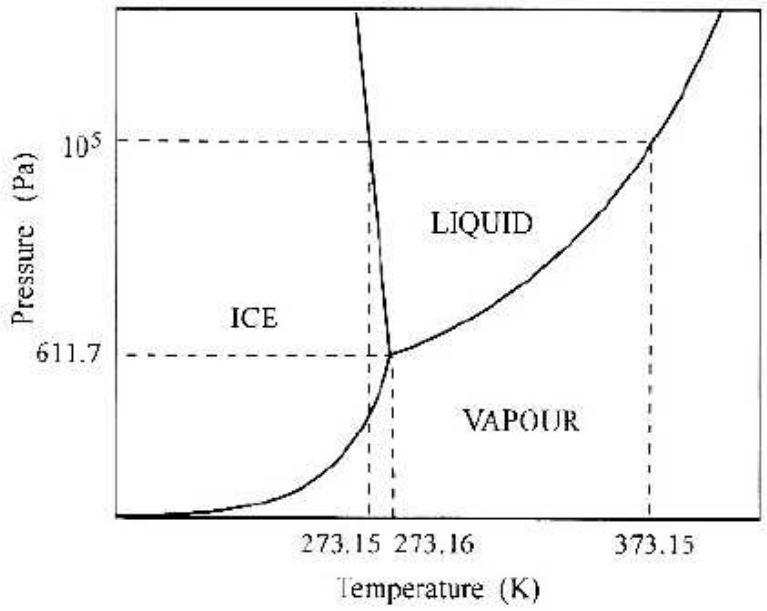

Figure 1.2 – Phase diagram for ice Ih, water and vapor (Travesset, 2008).

1.1.2 Water properties

Because of its polar nature water molecules in liquid or solid state will strongly interact and be surrounded by numerous other water molecules. The two lone pairs and two hydrogen atoms cause the water molecule to bond with up to four other water molecules, as shown in Figure 1.1. The water molecule will therefore be arranged at the centre of a tetrahedron formed by four other water molecules approximately 2.82 Å away (at 25 ºC) and at angles of 109.47º (Chaplin, 2008). The length of this bond varies with temperature and pressure (Eisenberg and Kauzmann, 1969), and at high temperatures the orientation of the water molecules are not fully tetrahedral. In simple liquids the number of surrounding molecules is rather high, but due to the directional hydrogen bond in water the number of neighboring water molecules is restricted.

Water has a range of anomalous properties, many of which are directly or indirectly related to the hydrogen bonding between water molecules. In fact, if the strength of the hydrogen bond had differed by only a few percents large changes in the physical properties of water would occur (Figure 1.3), which would result in significant consequences for life on earth. Among some of the anomalous properties are its large heat capacity and high thermal conductivity, which combined with water's relatively high enthalpy of fusion and vaporization, allow for moderation of the climate by buffering large fluctuations in temperature. The polar nature of the water molecule is also the reason why water is such a good solvent. Hydrophilic substances will be surrounded by the relatively small water molecules where the positive dipole of the water molecule attracts negatively charged components of the solvent. A typical example found in nature is NaCl, which consists of the Na^+ cation and the Cl^- anion. These ions are easily transported away from their crystalline lattice into solution with water.

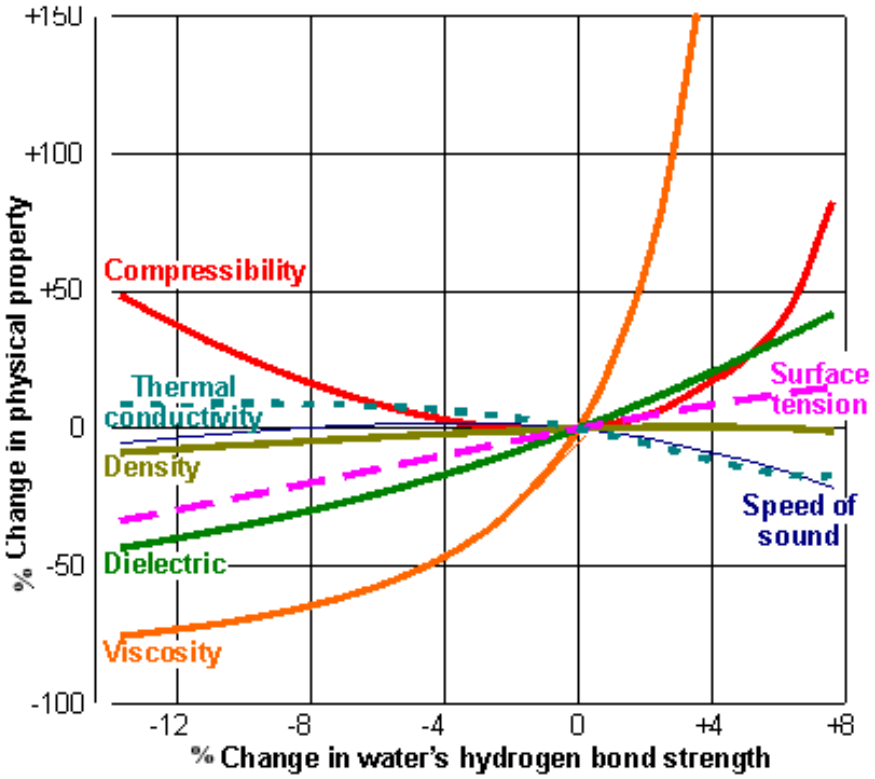

Figure 1.3 – Small percentage change in strength of hydrogen bond give rise to large changes in physical properties such as melting point, boiling point, density and viscosity (Chaplin, 2008).

One curiosity of water is the fact that in vapor phase it is one of the lightest gases known, as a liquid it is much denser than expected and at solid state it is lighter than expected. Just like any other liquid at room temperature, water becomes denser with lower temperature; however, at 3.98 ºC the water reaches a density maximum, and further lowering of temperature results in decreased density. In other words both increase and decrease in temperature at this point reduces the density of liquid water. This is a result of atom rearrangement in an ordered fashion where the shape of the water molecule and the hydrogen bond cause the molecules in the crystal to occupy more space in solid state than in liquid (Carrol, 2003). The length of the hydrogen bond is actually shorter than above 3.98 ºC, but each molecule has fewer neighbors, resulting in decreased density (Franks, 1972). This property, although not unique for water, is of great importance in nature as it prevents lakes and rivers from freezing solid. This property also causes convection currents where cooled water at the surface circulates to the bottom of the lake until the whole lake has a temperature of 3.98 ºC and further cooling will eventually result in freezing of the surface layers. The surface layers will eventually freeze and form ice. This normally occurs at 0 ºC, however, supercooling allows for liquid state until almost -42 ºC (Chaplin, 2008).

1.1.3 Hydrate and its similarities to ice

Ice has thirteen[a] different crystalline phases which exist at different temperatures and pressures (Travesset, 2008). Hexagonal ice (*ice Ih*) is the most common solid form of water, and due to tetrahydral bonded waters, it has some resemblance to gas hydrates. Ice Ih forms by freezing water at atmospheric pressure and is stable to 150 K. At temperatures lower than 150 K and at high pressures other phases of ice will form, as shown in Figure 1.4. Figure 1.5 illustrates the molecular structural lattice of ice Ih developed by Pauling in 1935, where none of the interconnected water molecules have the same directional orientation.

[a] Some literature refers to higher number of ice phases. Amongst these are Chaplin who refers to sixteen phases of ice (CHAPLIN, M. *"Water structure and science"*. http://www.lsbu.ac.uk/water/index2.html 2008).

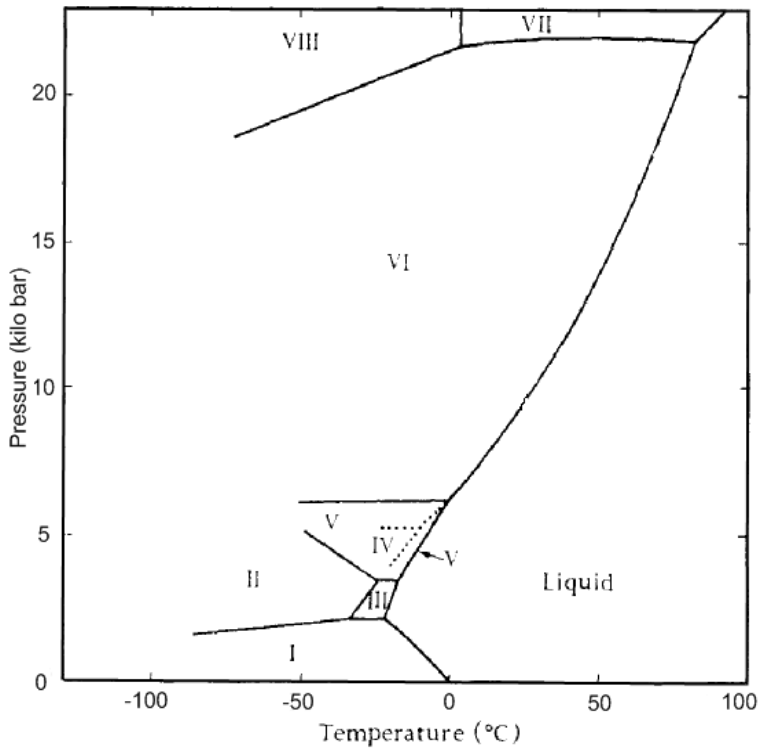

Figure 1.4 – Phase diagram illustrating stability regions for the different phases of ice. (Eisenberg and Kauzmann, 1969). This figure does not include all phases of ice, only the first nine.

The oxygen atoms are separated by a hydrogen atom or a proton in both ice Ih and hydrates, and the hydrogen bond is only 1% longer in the hydrate. In ice there is a tetrahedral O-O-O angle (109.5º) between the oxygen atoms connected through hydrogen bonding, which results in almost no geometrical distortion. In hydrates this angle only differs by a few degrees, 3.7º for structure I and 3.0º for structure II, which is less deviation than for the high pressure ices II, III, V and VI (Davidson, 1973). The angle between the two hydrogen atoms in the water molecule is similar as well for ice Ih and gas hydrates.

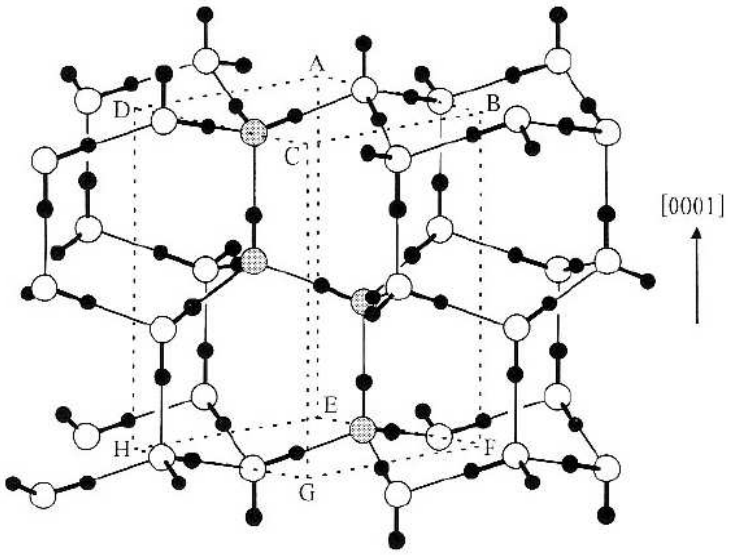

Figure 1.5 – Crystal structure of ice, where the open circles illustrate oxygen atoms and the dark circles represent the hydrogen atoms (Travesset, 2008).

A structural feature that distinguishes clathrate hydrates from the different ice structures is the predominance of planar five-membered rings in structure II and almost planar five-membered rings in structure I. Gas hydrates, on the other hand, form non-planar puckered hexagonal rings (Sloan and Koh, 2008). Comparisons of some properties among ice Ih and the two most common hydrate structures are shown in Table 1.1.

Table 1.1. *Comparison of some properties of ice and hydrates (Sloan and Koh, 2008).*

Property	Ice	Structure I	Structure II
Number of water molecules	4	46	136
Lattice parameters (at 273 K) [Å]	a=4.52, c=7.36	12.0	17.30
Dielectric constant at 273 K	94	58	58
H2O reorientation time [μs]	21	10	10
H2O diffusion jump time [μs]	2.70	>200	>200
Thermal conductivity [$Wm^{-1}K^{-1}$]	2.23	0.49+/-0.02	0.51+/-0.02
Density [g/cm^3]	0.91	0.94[b]	1.291[c]

1.1.4 Hydrate structures

Hydrates are formed by hydrogen bonded water molecules that interconnect to form a polyhedral cavity, which is capable of encapsulating a foreign hydrophobic molecule. These cavities are often built up by pentagonal and hexagonal faces, and studies have shown that the pentamer is the most likely structure to spontaneously arise in water at different temperatures, closely followed by hexamers (Stillinger and Rahman, 1974). These geometric shapes are therefore important when considering hydrates. The different faces combine to form different polyhedrons, shown in Figure 1.6, which contribute to form different hydrate structures.

[b] Based on methane hydrate density in large polyhedra.
[c] Calculated for 2,2-dimethylpentane $5(Xe,H_2S)\cdot 34H_2O$, SLOAN, E. D. & KOH, C. A. "*Clathrate Hydrates of Natural Gases",* 3rd edition. Boca Raton, CRC Press, 2008

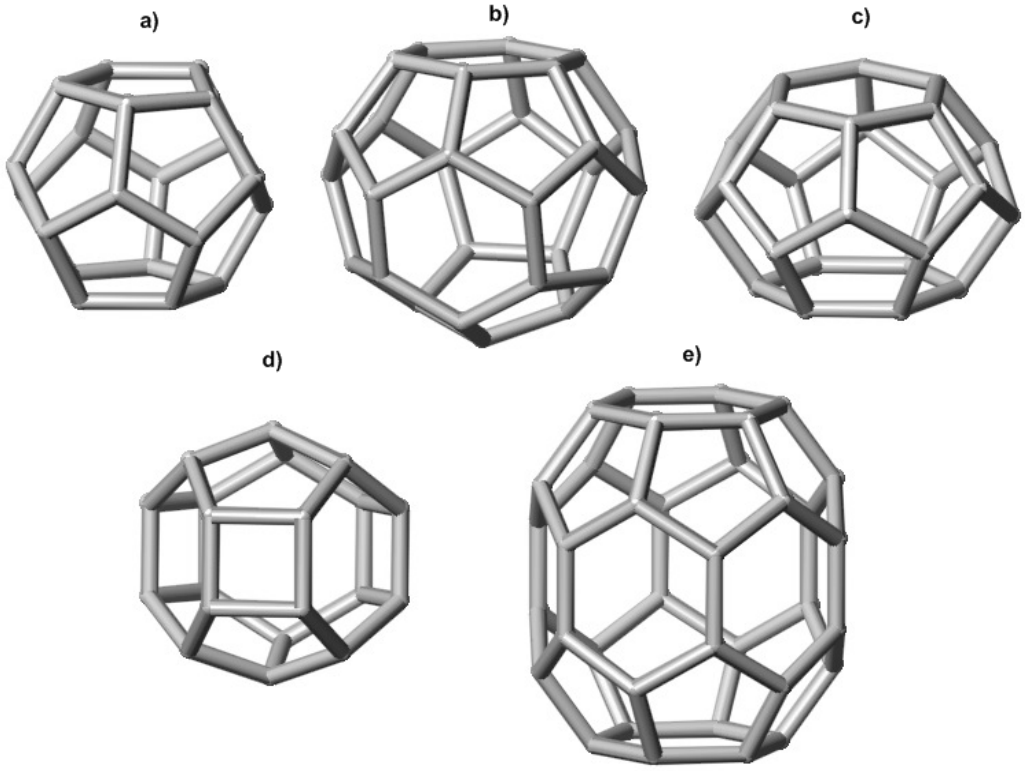

Figure 1.6 – Five different polyhedral cavities found in some of the most common hydrate structures: (a) pentagonal dodecahedron (5^{12}), (b) tetrakaidecahedron ($5^{12}6^2$), (c) hexakaidecahedron ($5^{12}6^4$), (d) irregular dodecahedron ($4^3 5^6 6^3$), and (e) icosahedron ($5^{12}6^8$). Modified from (Hester, 2009).

The pentagonal dodecahedron, which consists of twelve pentagonal faces, is a common polyhedron found in most hydrate structures. *Structure I* is made up by two pentagonal dodecahedra and six tetrakaidecahedra, a total of eight polyhedra per crystal cell. In this structure, the vertices are linked together (Sloan, 1991), and a total of 46 water molecules make up the structure. *Structure II* is made up by 16 pentagonal dodecahedra and eight hexakaidecahedra, where the faces of the 5^{12} cavities are interconnected, and a total of 136 water molecules constitute the crystal cell structure. In addition to the small 5^{12} cavity and a large cavity *structure H* uses an intermediate sized cavity and is therefore considered a bit more complex. It is made up by three pentagonal dodecahedra, two irregular dodecahedra, and one icosahedron, and a total of 34 water molecule make up a unit cell of structure H. Some properties of these structures are listed in Table 1.2.

Table 1.2. Main properties of the different hydrate structures (Sloan and Koh, 2008).

Hydrate crystal structures	I		II		H		
Cavity	Small	Large	Small	Large	Small	Medium	Large
Description	5^{12}	$5^{12}6^2$	5^{12}	$5^{12}6^4$	5^{12}	$4^3 5^6 6^3$	$5^{12}6^8$
Number of cavities per unit cell	2	6	16	8	3	2	1
Average cavity radius (Å)	3.95	4.33	3.91	4.73	3.94[d]	4.04[d]	5.79[d]
Number of waters per unit cell	46		136		34		

[d] From the atomic coordinates measured using single crystal x-ray diffraction on 2,2-dimethylpentane · 5(Xe,H_2S)-34H_2O at 173 K.

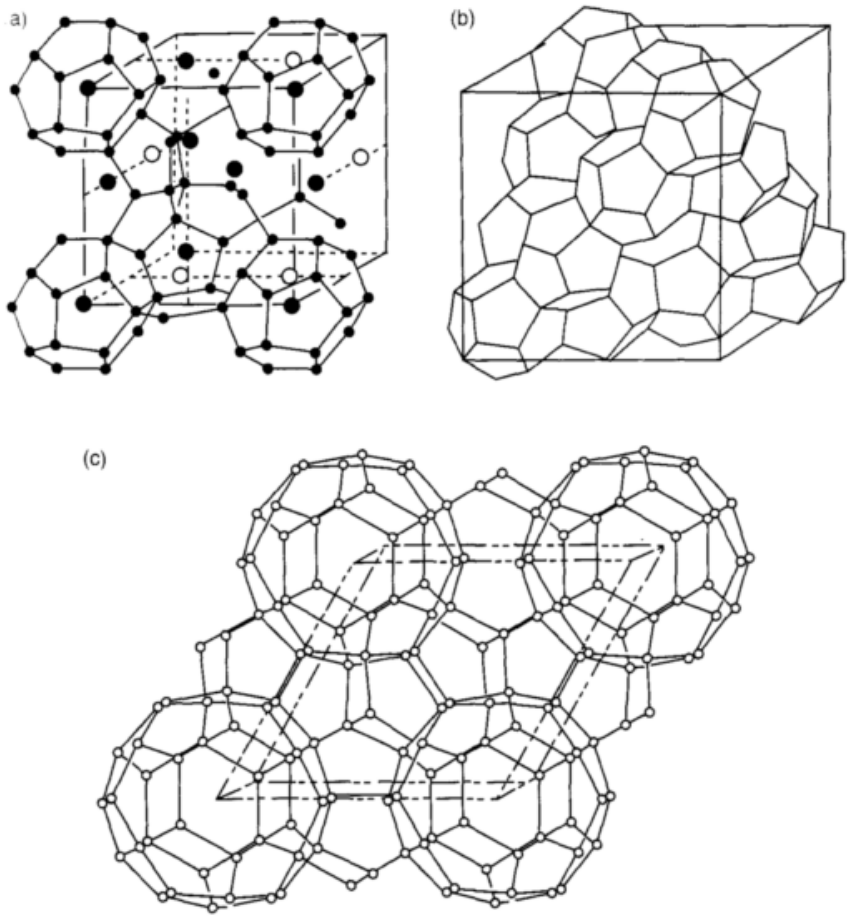

Figure 1.7 – Some common gas hydrate structures: (a) structure I, (b) structure II, and (c) structure H. (Sloan and Koh, 2008)

Several different structures have been observed to form hydrates so far, but structure I and structure II are considered to be the most important structures. Structure H was just recently discovered (Ripmeester et al., 1987), but is not considered that important due to the fact that it does not occur very frequently in nature (Lu et al., 2007, Hester, 2007). Structure I and structure II are both cubic structures, which can be seen from Figure 1.7, where each side of the cube is 12 Å for structure I and 17.3 Å for structure II. In order to stabilize a cavity a guest molecule is needed, and guest molecules will be further discussed in the following section.

1.1.5 Guest Molecules

In order to stabilize the cavity, a guest molecule that does not compete or interfere with the already existing hydrogen bonding is needed (Jeffrey, 1984). The preferred ratio of molecular to cavity diameter for the molecule to be able to stabilize the cavity is at least 0.76, however, this rule does not always apply. The cavity size and structure is dependent on the size of the guest molecule, and Figure 1.8 illustrates which gas molecules are able to stabilize the different hydrate structures. Structure I is stabilized by molecules with diameters between 4.2-6 Å in simple hydrate systems with only one guest molecule per crystal cell. Structure II is stabilized by molecules less than 4.2 Å and between 6-7 Å. For these structures, the shape of the guest molecule does not represent a major influence on the hydrate structure, whereas the shape of the guest molecule has a great impact on structure H, and it is of great importance to fill the large cavity in an efficient manner. As long as certain shape restrictions are obeyed, guest molecules of 7.1 to 9 Å can stabilize structure H. From Appendix A1 it is easily

observed that CH_4 can stabilize the pentagonal dodecahedra in each structure and also the tetrakaidecahedron in structure I, but for larger cavities larger molecules are needed.

Small and simple guests, such as CH_4 and hydrogen sulfide (H_2S), can stabilize both the small and large cavities of structure I. Other natural gas components which form structure I as simple hydrates are ethane (C_2H_6) and carbon dioxide (CO_2). Nitrogen (N_2), propane (C_3H_8), and iso-butane (C_4H_{10}) all form structure II, but some of these guest molecules can only fit into the larger cavity and consequently structure II often exists of mixtures of different gases. If smaller gas molecules are not available, hydrates might not be able to form. This is the case for benzene (C_6H_6) and cyclohexane (C_6H_{12}), which are dependent upon a help gas, such as CH_4 or xenon (Xe) (Sloan and Koh, 2008). Large molecules can only occupy the larger cavities, leaving the smaller cavities vacant. In this thesis, for simplicity, mainly one type of gas will be used during hydrate formation. Because CH_4 has the ability to stabilize both the small and the large cavity of structure I, this is the gas that will be used during experiments in this thesis. This is also by far the most common natural gas found in gas hydrate reservoirs.

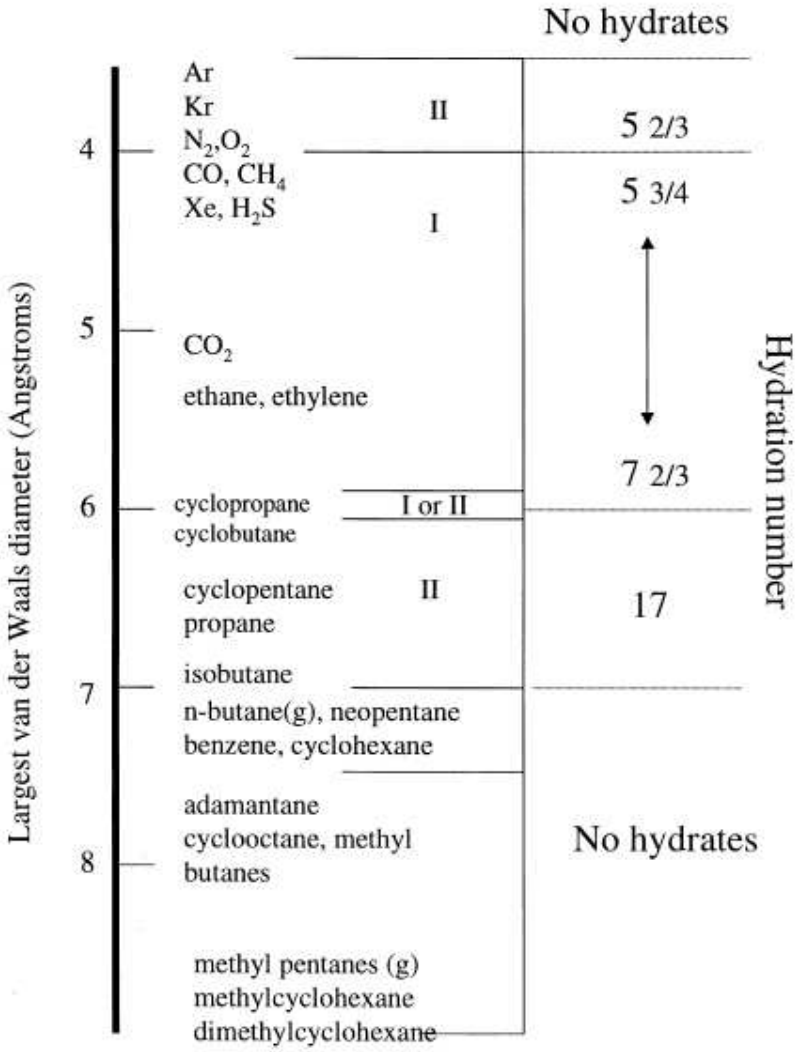

Figure 1.8 – Correlation between guest size, structure and hydration number for single guest molecules (Ripmeester, 2000). There are several more guest molecules than presented in this figure and these can be found in Appendix A1.

1.1.6 Hydrate formation kinetics

Kinetics of hydrate formation and dissociation is considered one of the most intriguing and challenging questions concerning hydrates. Knowledge on hydrate nucleation is especially imperative when maintaining flow assurance in production and transportation pipelines, but also for experimentalists investigating hydrate properties. Despite the fact that vast amounts of data are available through multiple experiments, it has been hard to find any correlation that gives information on when hydrate growth initiates. Experiments have shown that the length of the metastable state of the system (the induction time) is dependent on the apparatus setup, the presence of substrate material, the history of the water, water and gas composition, pressure and temperature, cooling rate, and if it is a dynamic or static condition (Makogon et al., 1999). However, even though the variables in a system are kept constant the induction time may vary. As a result the induction time is therefore considered a stochastic process, even though increased interface between the two constituents increase the probability of nucleation.

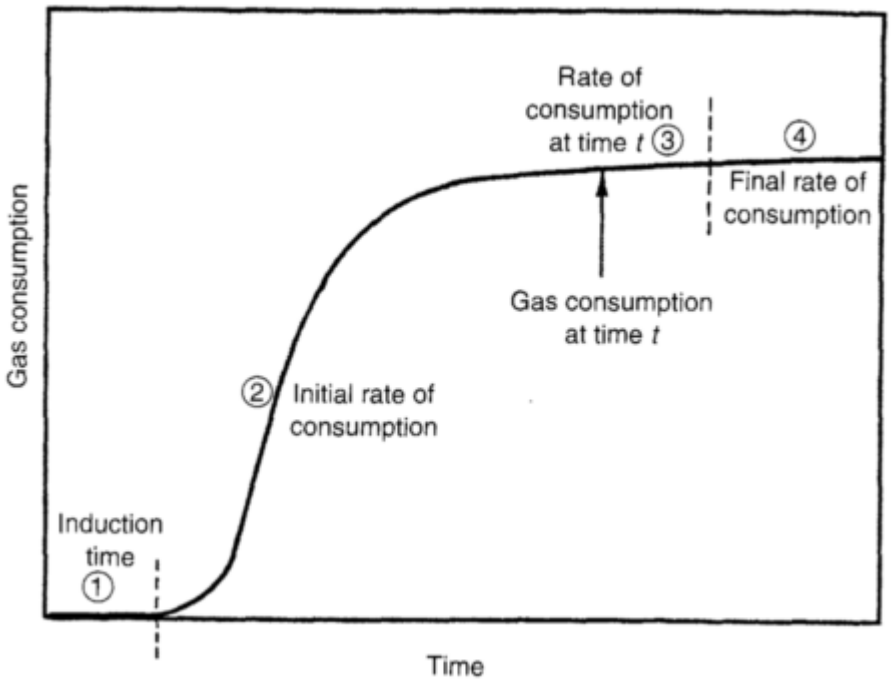

Figure 1.9 – Gas consumption during formation of hydrates. As the induction time comes to an end and hydrate growth has initiated the CH_4 consumption follows an exponential pattern with high initial consumption. Modified by (Sloan and Koh, 2008) from (Lederhos et al., 1995)

Nucleation, which is when a hydrate crystal starts forming, happens at the left corner of Figure 1.9. This is a random micro scale process, and can not be detected macroscopically. Once labile clusters have formed they will start to agglomerate by sharing faces, but until the crystal reaches a critical size, r_c (Figure 1.10), formation and dissociation occurs randomly. After critical size has been reached steady hydrate growth period has initiated.

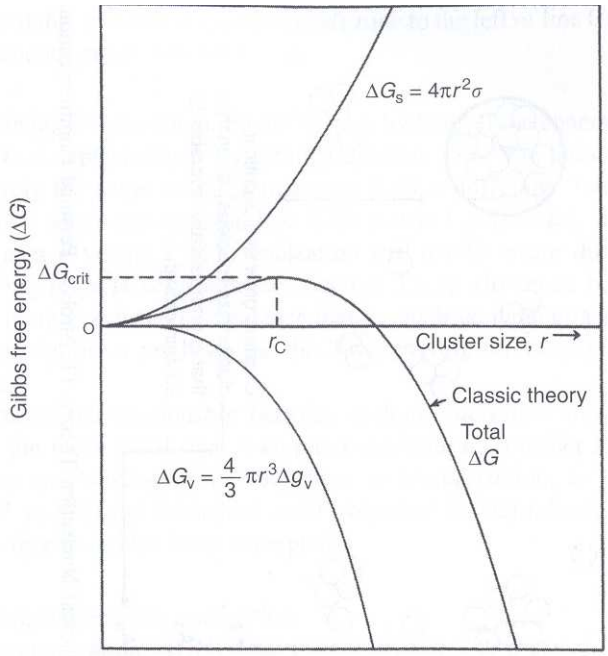

Figure 1.10 – Gibbs free energy as a function of cluster size (Sloan and Koh, 2008).

Two different types of nucleation are referred to in the literature, depending on the condition of the phases present. Homogeneous nucleation (HON) is not very common, but is a solidification process that occurs in the absence of impurities. For such a process to occur there has to be huge amounts of gas dissolved in the water, which is unusual for non-polar gases like CH_4. This would also result in a positive Gibbs free energy, which is unfavorable. Aqueous solutions used in the laboratory contain more than 10^6 particles per cm^3 (Mullin, 1993), so avoiding impurities is considered nearly impossible, even in laboratories. Heterogeneous nucleation (HEN), on the other hand, occurs at the interface between two different phases, as shown in Figure 1.11, where impurities like dust or surfaces are likely to be involved.

The induction time starts by the formation of the first crystal nuclei, and concludes by the appearance of a detectable hydrate volume. As mentioned, it is a stochastic process, and may take only a few nanoseconds or up to several months, depending on the system. This time delay is caused by:

- Rearrangement of hydrate interfaces
- Rearrangement throughout the hydrate
- Effects of the solid surface
- For the HEN case presence of a hydrate film[e] at the interface between the two phases will also increase the (macroscopic) induction time.

Considering free energy it is less likely to grow a hydrate nucleus in a free volume of gas and water than in the presence of micro-particles or a surface. A substrate is likely to have a wettability preference for one of the phases, resulting in a contact angle θ. For the HON case where no surface or substrate is present we have a critical Gibbs free energy for hydrate growth given by

[e]According to KVAMME, B., Personal communication (2009)

$$\Delta G_{critical} = 4\pi\sigma r_c^2 / 3. \quad (1.1)$$

For the HEN case the contact angle has to be considered as well, and equation (1.1) is therefore modified to

$$\Delta G'_{critical,HEN} = \phi \Delta G_{critical}, \quad (1.2)$$

where

$$\phi = \left[(2+\cos\theta)(1-\cos\theta)^2\right]/4. \quad (1.3)$$

If the contact angle θ = 180º the substrate has no wetting preference for the phase and the critical Gibbs free energy will thus be the same for the HON and HEN case. On the other hand, if the contact angle θ = 0º, which corresponds to complete wetting of the substrate, $\Delta G_{critical}$ = 0, and the critical radius required for catastrophic growth has been lowered effectively. In this study, gas hydrates has been formed in Bentheim sandstone, which has a strong water-wet preference (Graue, 2009),and effectively lowers the critical radius and induction time. Experiments (Long and Sloan, 1996) have shown that hydrate growth is initiated most frequently at the water-gas interface shown in Figure 1.11. This makes sense when considering the fact that the concentration of both constituents is higher here than elsewhere. According to Chaplin (Chaplin, 2008) nano-sized clusters of water will occur within about 250 nm of the interface where small gas molecules will bond to these surface clusters because of several van der Waals interactions. In a CH_4 and water system the nucleation usually occurs on the gas side of the interface because of the high amount of gas that is needed (15%). Such high concentrations are usually not found dissolved in water. Additionally, Gibbs free energy of nucleation is lower here.

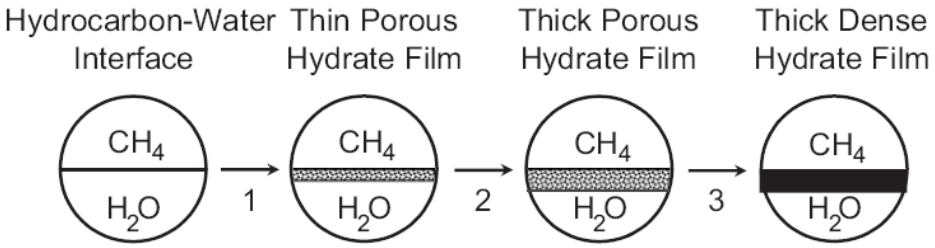

Figure 1.11 – Hydrate growth is more likely to occur at the interface between gas and water, where both constituents can easily be accessed. At first a thin and porous film forms that grows into the water phase. The end result is a thick and dense hydrate film. (Taylor et al., 2007)

Results from simulations on molecular level support this as well, and it is often explained by the significant concentration gradient at the interface with subsequent decrease in Gibbs free energy of nucleation. Once the growth period has initiated hydrate growth occurs very rapidly, and gas is being concentrated in hydrate cavities where the density of gas molecules actually is higher than in the gas phase. With time the consumption rate will decrease, as shown in Figure 1.9, and eventually the consumption rate will stop, due to lack of either gas or water molecules.

1.1.7 Conditions for hydrate formation

The gas hydrate stability region is restricted to the left of curve CD (Figure 1.12), where the nucleation driving force is very high and nucleation occurs easily. In the metastable region nucleation may also occur, but will probably have an increased induction time relative to the stable region. The driving force, as most processes in thermodynamics, is related to Gibbs free energy. Assuming an isothermal and isobaric process Gibbs free energy for a vapor and water system will be given as

$$\Delta G^{\text{driving}} = \Delta G^{\text{reactants}} - \Delta G^{\text{products}} = \Delta G^{\text{Water}} + \Delta G^{\text{Vapor}} - \Delta G^{\text{Hydrate}} \tag{1.4}$$

$$\Delta G^{\text{Water}} = x_w^{II}\left(\mu_i^{II} - \mu_w^{I}\right) = v_w\left(P^{eq} - P^{I}\right) \tag{1.5}$$

$$\Delta G^{\text{Vapor}} = \sum x_i^{II}\left(\mu_i^{II} - \mu_i^{I}\right) = RT\sum x_i^{II}\ln\left(\frac{f_i^{II}}{f_i^{I}}\right) \tag{1.6}$$

$$\Delta G^{\text{Hydrate}} = x_w^{H,II}\left(\mu_w^{H,II} - \mu_w^{H,I}\right) + \sum x_i^{H,II}\left(\mu_i^{H,II} - \mu_i^{H,I}\right) = v_H\left(P^{I} - P^{eq}\right). \tag{1.7}$$

Combining these equations leads to the following expression for the nucleation driving force:

$$\Delta G^{\text{driving}} = v_w\left(P^{eq} - P^{I}\right) + RT\sum x_i^{II}\ln\left(\frac{f_i^{II}}{f_i^{I}}\right) + v_H\left(P^{I} - P^{eq}\right). \tag{1.8}$$

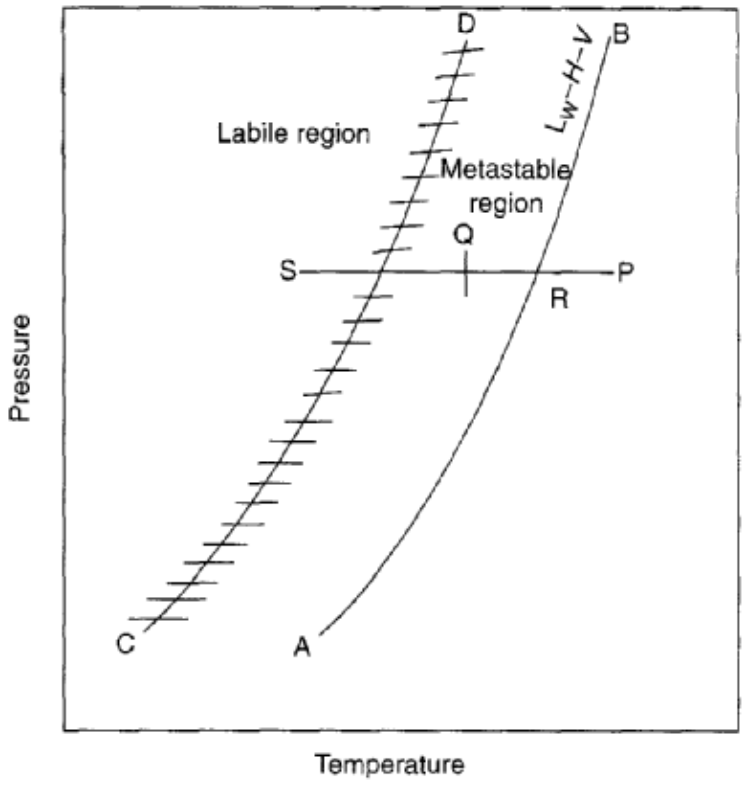

Figure 1.12 – Stability region for hydrate nucleation (Sloan and Koh, 2008).

From equation (1.8) it is easily observed that differences in Gibbs free energy may occur as changes in chemical potential, fugacity, pressure and temperature. By varying these parameters hydrate formation or dissociation can be controlled. Makogon (Makogon et al., 1999) summarized the following conditions for hydrate formation:

1. It has to be thermodynamically favorable ($\Delta G < 0$)
2. Availability of hydrate constituents (water and hydrate former)
3. Heat transport during hydrate formation to remove latent heat of fusion.

1.1.8 Theories on hydrate nucleation

Several different hypotheses have been presented on nucleation, whereas three different theories mainly are considered in today's literature. The only way to verify either one of these theories is through experimental work, but due to its stochastic and microscopic nature this is very challenging.

In the labile cluster nucleation hypothesis, illustrated in Figure 1.13, pure water occur in clustered structures but without guest molecules occupying the cavities (A). Dissolved guest molecules will be surrounded by labile clusters of water which combine to form different unit cells (B). Depending on the amount of water molecules available different polyhedra will form. Some labile clusters will agglomerate by sharing faces and thereby increasing the disorder (C). Once the critical radius has been reached steady growth will commence (D).

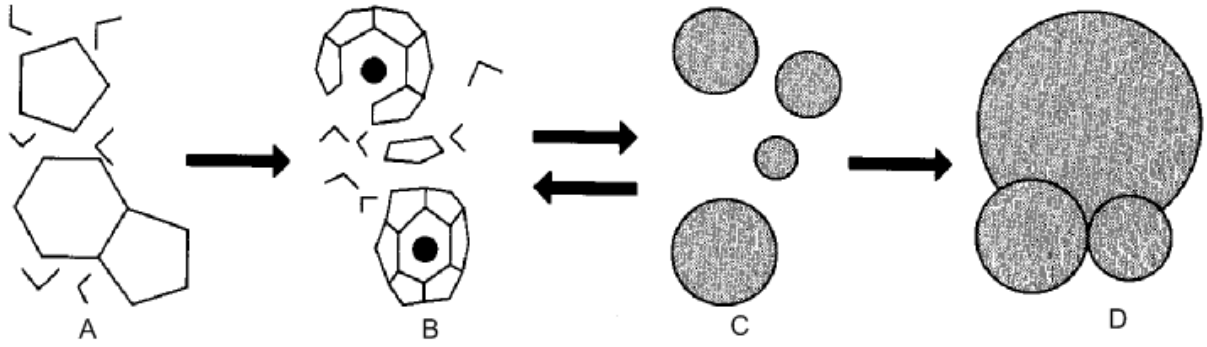

Figure 1.13 – Labile cluster nucleation hypothesis. Modified from (Sloan and Koh, 2008). A) Clustered structures of water with no guest molecules encapsulated in the clusters. B) Guest molecules are surrounded by labile clusters of water forming different unit cells. C) Agglomeration of labile clusters. D) Critical radius has been reached and steady growth commenced.

Another theory is the nucleation at the interface hypothesis suggested by both Long (1994) and Kvamme (2000).This hypothesis has been slightly modified in later publications (Kvamme, 2002b), and is illustrated by Figure 1.14. According to this theory gas molecules are transported to the interface between water and gas (A), where the gas adsorbs on the aqueous surface. The gas will then migrate to a suitable location for adsorption through surface diffusion (B), whereby the water molecules will form first partial and then complete cages around the adsorbed gas molecules (C). Labile clusters will start agglomerating and growing on the vapor side of the interface (D) until a critical size has been reached. The hydrate growth on the gas side of the interface has been estimated to be two magnitudes higher than on the water side (Kvamme, 2002a), and the gas side of the interface will thus dominate the hydrate growth.

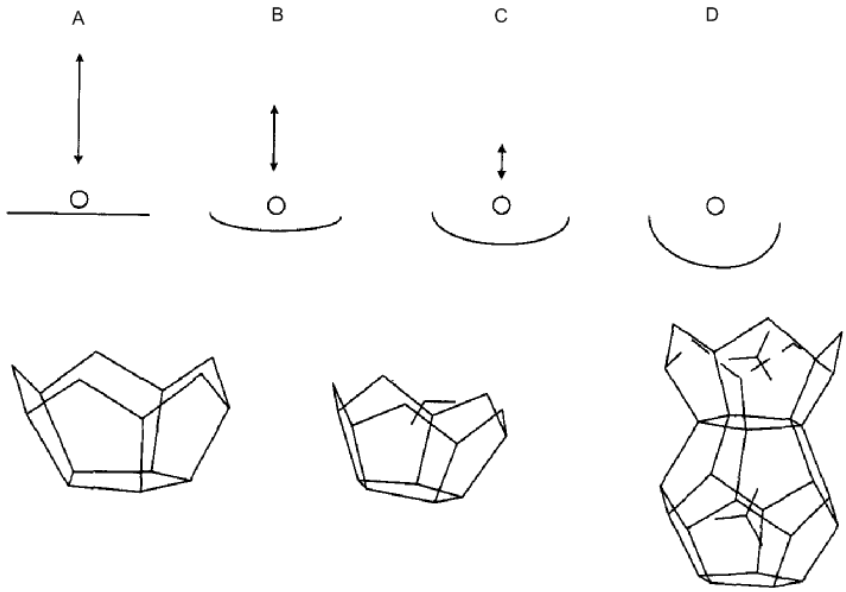

Figure 1.14 – Visualization of nucleation at the interface hypothesis. Modified from (Long, 1994). A) gas molecule is transported to the gas/water interface. B) The gas molecule migrates to suitable adsorption location. C) The gas molecule will be encaged in first partial then complete cages. D) Labile clusters agglomerate and start growing on the vapor side.

The third theory often referred to is the local structuring nucleation hypothesis, in which thermal fluctuations causes a group of guest molecules to be arranged locally in a configuration similar to the clathrate hydrate phase. Both large and small clusters are formed which reassembles the hydrate cages. These clusters may grow to form hydrate unit cells or agglomerations of such, or they may shrink and dissipate. Once critical size of the hydrate cluster has been reached secondary nucleation and rapid hydrate crystal growth may occur.

Nucleation is a stochastic process and considered unpredictable, which is illustrated by the fact that three slightly different hypothesis exist. During nucleation there are many unknown mechanisms involved in the hydrate formation process, and without experimental studies it is hard to verify these theoretical models. This applies for hydrate growth also, where several different hypotheses exist.

1.1.9 Hydrate inhibition

Flow assurance in production and transportation pipelines is the main reason for previous extensive hydrate research by several petroleum companies. High pressure and low temperature in pipelines, in addition to abundance of both water and guest molecules, makes hydrate formation inevitable. If hydrate crystals are allowed to agglomerate the hydrate will eventually form a plug that may prevent flow in the pipeline. These hydrate plugs, which sometimes take months to remove, may cause major economic impacts due to downtime in flowline operations. Dissociation of such plugs starts along the pipe wall, and differential pressure over the plug can cause the plug to become a high velocity projectile with velocities up to 300 km/hour (Sloan, 2003), thus exposing production facilities and crew at great risk. The stability region of hydrate is quite predictable and by using thermodynamic simulators as guideline the petroleum industry try to maintain production and transportation outside the labile region of Figure 1.12. However, as most production occurs at high pressure and low temperature this can not always be accomplished, in which case injection of hydrate inhibitors (chemical additives) or heating of pipe lines has to be applied.

Alcohols and glycols are examples of hydrate inhibitors, where differences in electronegativity cause the inhibitors to compete with the solid hydrate for water molecules. In addition the hydrocarbon end of the alcohol molecule causes the water molecules to form organized solved clusters. High concentrations are needed for the inhibitor to be effective, which often results in financial penalties due to too high concentration in refinery feedstock. Extensive research has resulted in new low dosage inhibitors that prevent hydrate growth or agglomeration. These are more attractive, both economically and environmentally, and examples are polymer molecules such as PVP (poly(N-vinylpyrrolidone)), VC-713, the terpolymer of N-vinylpyrrolidone, N-vinylcaprolactam and dimethylaminoethyl methacrylate, and anti-agglomerants (quaternary ammonium salts) (Koh, 2002).

Salt can also be used as a thermodynamic inhibitor to prevent hydrate formation; however, its use is a bit different from alcohols or glycols. Water molecules usually connect through hydrogen bonding, but when salt is present the salt will ionize and interact with these dipoles with a much stronger Coulombic bond than both the hydrogen bond and the van der Waals forces. Water will therefore be attracted to salt ions rather than to the hydrate structure and large clusters of water will form around the salt molecule. The ion binds the water in a more efficient manner than alcohol and glycol, but due to corrosion in metal pipes it is usually not used as a hydrate inhibitor.

In all experiments conducted in this thesis a brine solution was used for saturating the porous samples, in order to prevent swelling of clay present in the sedimentary material. Normal seawater has an average salinity of approximately 3.5 wt%, dominated by NaCl, and saline water is also found in offshore reservoirs. NaCl is one of the most common salts found on earth, and consists of the positively charged Na^+ cation and the negatively charged Cl^- anion that are bonded through an ionic bond. Earlier in-house experiments have investigated the impact of different salinities on hydrate growth (Husebø et al., 2008a), but did not investigate salinities over 6 wt%.

1.2 Gas Hydrates as an Energy Resource

The global energy demand is on a rise and is projected to increase by 50% from 2005 to 2030 (EIA, 2008). Concurrently, discovery of large conventional hydrocarbon accumulations is decreasing. In order to meet the future energy demand, alternative energy sources may have to be considered in the near future.

1.2.1 Hydrate distributions worldwide

Gas hydrates are generally found below the seafloor at ocean depths exceeding 300 m and in arctic permafrost regions, in areas where organic carbon has accumulated rapidly, mainly beneath the slope of both active and passive continental margins (Tréhu et al., 2003). Estimates of *in situ* CH_4 hydrates vary between 0.2 x 10^{15} m^3 and 3053 x 10^{15} m^3 (Appendix A2), where the most frequently cited estimate is 20 x 10^{15} m^3 (Kvenvolden, 1988). This represents over twice the energy found in all conventional fossil reservoirs combined. Even if conservative estimates of *in situ* gas hydrates turn out to be correct and recovery is low, production from gas hydrate reservoirs will still have a great impact as an energy source due to the sheer size of the resource. In addition, the gas is highly concentrated when stored in gas hydrates, where 1 m^3 of CH_4 hydrates corresponds to 164[f] m^3 of gas at standard conditions (Moridis et al., 2008), so the amount of energy stored in gas hydrates is vast. To recover the gas stored in gas hydrates energy is needed for the dissociation process, but modelling suggests that this energy could be less than 15% of the total recovery (Sloan and Koh, 2008). There are two orders of magnitude more hydrate in the ocean than on land, as indicated in Figure 1.15.

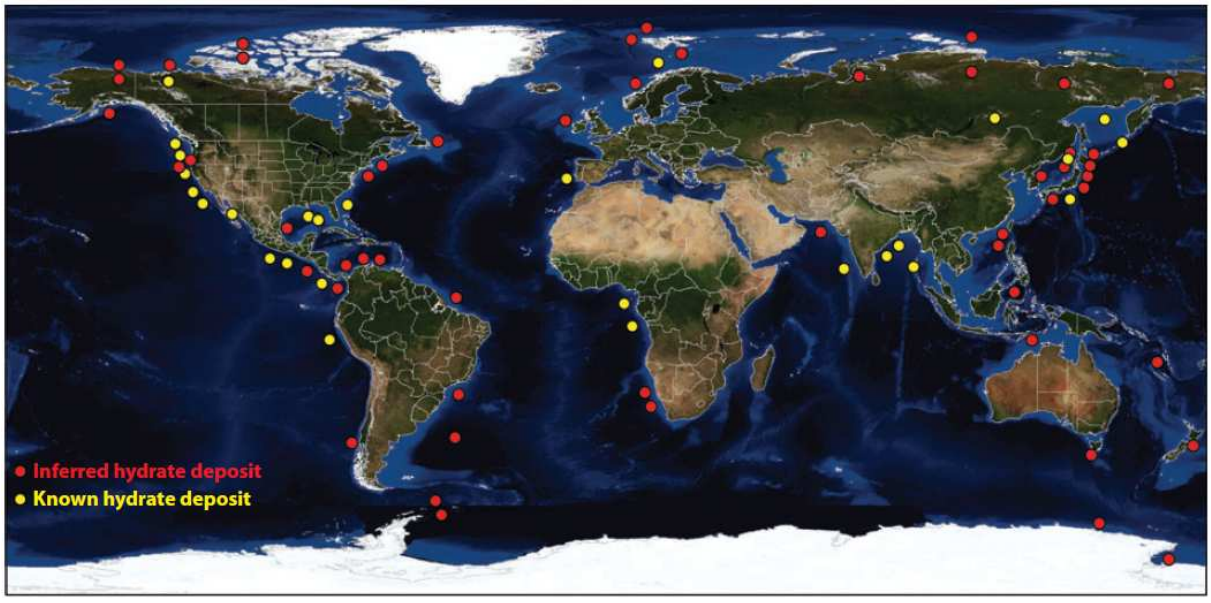

Figure 1.15 – Map of more than 90 documented hydrate occurrences (Hester and Brewer, 2009). Indirect hydrate markers, such as seismic reflectors and pore-water freshening in core samples, were used to identify the inferred hydrate deposits. Areas where hydrate samples have been taken are marked as known hydrate deposits. It is easily observed hydrate deposits are mainly distributed in marine environments.

[f] Number is dependent upon cage filling and hydrate structure. This number assumes 100% cage filling in structure I methane hydrate.

1.2.2 Potential role in the energy future

As more and more of the conventional fossil energy reserves are depleted, the focus needs to be shifted to other potential sources of energy and the future demand for cleaner energy is likely to increase. The advantage with CH_4 gas, compared to other fossil fuels such as oil and coal, is that it burns relatively clean upon combustion and causes fewer pollution problems and less CO_2. Figure 1.16 shows a comparison between gas stored in gas hydrates and in gas reservoirs, where the more promising aspects of the reservoirs are located at the top, while the more technically challenging are located at the base of the pyramid. Consequently, the volume of the challenging locations is in abundance and dominates the potential of the resource, but the saturation of these hydrate accumulations are low (~10% or less) and current technology does unfortunately not offer an economically feasible production scheme for these accumulations (Moridis and Sloan, 2007). However, even the topmost layer of the hydrate deposits pyramid offer vast amounts of energy. Current production targets include hydrate accumulations in sandstones and dense hydrate accumulations with associated fractured network. In order to provide sufficient production rate the reservoir is dependent on suitable permeability.

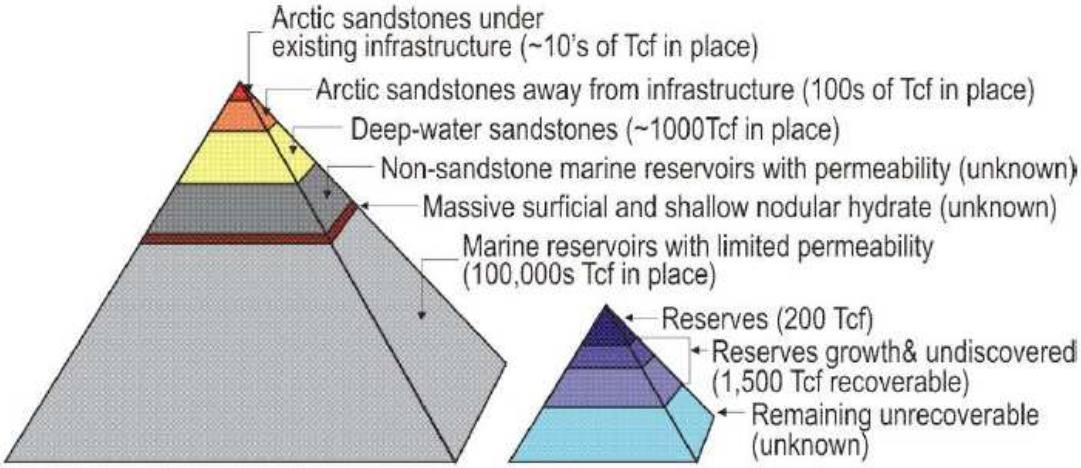

Figure 1.16 – Gas hydrate resource pyramid to the left and to the right is an example of a gas resource pyramid for all non-gas hydrate resources (Boswell and Collett, 2006). The shear size of the gas hydrate pyramid makes gas hydrates an attractive energy resource, even though the majority of the reserves are located in inaccessible reservoirs partly due to limited permeability.

1.3 Gas Hydrates in Porous Rock

Typically, gas hydrates are deposited in porous reservoirs and to simulate hydrate reservoir conditions outcrop rocks which closely resemble reservoir conditions will be used for this study. This section will introduce some basic core analysis terminology which are essential for further studies, especially permeability, which will be experimentally investigated in Chapter 4.

1.3.1 Porosity

Sedimentary rocks consist of grains of different sizes and shapes that have been consolidated into a rock. Despite cementation there is still some void space inside the rock not filled with sediments and this void constitute the *porosity*. The porosity is a fraction and therefore a dimension-less parameter, which is defined as the ratio of pore volume to bulk volume

$$\phi = \frac{V_p}{V_b} \tag{1.9}$$

where ϕ is the porosity, V_p is the pore volume and V_b is the bulk volume. Because porosity influences the hydrocarbon potential in a reservoir, it is an essential and important reservoir rock quality. The literature differs between effective and ineffective porosity. Catenary and cul-de-sac pores (Figure 1.17) are connected through a network of pores and constitute the effective porosity, while closed pores are isolated from the rest of the pore-network and thus result in ineffective porosity.

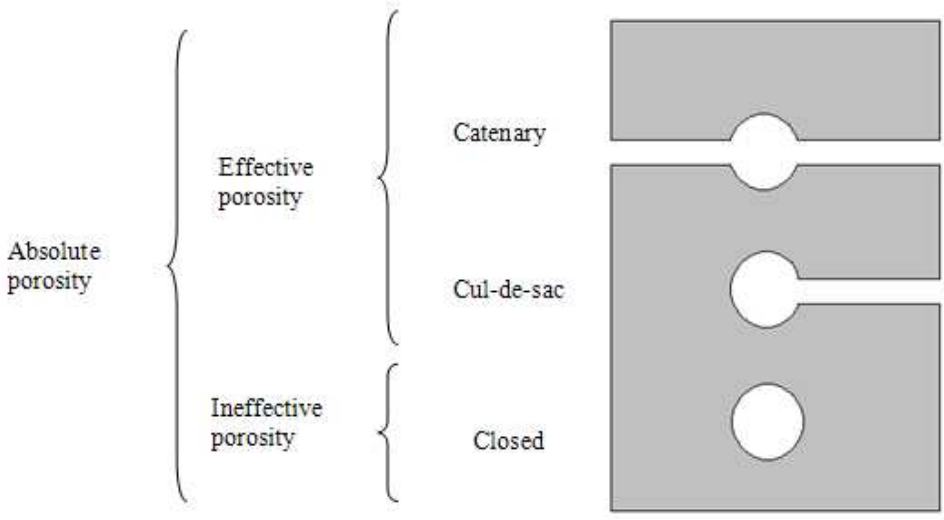

Figure 1.17 – Illustration of the different pore structures found in a sedimentary rock. Modified from Selley (1998).

1.3.2 Permeability

Absolute permeability

Permeability may in some cases be related to porosity and determines the fluid flow capacity through the porous medium. Permeability is a rock parameter and refers to the capability of the rock to transport fluids through its pores and pore throats. Darcy's law, in which permeability is defined, is an empirical law which can be written as

$$Q = \frac{KA}{\mu}\frac{\Delta P}{L}, \tag{1.10}$$

where Q is the flow rate [m^3/s], K is the permeability [D], A [m^2] is the cross-sectional area of flow, ΔP [Pa] is the differential pressure over the core with length L [m], and μ [Pa·s] is the viscosity of the fluid. In order to be able to use Darcy's law, the porous medium has to be 100% saturated with a single fluid that flows in a laminar manner without inducing any chemical reactions with the porous media. According to Darcy's law, the permeability is considered a scalar, but considering the inhomogeneous nature of the sedimentary rock it is intuitive that the permeability will differ in space and direction of flow. The permeability can therefore be treated as a tensor and is often higher horizontally than vertically due to sedimentation induced by gravity, which governs the grain arrangement.

Relative permeability

If the porous medium is saturated with non-miscible fluids, each fluid will constrict the flow area of the others and obstruct flow throughout the porous medium. This will result in a reduction in the effective permeability for each fluid compared to the absolute permeability. Darcy's law may be modified to express the current effective permeability for each fluid:

$$k_{i,eff} = \frac{q_i}{A}\frac{\mu_i L}{\Delta P}, \tag{1.11}$$

where i is a specific fluid, in most cases either water, oil or gas. The relative permeability is defined as the ratio between the effective and the absolute permeability:

$$k_{r,i} = \frac{k_{eff,i}}{K}, \tag{1.12}$$

where $k_{r,i}$ is relative permeability for fluid i, $k_{eff,i}$ is effective permeability for fluid i, and K is the absolute permeability. Because the flow rate is obstructed the relative permeability will always be less than the absolute permeability, resulting in a fraction less than one for each fluid present. The relative permeability is greatly dependent on the fluid saturation of the porous medium, as illustrated in Figure 1.18, where higher saturation results in subsequent increase in relative permeability.

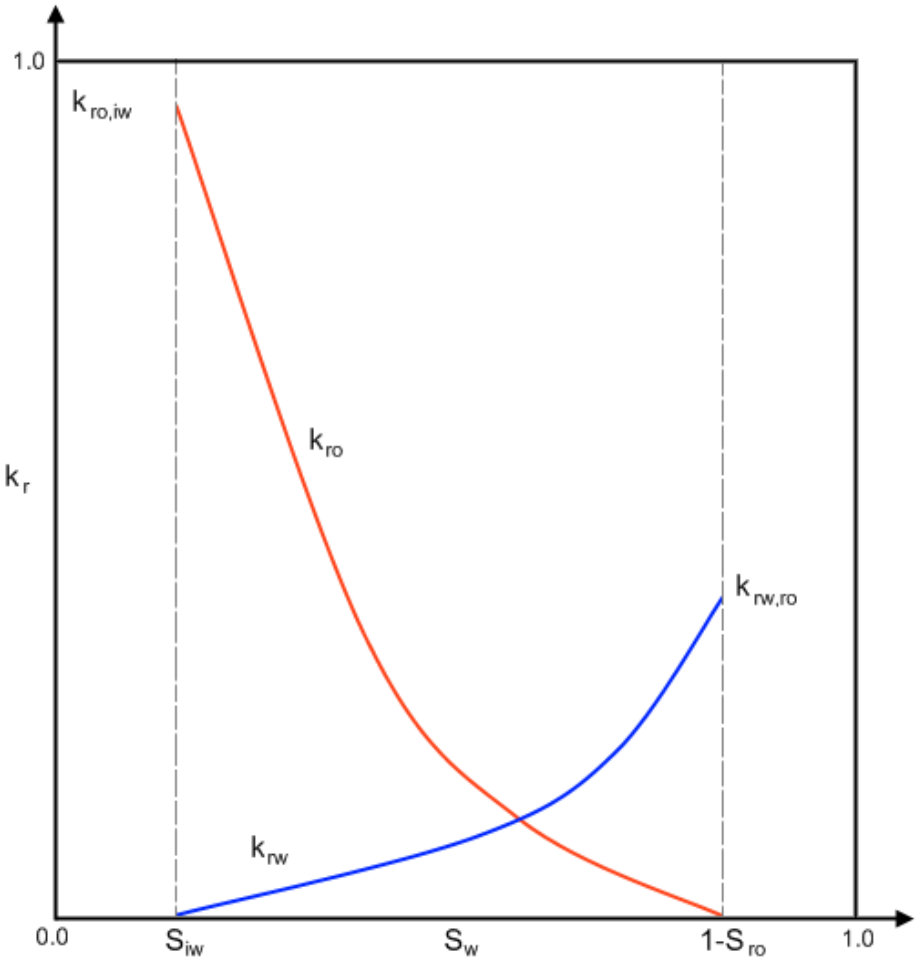

Figure 1.18 – Example of relative permeability curve for a porous media saturated with both oil and water. S_{iw} represents the irreducible water saturation while S_{ro} is the residual oil saturation. k_{rw} is the relative permeability for water and k_{ro} is the relative permeability for oil.

Gas permeability

Darcy's law is only applicable during slow and viscous flow, which results in a linear relationship between flow rate and pressure drop. When gas is used for permeability measurements, the fluid flow may not always be in the Darcy flow regime. The fluid flow is often in the Forchheimer flow regime, which is laminar flow with inertia effects, and Darcy's law will consequently have to be modified to account for this added resistance. Reynolds number, which is the ratio of inertial forces to viscous forces, is used to determine if the flow is laminar or not and can be calculated using

$$R_e = \frac{\rho v d_p}{\mu}, \tag{1.13}$$

where ρ is fluid density, v is the specific discharge, d_p is a variable representing grain diameter for the porous medium, and μ is the viscosity. As long as Reynolds number is less than 10 the flow regime is considered Darcian. If the flow rate is sufficiently high, Reynolds number will surpass 10 and the Dupuit and Forchheimer modification of Darcy's law has to be applied to describe the nonlinear flow. The Forchheimer equation is given as

$$-\nabla P = \frac{\mu}{\kappa} V + \beta \rho V^2, \tag{1.14}$$

where V is the flow velocity and β is the inertia resistance factor that has to be determined experimentally from the slope of the Forchheimer graph (Huang and Ayoub, 2008), which is given as the relationship between $1/k_{app}$ and $\rho V / \mu$, where the apparent permeability is given as

$$\frac{1}{k_{app}} = -\frac{\nabla p}{\mu V} = \frac{1}{k} + \beta \frac{\rho V}{\mu}. \tag{1.15}$$

The added resistance occurs as a combination of gas compressibility and alternating pore sizes, where gas is compressed and adds resistance to the flow in smaller pores and pore throats. In order to produce a Forchheimer plot, multiple flow rates have to be applied during the permeability measurements.

1.4 Gas Production from Hydrate Reservoirs

1.4.1 Gas production scenarios based on destabilization of hydrate

Current literature refers to two different groups of gas production schemes, where the first group is based on dissociation of hydrates by changing the reservoir conditions so that the gas hydrate is moved outside the stability region shown in Figure 1.19. In this group three different production methods are considered:

1. Hydrate dissociation through depressurization
2. Hydrate dissociation through thermal injection
3. Hydrate dissociation through inhibitor injection.

If the reservoir pressure is decreased into the unstable hydrate region, which is below or to the right of the phase boundary illustrated in Figure 1.19, the gas hydrate will start dissociating. This method is by many considered the most cost efficient production method, because the added energy during production is kept at a minimum. Thermal stimulation is another production method, where steam or hot water is supplied to the reservoir in order to move it outside its stability region. This production method requires a lot of energy, because liquid must be heated and then transported into the hydrate reservoir. In addition, hydrates do not conduct heat very well, and subsequently this method will not be very efficient. Injection of different inhibitors has also been considered, where the phase boundary shown in Figure 1.19 will be shifted to the left, thereby reducing the hydrate stability region. Other production methods have been considered as well, for example fire flooding, burial of nuclear waste, use of electromagnetic heating and solar and geothermal energy (Ning et al., 2008).

Both thermal injection and depressurization have been applied on field scales to assist production from gas hydrate deposits at Mallik (Mackenzie Delta, Canada) and the early production test in 2002 based on thermal injection showed a recovery of 470 Sm^3 gas (Yamamoto and Dallimore, 2008). A new production test was conducted in 2007 based on depressurization, where production was maintained for 60 hours, but was then shut in due to sand production. During the more successful period, a total of 830 Sm^3 gas was produced. In 2008 the pumping system was modified with additional sand control devices, which resulted in continuous production for almost six days. During this period stable gas flow and bottom hole pressure conditions were measured and the gas flow was ranging from 2000 to 4000 Sm^3/day, resulting in a cumulative gas volume of approximately 13,000 Sm^3. In order to provide economical feasibility, it has been indicated that rates larger than 500,000 Sm^3/day are needed (Sloan, 2003).

Messoyaka, located in the eastern Siberian permafrost, is another example of a gas hydrate reservoir produced through depressurization, with additional injection of a hydrate inhibitor (methanol). The reservoir mainly consisted of free gas, with assumed hydrate deposits acting as a cap rock. Production of the field was initiated in 1967 (Makogon, 1997). The Messoyaka field was in the metastable region with very low subcooling and a small pressure drop was sufficient to induce hydrate dissociation, which resulted in additional gas release to the reservoir. Consequently, 30% of the produced gas is assumed contributed from gas hydrates.

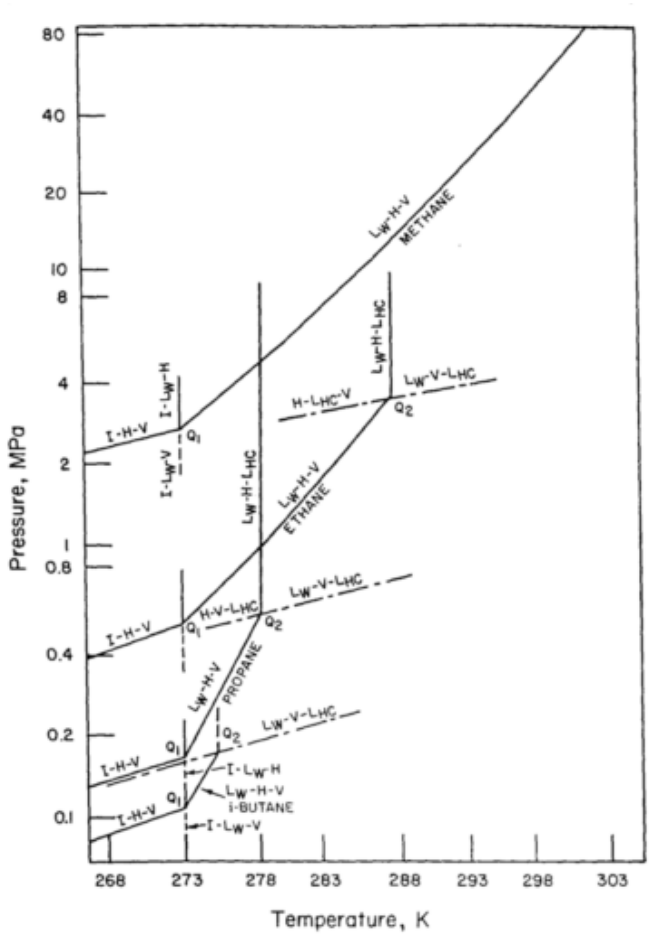

Figure 1.19 – Thermodynamic stability region for gas hydrate with different guest molecules (Sloan and Koh, 2008). The area above the phase boundary line displays the stability region for the hydrate. I denotes ice, L denotes liquid, V denotes vapor and H denotes hydrate. Subscripts W and HC are used to differentiate between water and hydro carbon fluids.

1.4.2 Gas production through replacement of guest molecule

The second group of production schemes is based on injection of a gas that provides thermodynamically more stable gas hydrates than the existing guest molecule does. CO_2 is one such gas and extensive experimental work supports possibility of replacing CH_4 with CO_2 (Ohgaki et al., 1996). CO_2 provides increased stability of the gas hydrate, as illustrated in Figure 1.20. The extent of the exchange is dependent upon the state of the CO_2, where gaseous CO_2 is more effective than liquid (Hester and Brewer, 2009). Several experiments have shown that exposing CH_4 hydrates to CO_2 will lead to an exchange process where the hydrates prefers occupation by CO_2, thus an exchange process takes place (Lee et al., 2003, Graue et al., 2006a, Jadhawar et al., 2005, Ota et al., 2005). This is also supported by simulations (Phale et al., 2006). Reasons for the exchange process is the mentioned difference in thermodynamic stability, but also due to the exothermic nature of CO_2-hydrate formation, which induces heat that may accelerate the exchange rate through rapid CH_4 hydrate micro scale dissociation. In fact, the released heat through CO_2 hydrate formation (-57.98kJ/mol) is higher than the heat required for CH_4 hydrate dissociation (54.49kJ/mol), which will accelerate the exchange process (Goel, 2006). In addition to provide increased support and stability, sequestration of CO_2 into hydrate stable regions also offers a favorable approach when looking at long-term storage of CO_2, which may halt the possible anthropogenic global warming.

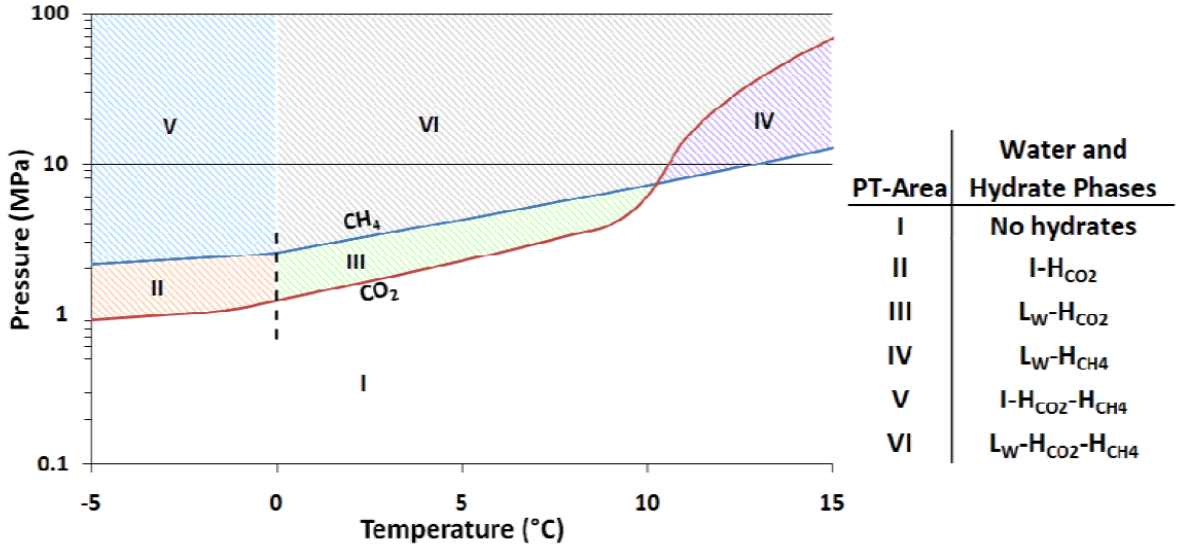

Figure 1.20 – Thermodynamic stability region for CH_4 and CO_2 (Husebø, 2008). From this figure it is easily observed that the stability region of CO_2 hydrate extends beyond that of CH_4 hydrate at lower temperature. I=Ice, L_w=liquid water, H_{CO2}=CO_2-hydrate, H_{CH4}=CH_4-hydrate.

1.5 Environmental Concerns during Utilization of Hydrates

There are several concerns and conceivable hazards involved when considering gas production from gas hydrates. CH_4, which is the most common gas found in hydrates, is considered a potential threat to the environment, and this alone raise concern due to potential release during production. Other problems involve loss of geomechanical stability during production and dissociation.

1.5.1 Loss of geomechanical stability

Gas hydrates form in the middle of the porous space without cementing or coating the grains (Murray et al., 2006) and because they can stand large amounts of stress, they give support to the matrix and overlying sediments. In some cases the matrix would be under-consolidated sediments of low shear strength if not for the presence of gas hydrates, which are 20 times stronger than ice Ih (Durham et al., 2003) and provides support to the overlying matrix. CH_4 hydrates are usually formed by migration of CH_4 along unstable fracture systems, which turns into solid gas hydrates once contacting water in the hydrate stable region. If the gas hydrates are removed by decomposition it can trigger catastrophic uncontrolled pore-collapse and plate shifting with additional liberation of CH_4 that has a significant effect on the global climate (Gunn et al., 2002). In the production scenarios suggested in Chapter 1.4.1, production is based on dissociation of the gas hydrate which will induce free water and free gas. The gas density in hydrate is higher than in free gas, so dissociation will increase the gas volume with a subsequent increase in pore pressure. If the local pressure exceeds the pressure provided by overlying sediments, fractures may occur and the gas is vented out from the previous hydrate site. The hydrate no longer provides stability to the under-consolidated sediment and massive landslides may occur, as illustrated in Figure 1.21. This represents a threat to production facilities and pipelines close to existing hydrate deposits; however, the geohazards involved would be far more substantial in an actual gas hydrate production scenario.

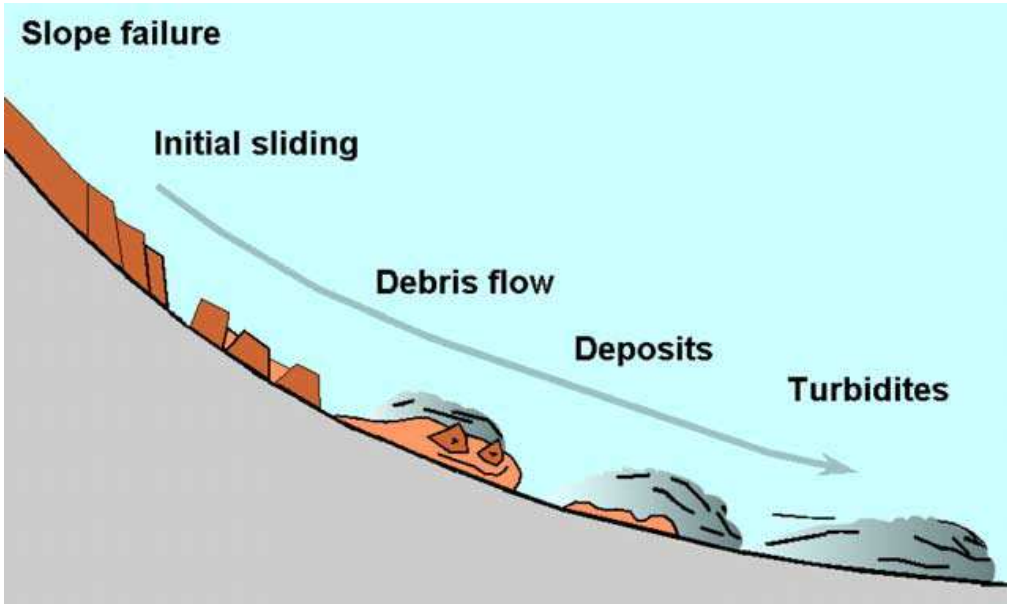

Figure 1.21 – Schematic illustration of the different stages during a landslide (Bryn et al., 2005). The hydrate maintains the stability of the sediment, but once dissociated initial slide occurs and unconsolidated debris is picked up during the slide resulting in displacement of water and possible creation of a subsequent tsunami.

1.5.2 Climate challenges

CH_4 absorbs infrared radiation approximately 25 times more efficient than CO_2 (Lelieveld et al., 1998) and consequently has a more aggressive effect on the climate than CO_2. Current concerns and focus are mainly directed on anthropogenic CO_2 emissions; and according to Etheridge and coworkers (1998) the CH_4 concentration in the atmosphere has increased from 700 ppb in 1800 to 1700 ppb today. Measures are provided in order to reduce greenhouse gas emissions; however, current emission budgets do not consider geologically-sourced CH_4 seepage. The estimated total contribution from geological sources to the atmosphere is approximately 45 Tg CH_4/year (Kvenvolden and Rogers, 2005). The actual flux of CH_4 from the earth is a lot higher, but microbial oxidation processes intercept and remove more than 50% of the CH_4 before it reaches the atmosphere, thus lowering the total flux.

Seepage of CH_4 from gas hydrates along with CH_4 from swamps and volcanic eruptions are considered natural macro seeps; however, the contribution from gas hydrates into the atmosphere is still unaccounted for. Nevertheless, empirical experiments, theoretical considerations and geological reasoning suggest that CH_4 from such systems may in fact reach the atmosphere. Hansen (2004) suggests that reduction in CH_4 emissions may outweigh the negative influence of CO_2 emissions. By sequestrating CO_2 into CH_4 hydrate deposits CO_2-hydrates form, which are less susceptible to temperature fluctuations (Figure 1.20). In this manner the CO_2 content in the atmosphere is lowered while CH_4 may be made accessible for production. Due to the gas hydrate stability increase the risk of dissociation and associated pore collapse is reduced. One of the production scenarios investigated in this thesis is based on exchange between liquid CO_2 and CH_4 hydrate and the additional environmental benefits achieved during this production scenario should be considered as well. However, if CO_2 is sequestrated into gas hydrates, this represents yet another threat due to potential leakage. At sufficiently high pressure CO_2 is in liquid state, where CO_2 hydrate formation may occur at lower temperature than those where CH_4 hydrate dissociates (Goel, 2006). If CH_4 hydrates dissociate and are not replaced by guest molecules, the geomechanical stability may be compromised, resulting in release of CH_4 and CO_2.

During its lifetime the earth has experienced several extreme global environmental changes. During the Latest Paleocene Thermal Maximum (LPTM) approximately 55.5 million years ago the water temperature was increased by 4 º to 8 ºC (Katz et al., 1999, Dickens et al., 1995, Bin, 2007). Dissociation of gas hydrates has been suggested as an important factor during extreme temperatures, where small temperature changes to the oceans resulted in massive dissociation of gas hydrates and consequent release of CH_4 with subsequent additional temperature increases. According to the controversial Clathrate Gun Hypothesis (Kennett et al., 2005), CH_4 hydrates stabilized and accumulated during cold intervals in the late Quaternary. Later temperature changes in the thermohaline circulation resulted in warming of water at intermediate depths, causing hydrate instability and subsequent catastrophic release of CH_4 into the ocean and atmosphere. As the gas hydrate dissociated sediment stability was compromised, resulting in sediment disruption on upper continental slopes. The release of CH_4 contributed to further warming of the atmosphere and oceans, again resulting in further CH_4 hydrate dissociation. Even though the hypothesis lacks general support (Hester and Brewer, 2009), the negative environmental influence of CH_4 should carry weight during decisions concerning gas production from gas hydrates due to the fact that massive gas hydrate dissociation and consequent CH_4 flux to the atmosphere may cause severe and irreversible damage to the environment.

Chapter 2

Imaging Techniques

2.1 Fundamentals of NMR

Nuclear Magnetic Resonance (NMR) was discovered independently by Felix Bloch (Bloch, 1946) and Edward Mills Purcell (Purcell, 1946) and has a wide range of applications in today's industrial and scientific societies. In the petroleum industry NMR is used as the basis of a suite of logging tools. The principle of NMR is based on quantum mechanics and Newtonian physics. Intrinsic angular momentum, often referred to as spin, is a fundamental property in quantum mechanics where the classical analogy describes particles rotating around their own axis. This creates an electromagnetic field, where the magnetic component of this field causes some nuclei to act as bar magnets. Large parts of the molecules found in the human body and hydrocarbons are comprised of hydrogen, which consists of one single positively charged proton that has a spin of S=1/2. The energy states for such a particle will be -½ and ½, where α denotes the lower energy state (½) and β denotes the higher energy state (-½) (Figure 2.1).

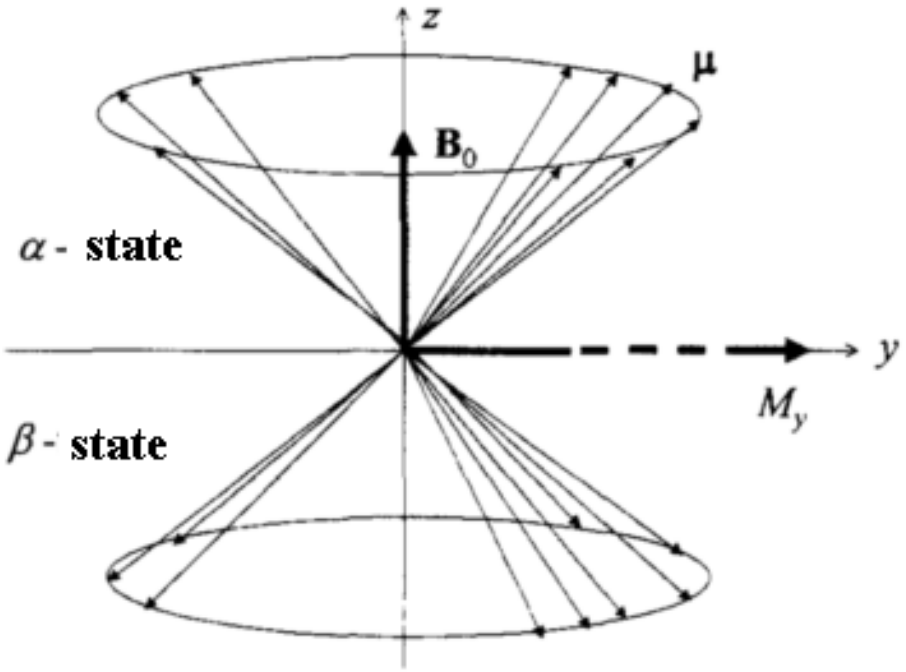

Figure 2.1 – Two different energy states for a proton in an external magnetic field (Lien, 2004).

Nuclei with unpaired protons will have an angular momentum $\vec{J}$, and a net magnetic field or a magnetic dipole moment given by

$$\vec{\mu} = \gamma \vec{J}, \tag{2.1}$$

where γ is the gyromagnetic ratio. Spinning unpaired protons in the presence of an external magnetic field with flux $\vec{B}$ will line up along the vector with the majority of dipole moments directed in positive flux direction of this field. The torque experienced by the magnetic dipole moment is

$$\vec{\tau} = \vec{\mu} \times \vec{B}, \tag{2.2}$$

and as long as $\vec{\mu}$ is parallel to $\vec{B}$, which is the preferred state of $\vec{\mu}$, the torque will be zero. The magnetization will then be the sum of the individual magnetic dipole moments

$$\vec{M}_0 = \sum_i^N \vec{\mu}, \tag{2.3}$$

and the magnetic flux at this state is referred to as $\vec{B}_0 = \vec{B}_z$. As long as no external force is applied the particles will stay at the lower energy equilibrium, and $\vec{M}_0 = \vec{M}_z$. If an external force is applied and $\vec{\mu}$ is rotated outside its state of equilibrium the potential energy to the system is increased according to

$$U = -\vec{\mu} \cdot \vec{B}. \tag{2.4}$$

If a 180 pulse has been applied and the magnetization vector is tipped 180º, from its direction at equilibrium, the energy difference between the two spin orientations for one proton becomes

$$\Delta E = 2\mu B. \tag{2.5}$$

When photons of energy ΔE irradiate the hydrogen atoms, some of the nuclei will make transitions from the lower α-state to the higher β-state by resonance absorption. The frequency of these photons are given through Planck's law

$$\Delta E = hf = \gamma \hbar B_0. \tag{2.6}$$

Nuclei in a magnetic field will rotate around the static magnetic field $\vec{B}_0$ according to Newtonian physics. This precessing frequency is called the Larmor-frequency, and is given by

$$f_L = \frac{\varpi_L}{2\pi} = \frac{\gamma}{2\pi} B_0, \tag{2.7}$$

which is the same frequency as the photons, given by Equation (2.6). Therefore, in order to get an image by NMR, a new magnetic field $\vec{B}_1$ is introduced which is orthogonal to both the angular momentum $\vec{J}$ and $\vec{B}_0$. In addition, it is critical that this new magnetic field rotates around $\vec{B}_0$ with the Larmor-frequency. If the frequency does not match the precessing frequency, no resonance will occur and no energy will be added to the protons. By transmitting an electromagnetic radio frequency (RF) wave $\vec{J}$ is flipped into the xy-plane where the individual spins will start precessing around the external magnetic field axis.

2.2 Relaxation Time

Nature tends to seek the lowest energy level, and once the RF pulse that has tipped the protons to a higher energy state is turned off, the spins will start relaxing back to equilibrium state. The protons will try to realign with the original $\vec{B}_0$ magnetic field by giving up their excess energy. During this process two different relaxation times, T_1 and T_2, may be measured, where T_1 is the spin-lattice relaxation time; the time it takes for the spins to realign along the z-axis. The magnetization during this process is given by

$$M_z(t) = M_0\left(1 - e^{-t/T1}\right) \tag{2.8}$$

for a 90º pulse, and it can be seen that the magnetization will increase with time in z-direction (Figure 2.2). T_2 is the spin-spin relaxation time, and is a measure of the decay of the M_{xy} component once the RF pulse is turned off. Once $\vec{M}_0$ is flipped into the x´y´-plane (the rotational frame), which is parallel or equal to the xy-plane (the laboratory frame), the magnetization will start dephasing, spreading out in a fan shape, as shown in Figure 2.3. This happens due to field inhomogeneities and interactions between spins. The decay of M_{xy} is given by

$$M_{xy}(t) = M_0 e^{-t/T2} \tag{2.9}$$

and with time the magnetization decreases.

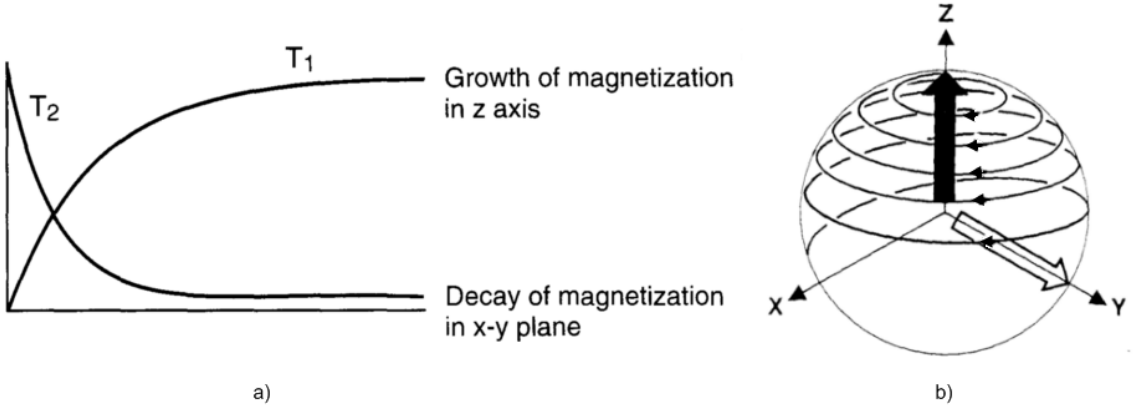

Figure 2.2 – Relaxation of the magnetic signal (figure a) is taken from (Hashemi and Bradley, 1997), while b) is modified from Vlaardingerbroek and den Boer (1996)). The z-component of the magnetic field increases with time, while the planar component decreases. b) illustrates how the magnetization progresses in a spiral motion with time.

2.2.1 The spin echo pulse sequence

The spin echo sequence (Hahn, 1950) is the most frequently used sequence. First a 90º pulse tips the net magnetization M_0 into the xy plane, and at this point $M_{xy} = M_0$. The signal will start dephasing as shown in Figure 2.3, due to inhomogeneities and spin interactions. The spins will precess with different frequencies due to inhomogeneities, and the different magnetic dipole moments will spread out in a fan shape. Eventually they will be totally out of phase and cancel each other out, resulting in a zero net magnetization vector in the x-y-plane. By applying a refocusing 180º pulse over the x-axis some time τ after the 90º pulse, the magnetic dipole moments that were lagging behind are now leading the group, while the magnetic dipole moments that were moving fastest are now lagging behind. At time 2τ the magnetic dipoles are gathered again into one magnetization M_{xy}, and the echo time can be measured. However, the magnetization is smaller than the original M_0, due to the fact that the signal has been decaying in z-direction as well, moving upwards as a spiral as shown in Figure 2.2. This process will be repeated until $M_z = M_0$, when a new 90º pulse is applied to tip the magnetization down in the x-y plane. Because several echoes are recorded between each 90º pulse multiple T_2 decays are measured for each T_1 measurement.

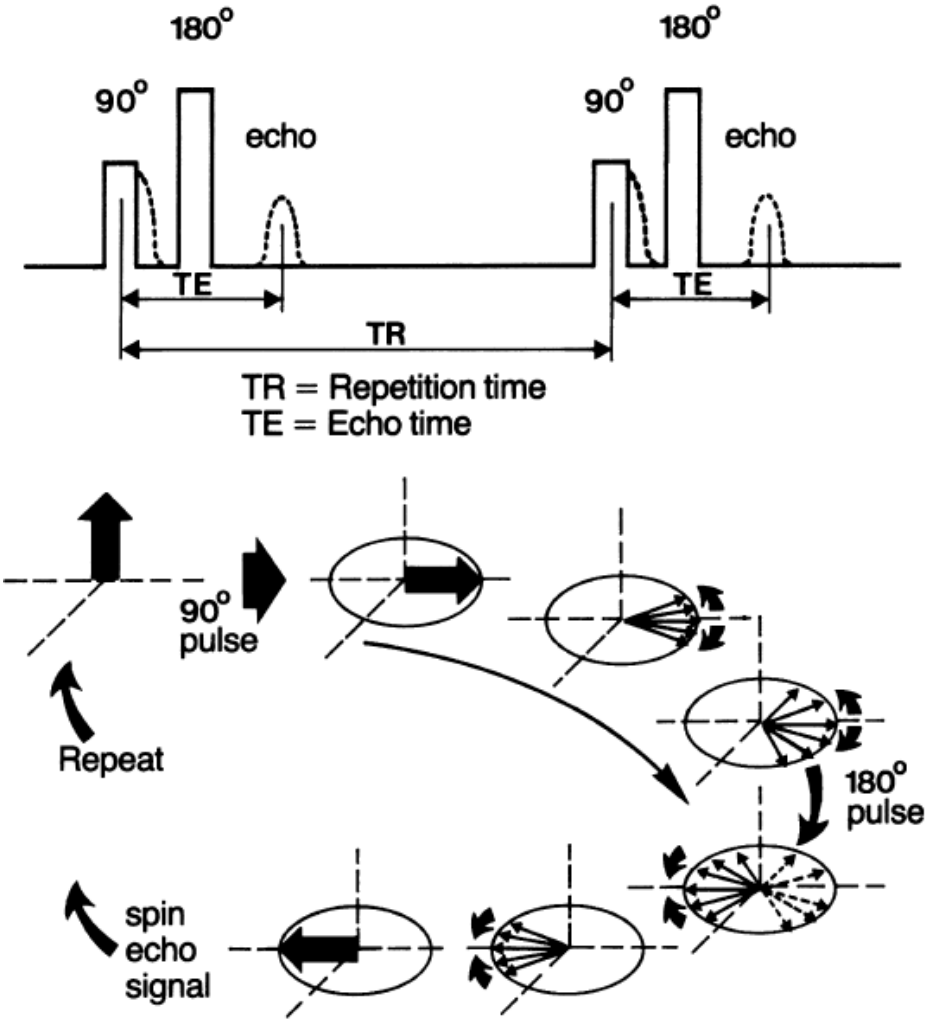

Figure 2.3 – Illustration of a 90º spin echo pulse sequence. (PhillipsMedicalSystems, 1984).

2.3 Applications of MRI in Hydrate Experiments

MRI is an imaging tool based on the same principles as NMR. MRI is a useful tool that can give three types of information (Coates et al., 1999):

- Information about the quantities of the fluids in the rock
- Information about the properties of these fluids
- Information about the sizes of the pores that contain these fluids

In this thesis a high field superconducting magnet cooled by liquid nitrogen is used. The MRI, a Unity/Inova-Imaging 85/310 spectrometer, is operating at a frequency of 85.7 Hz, corresponding to a the magnetic flux density of approximately 2 Tesla. The MRI has been used to look at 1D intensity profiles over the core and 3D images. These 3D images formed the basis for analysis done in this thesis. The signal to noise ratio (SNR) increases with the time scan period, and during this thesis scan times varied between 1 to 18 hours, where 2,4, and 9 hour scans were the most common. Initially, liquid water and CH_4 gas saturated the pores, which both contain hydrogen and therefore are visible in the MRI. The relaxation time for liquid and vapour is relatively fast. For gas hydrate and ice the relaxation time is very fast, and can therefore not be detected using standard imaging sequences. Some free gas is still present in the pores, however, this is often in the background signal range, and is not detected. Changes in MRI intensity will therefore make it easy to discern the progression of hydrate formation throughout the core (Baldwin et al., 2003).

Part II

Experimental Descriptions

Chapter 3

Experimental Setups and Procedures

Several different types of gas hydrate experiments have been conducted in this study, where the main objective was improved basic understanding of the processes involved during hydrate formation and gas production from gas hydrate deposits. Salinity has been shown to impact hydrate growth and induction time and has been investigated through six different experiments, using a range of salinities between 1 wt% and 10%. In addition, experiments looking at depressurization induced CH_4 production and injection of CO_2 into CH_4 hydrate deposits have been conducted to observe the production potential of each production method and to compare these results. In all experiments, CH_4 hydrates were formed in a porous Bentheim sandstone core at high pressure (8.37 MPa) and low temperature (4 ºC). For these experiments an already existing experimental setup at the University of Bergen was used. However, due to repeated problems with the experimental setup at the University of Bergen, two new setups were designed and built as a major part of this work and were based on a different design to reduce these problems. In addition, experiments were conducted using an experimental setup provided by ConocoPhillips in Bartlesville, USA. The following chapter will describe the experimental setups and procedures during these experiments.

3.1 Properties of Porous Media

Core samples from hydrate reservoirs are rare and often corrupted during coring procedure due to the lack of pressure maintenance during transport to the surface and other core retrieval challenges. Coring is also very expensive. Using an outcrop analogue as reservoir rock is therefore a good alternative. Sandstone is a clastic sedimentary rock, a typical reservoir rock usually composed of quartz and feldspar with generally high porosity and permeability. Bentheim sandstone has been used for all experiments in this study, and provides an ideal starting point for experiments on hydrate production scenarios. Bentheim sandstone has a grain density of 2.65 g/cm^3, and the mineralogy is 99% quartz, with small amounts of the clay mineral kaolonite (Graue et al., 2006a). This sandstone is consolidated fairly homogeneous, with a porosity of 22-23% and permeability of 1.1 D. This seems to be in accordance with the porosity reported by others (Klein and Reuschlé, 2003). The cores were acquired from a Bentheim quarry in Lower Saxony, Germany, and are strongly water-wet (Graue, 2009). The pore geometry is relatively uniform, with a pore diameter of 125 microns. Typical core size used in the experiments presented here is 5.15 cm in diameter and 10 cm in length. Further details on core properties such as weight, length and diameter can be found in Appendix B1.

3.2 Experimental Setups

3.2.1 Experimental setup based on open cooling bath (setup I)

Previous extensive gas hydrate research has been conducted at the University of Bergen (Husebø, 2008, Ersland, 2008). An existing gas hydrate experimental setup (Figure 3.1) was therefore available, but several modifications were needed due to major leaks and limited experimental possibilities. These modifications included a bypass that provided simultaneous gas injection at both ends of the core to prevent water displacements from the core into tubing during increase of pore pressure. Additional valves and a Validyne DP 303 bi-directional wet-wet differential pressure transducer were installed for permeability measurements. The voltage from the Validyne transducer was converted by a Validyne UPC 2100 acquisition card from analog to digital signal. To allow for gas production from CH_4 hydrates during CO_2 injection, a vacuum pump was added to remove excess CH_4 prior to CO_2 injection, and several valves and additional lines were also added. All salinity experiments conducted in this thesis was performed using setup I.

Figure 3.2 shows a detailed cross-sectional illustration of the high pressure Hassler core holder used for these experiments, which was connected to two Quizix C-5000-10K-SS pumps that provided confining pressure by injecting high viscosity oil into the core holder. Two Quizix C-5000-2.5K-HC pumps were used for CH_4 injection to the core, and PVT (pressure volume temperature) data was used to monitor hydrate formation. The gas concentration in gas hydrates is higher than in free gas, and during hydrate formation gas will therefore be delivered from the pumps in order to maintain constant pressure. This gas consumption is logged and gives information on when hydrate growth initiates and the number of moles of gas consumed during hydrate growth. The core holder (Figure 3.2) was fully submerged into an open external bath, where a Thermo Neslab RTE-17 refrigerated bath was circulating cooled antifreeze. The flux of antifreeze from the refrigerated bath was controlled through two valves, one on the inlet and one on the outlet. These were highly sensitive, and small adjustments to these sometimes resulted in flooding of the open bath. In some cases experiments were lost due to loss of cooling. In addition, this setup often resulted in a mess due to problems with flooding.

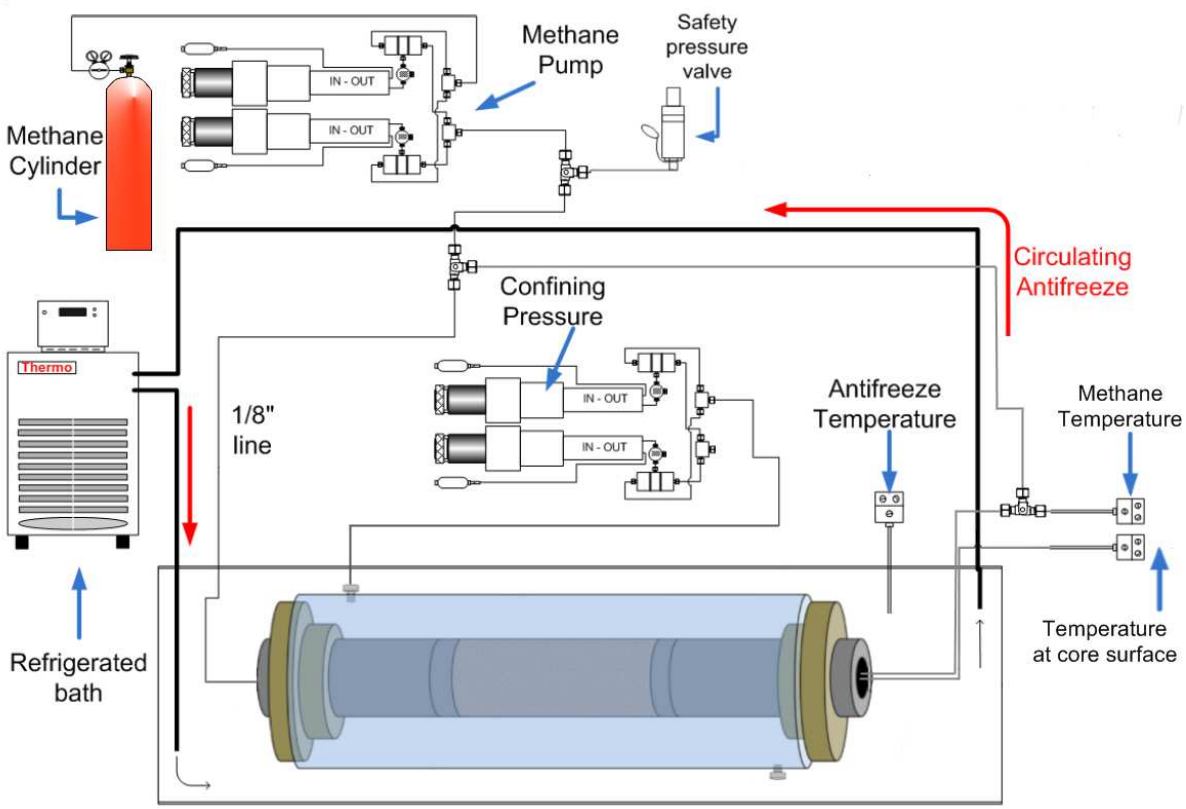

Figure 3.1 – Illustration of experimental setup I, modified from Husebø (2008). The blue core holder is submerged in an open cooling bath (the grey rectangle) and due to the sensitive nature of the valves controlling the flux of circulating antifreeze the open bath was frequently flooded.

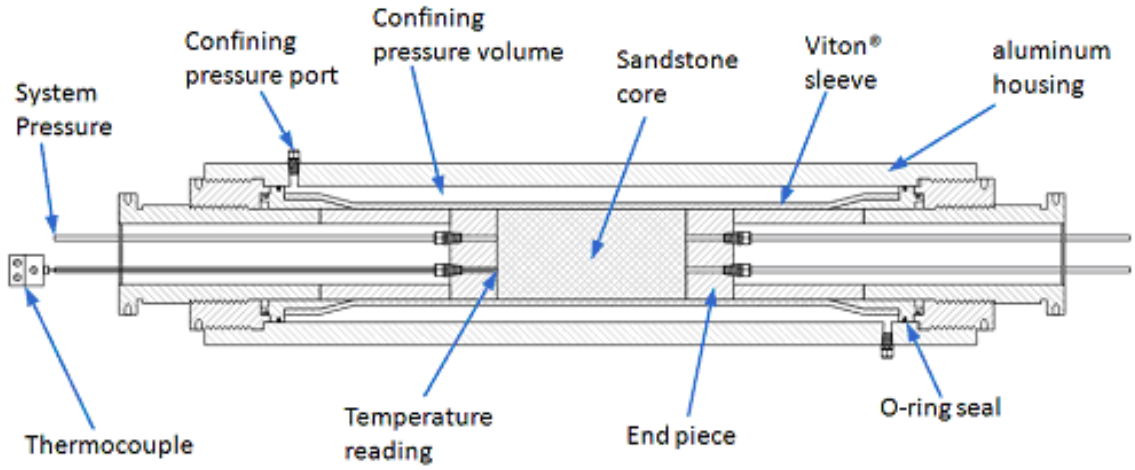

Figure 3.2 – Detailed cross-sectional illustration of core holder used in experimental setups I and II (Husebø, 2008).

3.2.2 Experimental setup with cylindrical cooling jacket (setup II)

To avoid the reported flooding problems, an additional experimental setup (Figure 3.3) was designed and built as a major part of the work presented in this thesis. In addition to resolving the flooding problem it would also allow for simultaneous gas hydrate experiments. To prevent flooding, a cylindrical closed cooling jacket was designed and fitted to a standard Hassler RCH series core holder (Appendix B2), where antifreeze could circulate without causing any flooding. The cylindrical cooling jacket does not cover the whole core holder, but provides sufficient cooling to the Bentheim sample located in the middle of the core holder. This setup was also prepared for permeability measurements and CO_2 injection, and much of the setup was therefore designed based on the modified setup I. For confining and CH_4 pressure two Isco D-series pumps were used (100 DM and 260 D), and a Thermo Neslab RTE-17 refrigerated bath circulated cooled antifreeze into the cooling jacket. This setup was not completed until the very end of this study and no experimental results from this setup are therefore presented in this thesis.

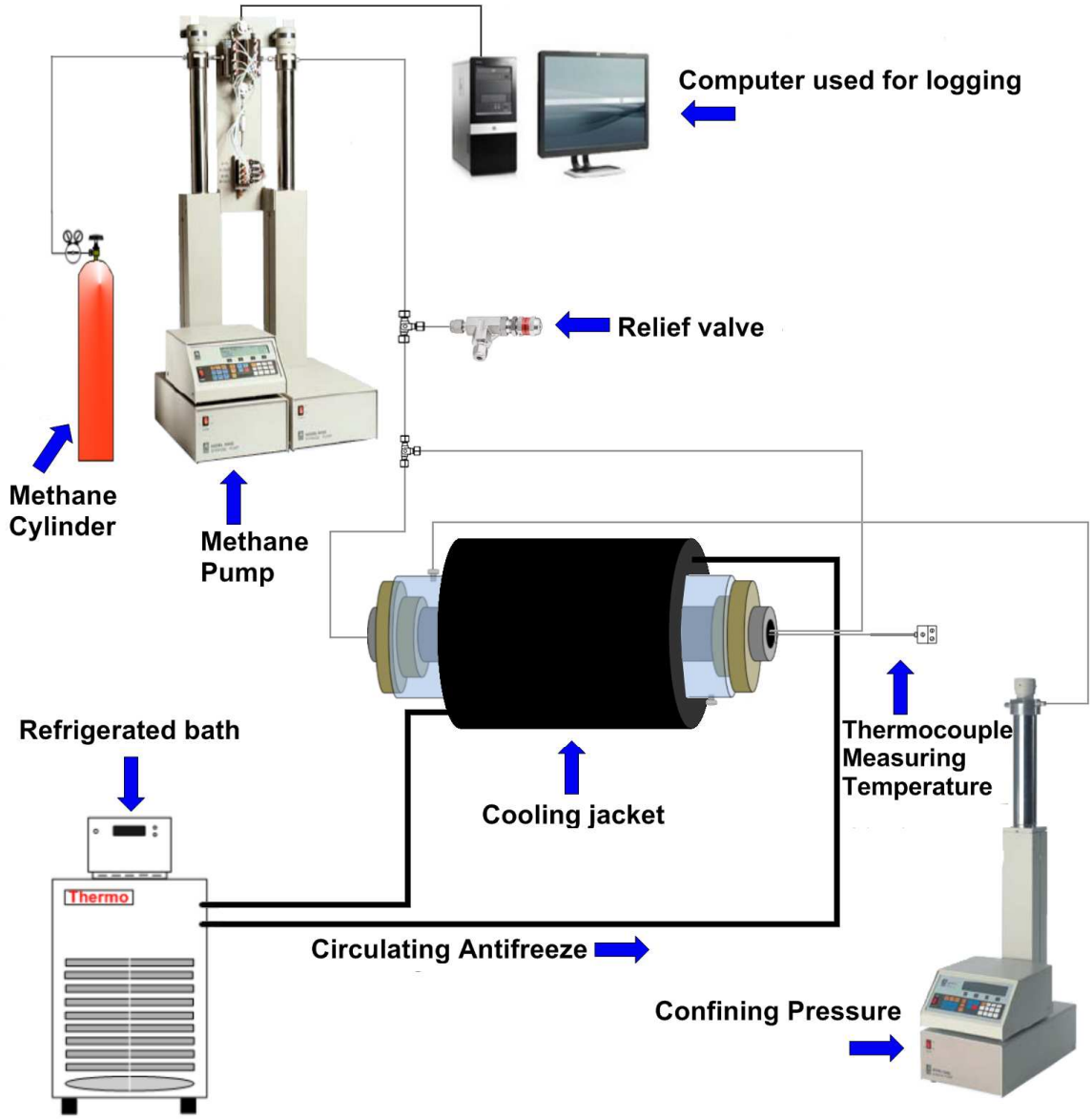

Figure 3.3 – Experimental setup II, where antifreeze was circulated in a cylindrical closed cooling jacket instead of in an unstable open bath.

3.2.3 Experimental setup with resistivity core holder (setup III)

Hydrate saturation is determined using PVT data in all setups; however, it would be advantageous to have additional monitoring possibilities during hydrate growth. A third setup was therefore designed and built as a major part of the work presented in this study, implementing an additional mean for confirmation on hydrate saturation. This setup was installed with a Temco EHCH resistivity core holder, which allows for *in situ* electrical resistivity measurements. An electrical current at 1000 KHz is connected to the inlet line and two metal rings (electrodes) that are situated in the sleeve with 2.54 cm spacing measure the voltage drop over the core. When the electrical current and voltage drop is known, the resistivity can easily be calculated. The resistivity is converted into water saturation through Archie's law. Pure water is a perfect insulator, but even deionized water is not completely free of ions, and is therefore not fit as an insulator. An impurity such as salt results in high electrical conductivity due to ion separation of salt in the aqueous solution and allows electrical current to flow freely. In a 50% brine saturated Bentheim sandstone the brine will therefore act as an electrical conductor, while the sedimentary rock essentially acts as an insulator. Upon hydrate formation, water saturation decreases as water and gas combine to form hydrate. Hydrate is an insulator too, and increased resistivity may therefore indicate hydrate formation. This allows for an additional measure of hydrate formation. However, upon hydrate formation impurities such as salt are not included in the hydrate crystal, and the salinity of the remaining pore water will be elevated, thus reducing the resistivity. The tortuosity, on the other hand, is going to increase and result in increased resistivity. In accordance with this, Liu et al. (2008) reported a minor decrease in resistivity as long as the hydrate saturation was below 20%. For gas hydrate saturations above 20% the resistivity increased.

Gas flow in hydrate deposits is often limited and restricted to diffusion through excess water. Resistivity and gas permeability are both affected by the amount of free water, and this setup was therefore also installed with a Validyne DP 303 differential pressure transducer, to establish how the two parameters correlate. To provide confining pressure, an air driven hydraulic Haskel MS-188 pump was used to inject high viscosity mineral oil, and for pore pressure an Isco D-series pump was used. The cooling mechanism is identical to setup II, where a Thermo Neslab RTE-17 refrigerated bath circulates cooled antifreeze into the cooling jacket.

3.2.4 Experimental setup with MRI

The second part of the experimental schedule was performed using an experimental setup at the ConocoPhillips Technology Center in Bartlesville, Oklahoma, USA. This experimental setup has the advantage of an MRI that can be used for monitoring dynamic *in situ* phase saturation development. Due to the strong magnetic field of the MRI only non-magnetic components can be used. This poses a challenge due to the high pressure conditions needed to form gas hydrates, and standard core holders can not be used due to their magnetic property. A Hassler core holder with fiber glass housing has been designed and constructed by Temco Inc©, Tulsa, OK, that is compatible with the high magnetic field. Details from the core holder can be seen from Figure 3.4. In Figure 3.5 the refrigerated bath, confining pressure pump and the pore pressure pumps are placed in a safe distance from the MRI, where the equipment is not sensitive to the magnetic field. A Quizix QX-6000HC-1-0-C-L-0 high pressure pump was used to provide confining pressure, while Quizix C-6000-10K-HC-HT was used for injection of both CH_4 and CO_2. During permeability measurements a Quizix C-6000 was filled with N_2,

and a Quizix SP-5200 pump was used to remove excess CH_4 in the system prior to N_2 permeability measurement.

Fluorinert FC-40 was used as confining fluid due to its lack of hydrogen atoms and does therefore not reveal a signal to the MRI (cf. Chapter 2). In addition, the low dielectric properties of the Fluorinert minimize the radio frequency loss. The system temperature was held constant at 4.0 ± 0.1 ºC by circulating cooled antifreeze fluid in an insulated PVC tube using Thermo Neslab RTE-17 refrigerated bath. Fluorinert was circulating in the inner tube and antifreeze in the outer tube (Appendix B3). A Quizix QX-6000 pump was set to deliver Fluorinert at approximately 10.79 MPa and a reciprocating pump was ensuring circulation of the pressurized Fluorinert.

Processing of raw data from the MRI

The MRI provides large amounts of unprocessed data. To structure and analyze these data an in-house IDL-based software, ROI v.2.01, was used (Husebø et al., 2007). This software uses several algorithms to identify intensity averages and corrects the acquired signal for noise. However, to visualize the data T3D v.1.1.3 (Fortner Research, LLC) was used, which displays the data in a useful interface, and was used to visualize the MRI-acquisitions.

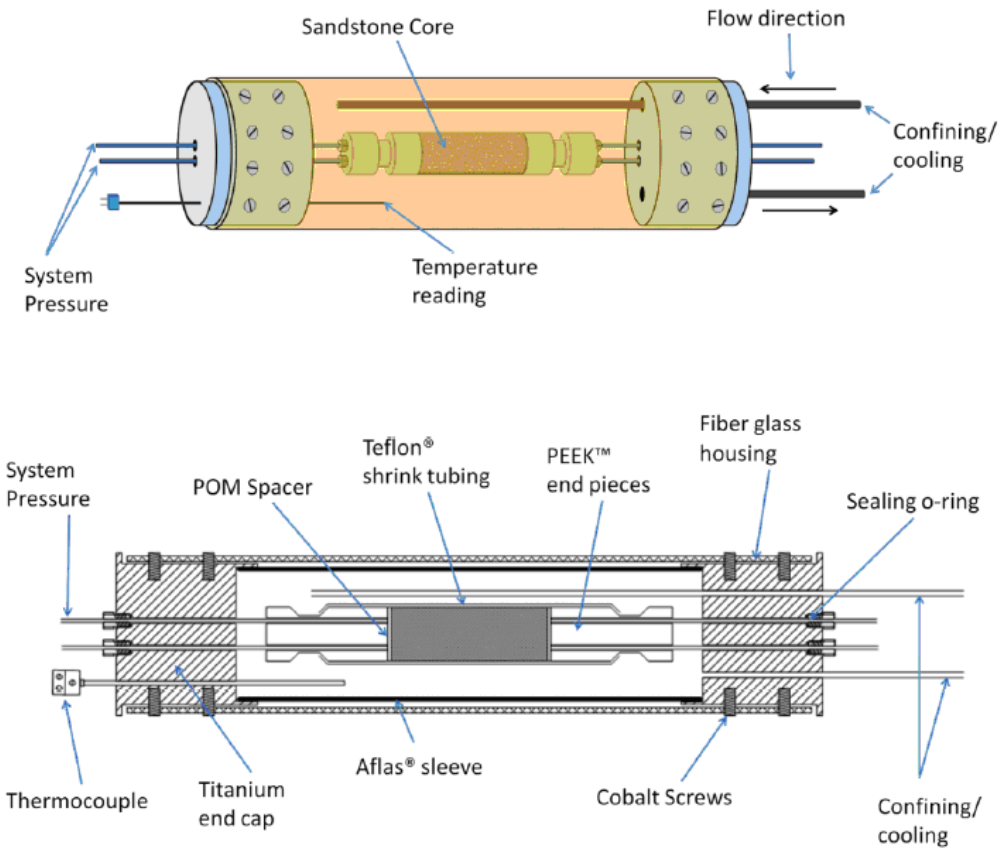

Figure 3.4 – Detailed illustration of the specially designed Hassler core holder (Husebø, 2008). The housing of the core holder is made of fiberglass and resin and is capable of handling pressures used for these experiments. Due to micro porosity of the housing, an Aflas™ sleeve is required as well. Titanium end caps are attached to the housing by non-magnetic cobalt screws.

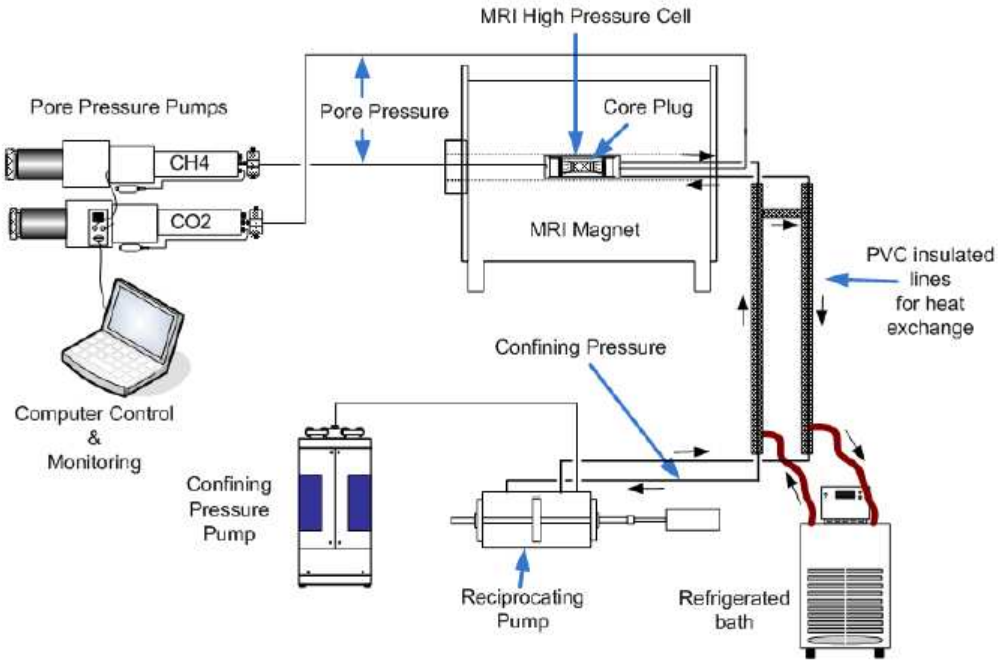

Figure 3.5 – Experimental setup used at ConocoPhillips in Bartlesville (Husebø, 2008). All magnetic equipment is located in safe distance from the MRI. Confining and cooling is provided by Fluorinert FC-40, which is circulated through the system by the reciprocating pump.

3.3 Experimental Procedures

3.3.1 Experimental procedure on salinity experiments

Hydrate formation and induction time is expected to be influenced by salinity. Salt is a hydrate inhibitor, and if the salinity is sufficiently high hydrate formation will be prevented. Salt therefore has a major impact on both thermodynamic stability of the gas hydrates and on hydrate growth, and experimental studies on impacts of salinity on hydrate formation are considered important. Previous experiments have tried to establish the effect of salt on hydrate growth (Husebø, 2008). A study is presented here using a range of salinities between 1 wt% and 10 wt%, investigating impacts of different salinities on CH_4-hydrate formation. A predetermined amount of NaCl was added to deionized water to make the appropriate brine solution. The strongly water-wet core was then partially saturated with brine through spontaneous imbibition by submerging the core into the brine solution. This method distributes water fairly uniformly in the core at S_w = 50%, which was confirmed by 3D MRI images (Ersland, 2009). When a brine saturation of approximately 50% was reached, the core was placed into the core holder, where confining pressure and CH_4 pressure were applied. These pressures were incrementally increased until the confining pressure was 10.44 MPa (1500 psig) and CH_4 pressure was 8.37 MPa (1200 psig). Once the system had stabilized, an estimate was made on the gas leakage rate. At high pressure, small gas leaks are inevitable due to the low viscosity of the gas. The leaks were constantly monitored and always maintained at a low level. Once the system had been pressurized, it was brought to 4.0 ± 0.1 ^oC, by circulating cooled antifreeze through the system. All hydrate experiments are based on material balance, and PVT data was therefore constantly monitored. CH_4-hydrates are stable at these conditions and hydrate growth was observed as a sudden increase in CH_4 delivery rate from the pumps due to increased CH_4 concentration in hydrate phase. The initial CH_4 consumption rate was very high due to large interface between the two constituents and decreased as a function of time. Once the growth had stabilized the data was analyzed and corrected for leaks.

3.3.2 Experimental procedure during gas production by depressurization

Depressurization induced gas production from gas hydrates is by many considered the most economical feasible production method (Sloan and Koh, 2008). In this study gas production from CH_4-hydrates was investigated through a depressurization test, based on constant pressure, to investigate the feasibility of this production method. When gas hydrate is brought outside its stability region, hydrate dissociation will occur and continues until a new equilibrium has been established. The production method was therefore based on stepwise pressure reduction once no gas production was observed. A 14 cm long Bentheim sandstone core was positioned between two *Polyoxymethylene* (POM) end spacers and two *Polyetheretherketone* (PEEK) end pieces. Teflon shrink tubing was wrapped around to prevent the CH_4 from contacting the confining liquid. A predetermined amount of 0.1 wt% brine solution was injected at each end to saturate the core, and vacuum was pulled on the inlet and outlet to distribute the water. A 1D profile was taken by the MRI to confirm that the brine distribution was relatively homogeneous. Titanium end caps were then placed at each end, and non-magnetic cobalt screws were used to lock the core holder to the end caps. The MRI high-pressure cell was centered inside the MRI and connected to the confining pump system and the pore pressure pumps. The confining and pore pressure were then incrementally increased to 10.44 MPa and 8.37 MPa, and a 3D MRI image was taken at room temperature. The system was then cooled, and after a couple of hours the temperature at the

core surface was at 4.0 ± 0.1 ºC, well within the CH_4 hydrate stability region. Hydrate growth was now initiated, and both pump logs and *in situ* MRI images were used to monitor the hydrate formation. Once the growth had stabilized and no CH_4 consumption was observed, the pressure was reduced to 4.24 MPa (600 psig) in incremental steps, and at current temperature this was still well within the hydrate stability zone. No hydrate dissociation was observed at this pressure. After the system had equilibrated, the pressure was reduced to 3.96 MPa (560 psig). Once equilibrated, the pressure was further reduced in incremental steps of ~0.07 MPa (10 psi) until all the CH_4 had been recovered. The pumps were set to maintain constant pressure during the production period, and the pumps therefore retracted during the dissociation of hydrate due to the higher concentration of CH_4 in gas hydrate state.

3.3.3 Procedure during CO_2 injection into two longitudinal POM spacers

Injection of CO_2 into gas hydrate deposits has been suggested as a production alternative, where CO_2 provides thermodynamically more stable gas hydrate and induces an exchange process upon which CH_4 is released and made accessible for production (Chapter 1.4.2). To increase the interface between CH_4-hydrate and CO_2, previous experiments have used single longitudinal mechanically fractured cores, where the fracture was kept open by a POM spacer (Husebø, 2008). This is an efficient way to increase the contact area between the two constituents. In this study two experiments were conducted, using the same 10 cm long Bentheim sandstone after comprehensive cleaning. The core had two longitudinal spacings (manufactured fractures), which were kept open by two POM spacers, as shown in Figure 3.6 (spacer information in Appendix B4). With an additional fracture, the contact area between CH_4 hydrate and CO_2 is infectively increased. This was done to investigate if the exchange rate between CO_2 and CH_4 could be increased, which would indicate that some of the limit within this production scheme lies within diffusion of CO_2 through the established CH_4 hydrate. Each of the core pieces were saturated to approximately 57% using a 0.1 wt% and 3 wt% brine solution respectively for the two experiments. The pieces were then assembled with the longitudinal POM spacers and positioned between two POM end spacers and two PEEK end pieces. Teflon shrink tubing was wrapped around these parts in order to prevent the CH_4 from contacting the confining liquid. At this time a 1D profile was taken to confirm approximately homogeneous brine saturation. Titanium end caps were then placed at each end, and non-magnetic cobalt screws were used to lock the core holder to the end caps. The MRI high-pressure cell was centered inside the MRI and connected to the confining pump system and the pore pressure pumps. The confining and pore pressure were then incrementally increased to 10.44 MPa and 8.37 MPa, and a 3D MRI image was taken at room temperature. The cooling system was then turned to 4.0 ± 0.1 ºC in order to bring the core into the hydrate stability region. Hydrate formation was monitored both through CH_4 delivery from the pumps and by loss of MRI intensity, as a result of free water converting into gas hydrates. Once the growth had stabilized and no CH_4 consumption was observed, N_2 gas was flushed through the spacers to remove excess CH_4. The system was then flushed with liquid CO_2, after which CO_2 was used to maintain 8.37 MPa pore pressure. An exchange process now occurred, induced by the increased thermodynamic stability offered by CO_2, where CH_4-hydrate dissociated on micro-scale and was left accessible for production, while CO_2 stabilized the empty water cavities and maintained structure I hydrate. CH_4 diffused and accumulated into the POM spacer, where it was monitored as increase in MRI intensity. Once no change in MRI intensity was observed the fracture was flushed once more with CO_2, and continued CH_4 production was observed.

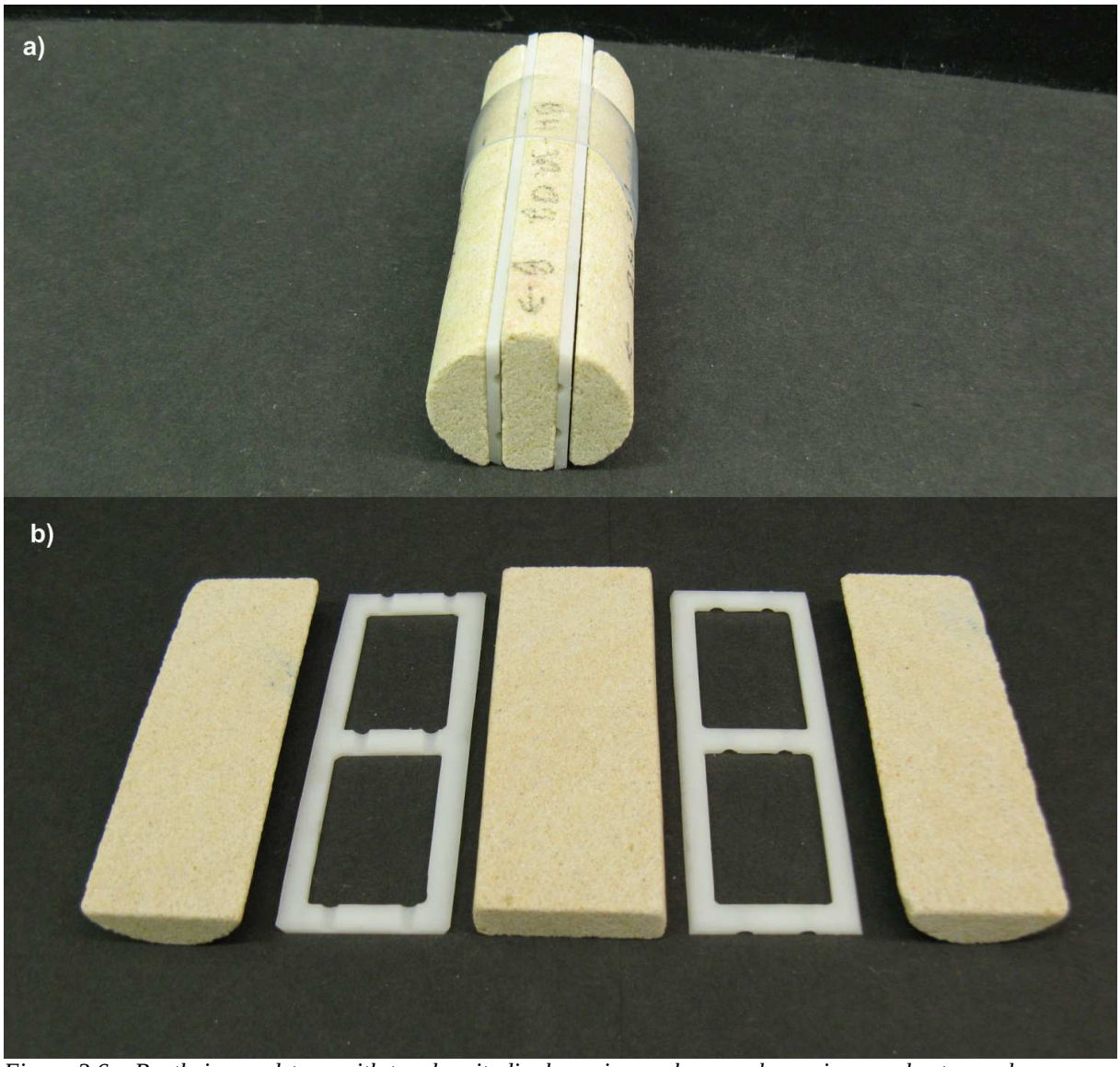

Figure 3.6 – Bentheim sandstone with two longitudinal spacings, where each spacing was kept open by an open POM spacer. a) shows how the core was assembled, while b) illustrates the accumulation volume of the two POM spacers.

3.3.4 Procedure with core partially saturated with hydrate and free water

Access to free gas is often the limiting component during hydrate formation in gas hydrate reservoirs. Initially, the reservoir is completely saturated with water, but due to gas migration from underlying sediments, gas is introduced to the reservoir. Gas hydrates will form if the pressure is sufficiently high and temperature is low, but due to limited amount of guest molecules the hydrates will never completely saturate the porous reservoir. A typical gas hydrate reservoir will thus be partially saturated with gas hydrate and partially with free water. Chapter 1.4.2 discussed injection of CO_2 into CH_4-hydrate as a possible production scheme. Free water, in addition to gas hydrates, are bound to be adjacent to the injection wellbore where CO_2 is introduced to the reservoir. This study was conducted to investigate how free water would respond to presence of CO_2 and how the permeability will evolve during injection of CO_2. CO_2 can stabilize structure I hydrates, and it was therefore expected that the free water would convert into gas hydrates as CO_2 was injected. Two 10 cm long Bentheim cores with 3.73 cm diameter were used during this research. Teflon shrink tubing

was recently discovered to be permeable to CO_2, and the core was therefore wrapped in Saran heavy duty plastic wrapping. The core was then assembled between one POM spacer at the producing end of the core and two PEEK end pieces (Figure 3.7). Teflon shrink tubing was then wrapped around these parts in two layers to prevent the CH_4 from contacting the confining liquid. A specific amount of brine with 0.1 wt% was then injected at the injection end of the core, and water was distributed in the core both through spontaneous imbibition and by applying a vacuum pump. A 1D profile of the core saturated with brine was acquired to assure a relatively homogeneous saturation. Titanium end caps were then mounted at each end, and non-magnetic cobalt screws were used to lock the core holder to the end caps. The high-pressure cell was centered inside the MRI and connected to the confining pump system and the pore pressure pumps. The pressure was increased in incremental steps to respectively 10.44MPa and 8.37MPa. A 3D MRI image was taken at room temperature to get an initial intensity estimate. Cooling was then set to 4.0 ± 0.1 ºC, which is sufficiently cold to provide hydrate stable conditions at 8.37 MPa. Hydrate formation was monitored by PVT data from pump logs and corroborated by MRI data. Water has high density of hydrogen atoms and therefore reveals a strong signal in the MRI. Loss of MRI intensity indicates hydrate formation.

Before hydrate formation was initiated, calculations were made to ensure that at least 25% of the injected water did not convert into hydrates. These calculations were based on data from previous experiments and indicated consumption of 0.00958 moles of CH_4 for each ml of water present. Once target hydrate saturation had been reached, the end spacers were flushed with N_2 to remove excess CH_4 from the spacers, thus limiting further hydrate growth. Soon afterwards, N_2 was injected through the core while a Validyne DP 303 differential pressure transducer was providing pressure data for permeability measurements. One pore volume of CO_2 was flushed through the core at constant rate of 0.5 ml/hour, during which CO_2 hydrate formed. Once one pore volume had been injected, CO_2 was injected at several different rates to provide endpoint permeability readings. CO_2 was used to maintain pressure at the end of the test, where an intensity build-up was observed in the POM spacer, indicating an exchange process between the initial CH_4 hydrate and CO_2.

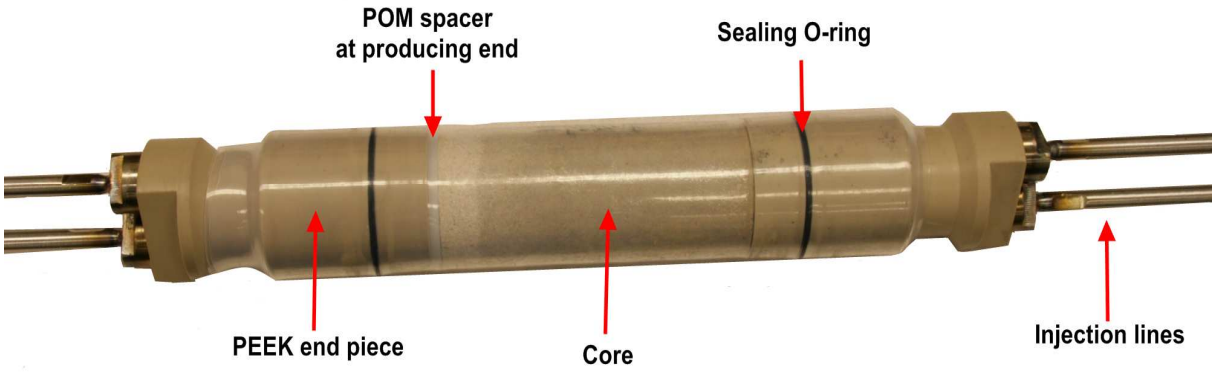

Figure 3.7 – Core assembled between two PEEK end pieces, wrapped in Teflon shrink tubing. The core displayed in the figure is being saturated with brine, where the water is imbibing towards the left side (producing end) of the core.

Chapter 4

Experimental Results and Discussion

A series of experiments have been performed to investigate properties of gas hydrates and hydrate formation, as well as different production schemes of gas hydrates in porous media. Salinity impacts on hydrate growth pattern and induction time has been a major part of the experimental work presented in this thesis. CH_4 production from CH_4-hydrates has been studied through both depressurization and injection of CO_2 to establish the feasibility of the production methods. Research on gas production schemes from hydrates is important to establish the resource potential of gas hydrates. This chapter will cover the results and discussion of the experiments.

4.1 Salinity Impacts on Hydrate Growth and Induction Time

Salt affects the thermodynamic stability of gas hydrates (Chapter 1.1.9), where water of sufficiently high salinity will prevent hydrate formation. Salinity is therefore an important parameter when estimating the amount of natural gas hydrate available. For lower brine salinity, the extent of inhibition is reduced but will still affect the hydrate growth and induction time. During hydrate formation only water and gas is consumed in the hydrate crystal, resulting in displacement of salt previously bound to the water. A salinity gradient will therefore be present at the hydrate formation front, where the salt concentration will increase as gas hydrates form. Further hydrate growth will be inhibited once the salinity is sufficiently high and the thermodynamic conditions for hydrate formation have been altered. According to calculations with CSMGem (Sloan and Koh, 2008), the brine salinity that prevents hydrate from forming is 14 wt% for sodium chloride (NaCl) solution. CH_4 hydrates were formed on several occasions in this study with different brine solutions to investigate how differences in salt concentration influenced both the induction time and the amount of hydrate formed during the growth period. *Fill fraction* was used to classify hydrate growth, and was defined as the amount of CH_4 in the hydrate relative to the theoretical amount of structural cages capable of holding a CH_4 molecule, if all of the accessible water was part of the hydrate structure. The fill factor for structure I is reported as eight gas molecules per 46 water molecules, but the gas hydrates are nonstoichiometric and may have some vacant cavities. In other words, 8/46 is not a fixed constant. Variations in this constant will compromise the calculations used during this data analysis, where a lower hydrate number would result in a fill fraction lower than 1.0. In this study 100% cage filling was assumed, with consumption of 8 gas molecules per 46 water molecules. Previous experimental results at the experimental conditions used in this thesis have shown a cage-filling of approximately 90%, thus reducing the gas to water ratio to 7.2/46 (Ersland, 2009). Circone et al. (2005) conducted a series of experiments on cage filling for CH_4 hydrates and reported a hydrate stoichiometry of n_w = 5.81-6.10 H_2O, with an average composition $CH_4 \cdot 5.99(\pm 0.07)H_2O$. This

corresponds to 7.7/46, and is not too far from the assumed 8/46 gas/water molecular ratio. Previous results and work have been presented by Husebø et al. (2008a).

4.1.1 Salinity impacts on hydrate growth

Hydrate growth period in these experiments is defined as the period during which detectable hydrate formations is observed. It has been established in previous experiments (Husebø et al., 2008a) that salinity impacts the growth pattern of gas hydrates; however, these experiments did not consider the effect of higher salinities. Six different cores were used for the experiments conducted in this thesis (H15-H20) and core data are given in Appendix B5. All cores were prepared according to the procedure discussed in Chapter 3.3.1. Once the system had been pressurized and cooled to hydrate stable conditions, gas hydrate formation initiated. Figure 4.1 illustrates a typical pump log curve for this process. At 0 hours the core was at room temperature and had already been pressurized to 8.37 MPa. At a) the system was kept at room temperature to allow for an estimate of the leakage rate. At b) cooling was initiated, which resulted in increased gas density with subsequent CH_4 injection from the pump to maintain constant pressure. This is illustrated in Figure 4.1 by the CH_4 consumption increase from 0 to 5 ml. After hydrate stable conditions were reached no additional CH_4 consumption was observed due to the induction time of the system. At c) the induction time concluded and steady growth was initiated, which resulted in exponential consumption of CH_4. The last 24 hours of the experiment were used to make an additional estimate of the leakage rate. A number of salinities were investigated, and the difference in hydrate formation rate can be seen in Figure 4.2. The induction time is excluded from this plot and will be discussed in detail later in Chapter 4.1.3.

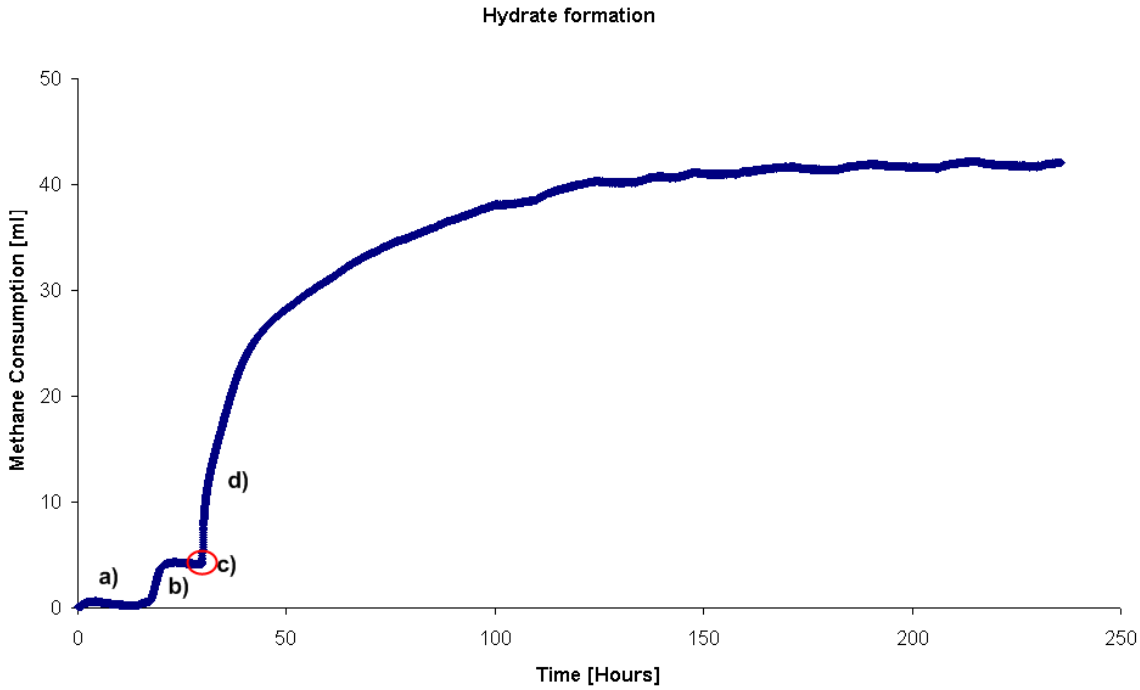

Figure 4.1 – CH_4 consumption during various stages of hydrate formation. To the left of the figure the system has already been pressurized to 8.37 MPa, and a) represents the pre-cooling period that allows the system to stabilize. This period is used to make a preliminary estimate of the leakage rate. At b) the system starts cooling, resulting in increased gas density, and the pumps therefore deliver gas to the system to maintain constant pressure. At c) the induction time comes to an end (marked with a red circle), and at d) steady growth takes place and continues until lack of available host molecules (water) or guest molecules (CH_4).

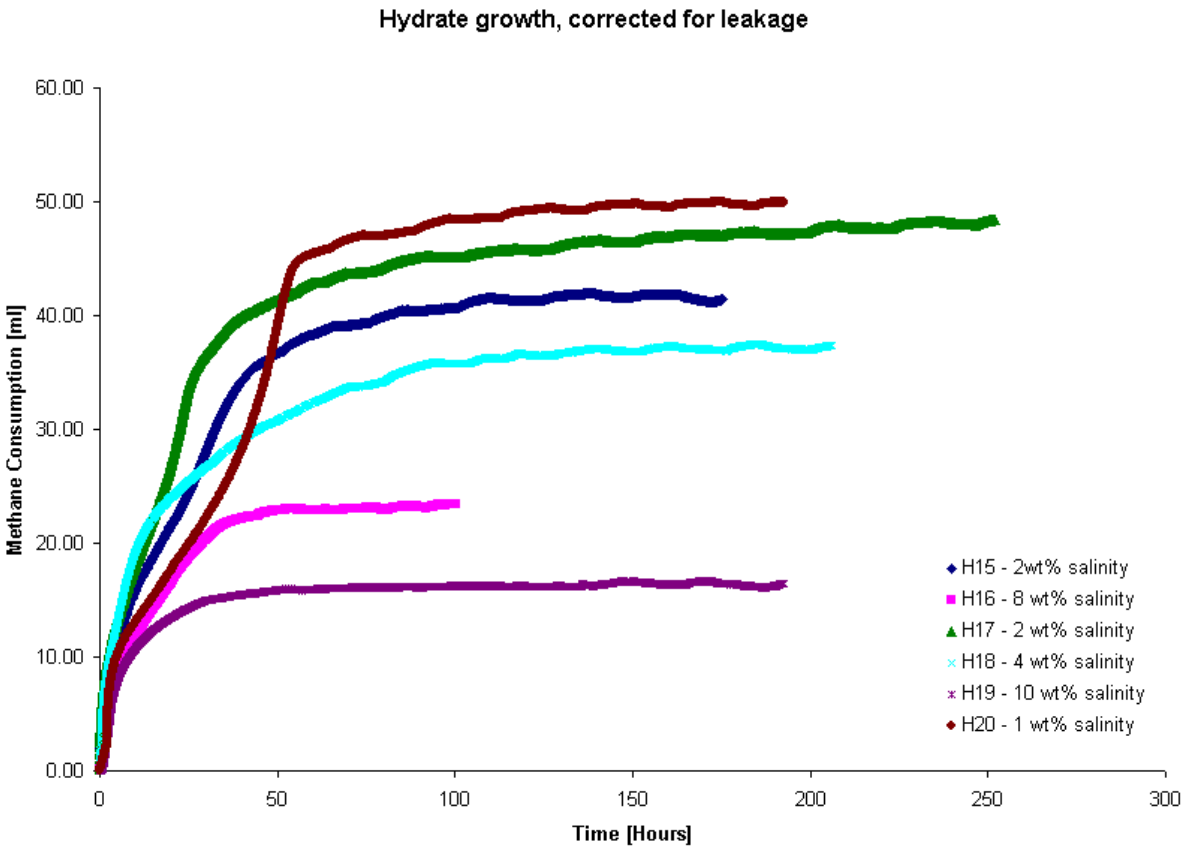

Figure 4.2 – CH_4 consumed during hydrate growth. The experimental results presented in this figure do not consider small differences in core length and brine saturation. This figure merely considers CH_4 consumption during the growth period for the different experiments.

Most curves in Figure 4.2 followed the same exponential pattern with high initial CH_4 consumption which decreased with time, and it is easily observed that the total consumed CH_4 was higher for the lower salinities. When 1 wt% salinity was used, 50 ml CH_4 was consumed (at 8.37 MPa and 4 ºC), while for the 10 wt% salinity experiment only 16 ml was consumed. Salinity impacts on fill fraction will be discussed in Chapter 4.1.2, where differences in core length or differences in moles of water present will be emphasized.

Variations in hydrate growth pattern

Sample H20 constituted an anomaly to the other exponential hydrate growth patterns in Figure 4.2. This core was saturated to nearly 60%, which is higher than the other cores, and as such the difference in growth pattern might indicate that the hydrate growth is affected by initial water saturation. Higher water saturation results in less surface area between water and gas. It also leaves less pore space available for the CH_4 to occupy with a subsequent reduction in relative gas permeability. These two factors may contribute to the reduction in initial hydrate formation rate. It is interesting to note that the CH_4 consumption rate is reduced after only 6 hours, but increase again after approximately 35 hours. At 57 hours, the consumption rate suddenly leveled out. During the experiment CH_4 diffuses through the core, resulting in a more even distribution, which may help explain the increase in CH_4 consumption due to the increased interface between gas and water.

4.1.2 Variations in fill fraction as a function of salinity

In structure I hydrates the gas/water molecule ratio is 8/46, meaning that there are eight cavities within the lattice of 46 water molecules capable of encapsulating a gas molecule. The *fill factor* is defined as the ratio of filled cavities in the structure, so if all of the cavities on the structure are occupied by a hydrate former, the fill fraction will be 1.0. The experiments presented here are performed without any *in situ* imaging, so the fill fraction is calculated under the assumption that all of the water has converted to hydrate and the consumed CH_4 is occupying hydrate structural cavities. These calculated fill fractions are presented in Appendix B5 and visualized in Figure 4.3, where the fill fractions are plotted as a function of salinity. The distribution of fill fraction follows a clear decreasing trend with increased salinity and seems to align along the theoretical red line based on theoretical calculated values using CSMGem. All experimental values align with the red line within a 14% deviation; however, most values are within ±7% of the theoretical value. The fill fraction therefore shows a clear dependency on the salinity of the accessible brine. Salinity is important when estimating available CH_4 in hydrate reservoirs, where salinity measurements of brine adjacent to gas hydrate deposits may help identify the size of the gas hydrate deposit.

Several points are located above the theoretical red line, which could indicate that the gas leaks adjusted for during calculations are more extensive than first assumed. An initial gas leak estimate is made prior to hydrate formation and compared with a gas leak estimate from the last 24 hours after hydrate formation. The last estimate is often what makes the foundation for the gas leak estimate. If the gas leakage rate was to evolve and fluctuate during hydrate formation, it would be impossible to detect. This could help explain why some of the data are above the red line. The final gas leak estimate may have been compromised due to the fact that gas hydrates are solids which obstruct gas flow, thus reducing the leakage rate during the time of the experiment. However, the accordance between the theoretical red line and the experimental values is still good, and the overall conclusion is that there is a clear dependency between fill fraction of CH_4 hydrates and salinity.

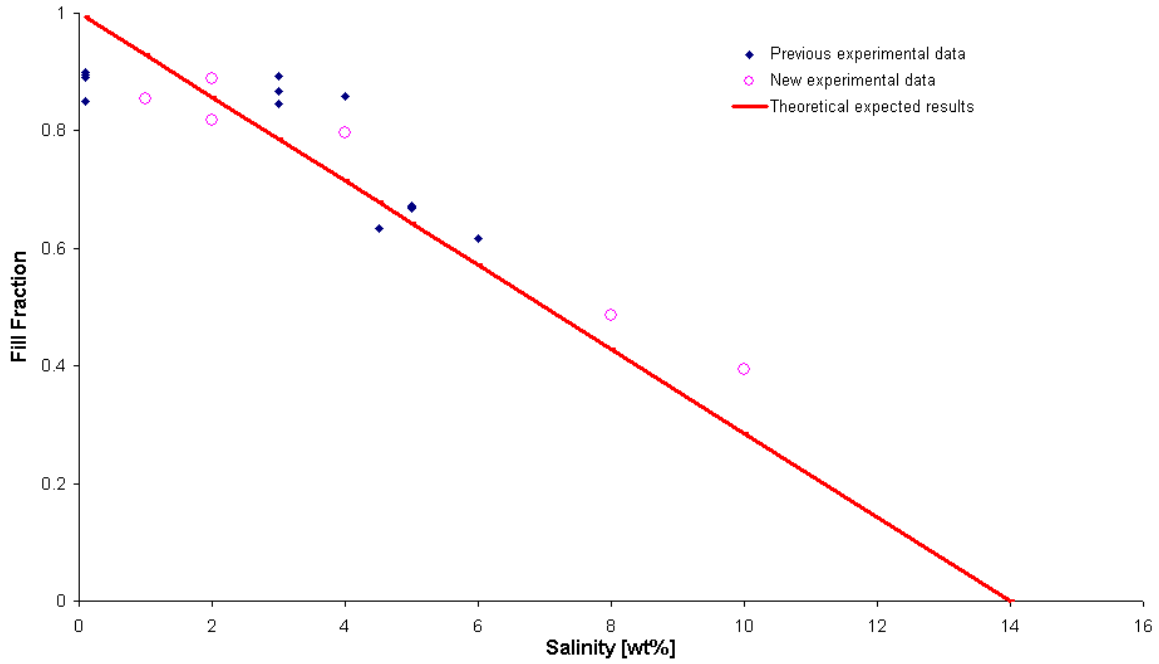

Figure 4.3 – Fill fractions from the different samples plotted as a function of salinity. The blue squares are previous data (Husebø, 2008, Ersland, 2008), while the red line is based on simulated results from CSMGem. The pink open circles are data acquired during this thesis, and the data seem to align along the simulated line.

There is a theoretical limitation to the assumption basis for calculating the fill fraction for these experiments. The assumption is that all the water is included in the hydrate structure. This means that a fill fraction of one is impossible to reach if there is residual water in the core after hydrate formation. The Bentheim sandstone is a strongly water wet porous media (Graue, 2009). Experiments have shown that hydrate formation in highly water wet cores occurs in the middle of the porous media (Kleinberg et al., 2003), and capillary forces will prevent hydrate formation in capillary bound water (Clennell et al., 1999). Hydrate growth will therefore never occur in small pores due to extensive capillary forces, and water in these pores will not contribute to form cavities that encapsulate the gas molecules. As a result of this, the calculated fill fraction will never be 1.0. Even for low salinities, between 0.1 and 4.0 wt% salinity, the fill fraction never exceeded 0.9, but remained stable between 0.8 and 0.9. This may indicate that the fill fraction is reduced by approximately 0.1 due to the capillary nature of the core. Another interesting observation is the lack of salinity impacts of low salinities. Only after the salinity concentration has exceeded 4 wt% does the salt seem to inhibit gas hydrate formation. A plausible reason for this could be that the effect of the capillary forces outweighs the negative influence of the salt for lower salinities, and during hydrate formation the salt is displaced and elevates the salinity of the remaining water. At higher salinities, the thermodynamic stability is reduced and the influence of salt on hydrate growth is inevitable. The effect causing this decrease in fill fraction is only speculation and is not quantifiable in either of the setups used in this study.

During hydrate formation, gas permeability is reduced in an effective manner, thus reducing the gas flux to parts of the core. In some cases, the gas hydrate may block pore-throats, and gas can only access the blocked area by diffusion through the limited water layers between mineral surfaces and the gas hydrate (Kvamme, 2006). These occlusions may reduce CH_4 consumption if gas is restricted from accessing free water due to extensive hydrate blocking of pores.

The fill fraction results show clear dependency on the salinity of the accessible brine and results acquired through this study corroborates previous work (Husebø et al., 2008a). Husebø et al. (2008a) used *in situ* MRI on some experiments to monitor the progression of hydrate formation, and concluded that the hydrate formation rate was more affected by initial brine distribution than salinity. This was not quantified in this study due to lack of imaging possibilities; however, the results show consistency considering the fact that experiments have been conducted using different setups. Some of the data on Figure 4.3 seem ambiguous, especially values for 2, 3 and 4 wt% salinity. However, the deviation from the average value for these data is less than ±4%. The deviation of the three data points at 5 wt% is ±0.15%, indicating excellent reproducibility.

4.1.3 Salinity impacts on induction time

Salt ions change the chemical potential of liquid water and therefore act as a hydrate inhibitor (Chapter 1.1.8). Even though the induction time is a stochastic variable (Chapter 1.1.9), it is expected to increase with increasing NaCl concentration due to its hydrate inhibitor effect. In this work, induction time is defined as the period from hydrate stable conditions were reached until stable hydrate growth was initiated. This was easily observed from PVT data. Figure 4.4 visualizes the induction time for experiments conducted in this study, and the added exponential trend line provides a fit with R^2 = 99.53%. It is unlikely that the fit would be maintained if several data points were added. The graph only contains values from the six experiments from this study, which is not adequate to conclude with scientific precision; however, it clearly indicates that increased salinity increases the induction time. Previous researchers report very stochastic behavior of induction time (Husebø, 2009). It would have been interesting to run experiments using even higher salinities to investigate at what salinity hydrate formation was prevented. On the other hand, if the added trend line should in fact provide a sufficient fit, the expected time for hydrate formation to occur using 14 wt% salinity would be nearly 5000 hours. The induction time span in these experiments was from approximately 1 hour at 1 wt% salinity to 371 hours at 10 wt% salinity.

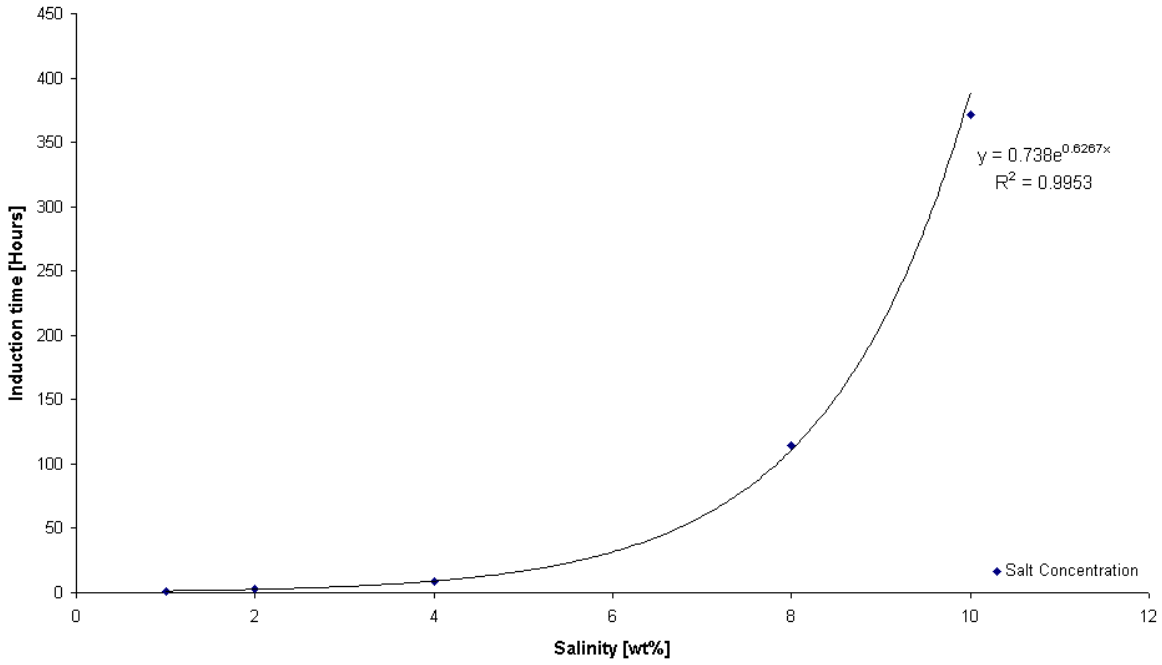

Figure 4.4 – Induction time as a function of salinity, where the two data points at 2 wt% salinity coincide. The added trend line provides a great fit, but the data points are too few to decide on an exponential relationship between induction time and salinity.

4.2 Production from CH_4 Hydrates through Depressurization

Production through depressurization is considered by many the most economically feasible gas hydrate production method (Chapter 1.4.1) and involves pressure reduction to a pressure below the hydrate dissociation threshold at the prevailing local temperature (Zhou et al., 2009). In particular, this production method is promising in *Class 1* deposits, containing either gas hydrates and free water (*Class 1W*) or gas hydrates and free gas (*Class 1G*). In these classes, depressurization-induced dissociation is predicted to result in production of large volumes of gas at high rates over a long period of time (Moridis et al., 2007, Moridis and Kowalsky, 2006). Depressurization tests and gas production by pressure depletion has been conducted on several hydrate deposits to determine their resource potential (Moridis et al., 2008). Gas production through depressurization was investigated in this study on Class 1G hydrate deposits, where all the water was assumed converted into gas hydrates with only free water and CH_4 hydrate left in the core. This represents an ideal hydrate production scenario, where free gas will provide additional recovery to the released CH_4 from gas hydrates. The depletion was based on constant pressure, where pressure was decreased in incremental steps once no dissociation was observed. This process was repeated until no further production was observed. Experimental data from this experiment can also be found in a previous publication (Husebø et al., 2008b).

4.2.1 CH_4 hydrate formation

CO_2 injection into CH_4-hydrates, taking advantage of the implicit CO_2 sequestration, has been the main focus on gas production from hydrates at the University of Bergen. To compare the gas production efficiency it is beneficial to have other production methods to compare to. The efficiency of gas production from hydrates through pressure depletion was tested in a depressurization experiment. CH_4 hydrates were formed in a 14 cm long whole Bentheim core, which was saturated to approximately 50% and assembled as described in Chapter 3.3.2. Hydrate formation was monitored by PVT data in conjunction with *in situ* MRI images. Figure 4.5 compares normalized inverted data from the MRI with normalized data from the pump logs. The correlation between the two curves confirms the advantage of using MRI to monitor changes in hydrate saturation in the porous media.

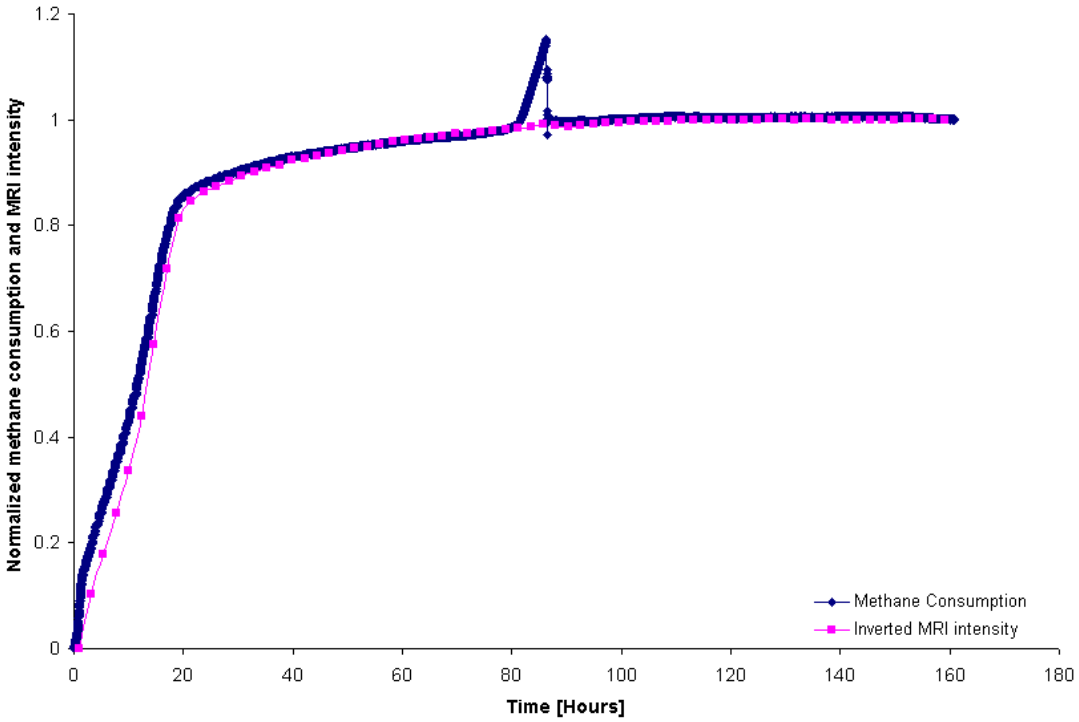

Figure 4.5 – Comparison between normalized CH_4 consumption (material balance) and normalized inverted MRI intensity of free water during hydrate formation. The spike in the CH_4 data is due to loss of confining pressure.

Confining pressure was temporarily lost after 81 hours due to problems with the confining pump, which resulted in a pressure drop in confining pressure to just below 8.37 MPa. This could have resulted in gas leaking into the confining liquid, considering that the pore pressure was maintained at 8.37 MPa. However, the Aflas^{TM} sleeve stayed in place, and once confining pressure was increased the CH_4 consumption stabilized at expected value. The spike in Figure 4.5 was a result of confining liquid no longer providing pressure on the sleeve, thus allowing gas to accumulate between the core and the spacer. Despite the addition of gas to the system the MRI intensity did not seem to change notably. As previously mentioned, CH_4 gas is less hydrogen dense compared to water and does not influence the MRI intensity as effectively as water. The bulk gas mainly accumulated between the core and the spacer. This area was therefore not included as a region of interest in the ROI software.

Once hydrate had stopped forming (at 8.37 MPa), the pore pressure was reduced in incremental steps to 4.24 MPa (600 psig). At current temperature, 4 ºC, this was still within the hydrate stability region. After the system had equilibrated, the pressure was reduced to 3.96 MPa (560 psig), and at this point some of the hydrate did dissociate (Figure 4.6). Upon equilibration, the pressure was decreased once more to 3.89 MPa (550 psig), resulting in far more substantial production. At 3.82 MPa (540 psig) even more gas was produced. The production is also visualized in Figure 4.7, where *in situ* MRI images revealed increased intensity from free water as the gas hydrate dissociated.

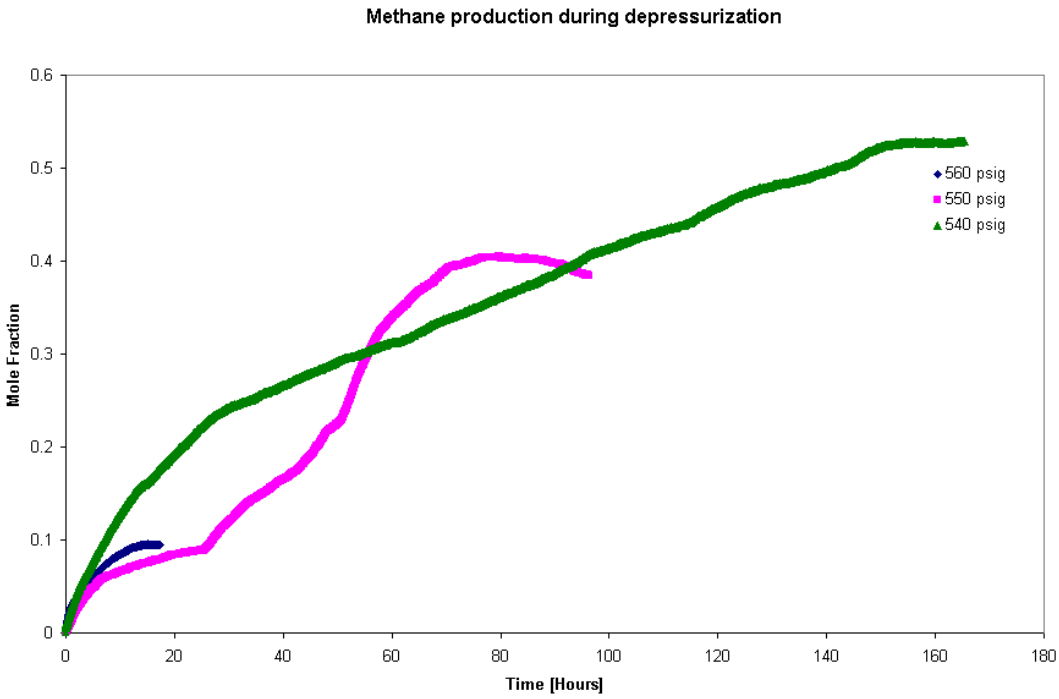

Figure 4.6 – CH_4 production from the gas hydrate during depressurization at different pressures. Production was converted into moles to consider differences in density at different pressures and then plotted as mole fraction by normalizing to moles of CH_4 originally converted into hydrates.

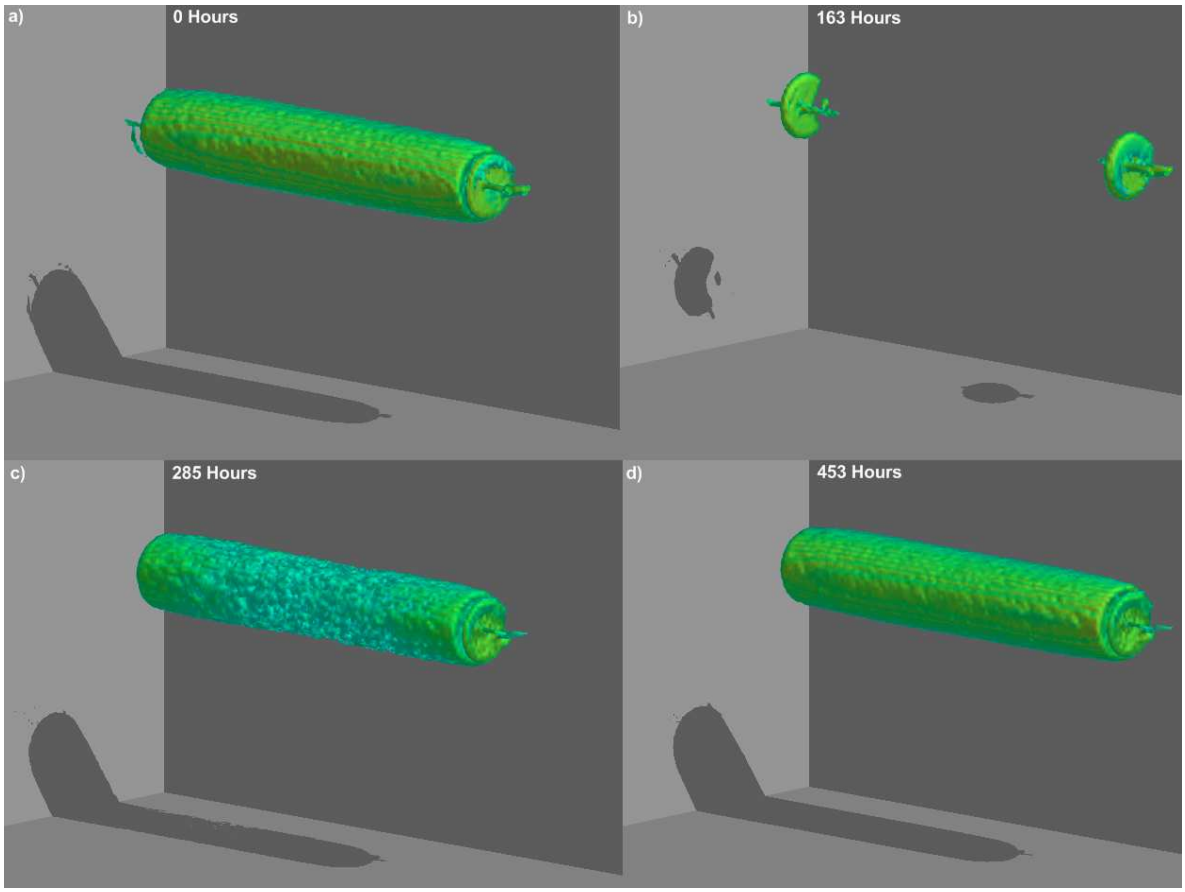

Figure 4.7 – Visualization of changes in MRI intensity during hydrate formation and dissociation using T3D©Fortner Research, LLC: a) 2 hour 3D image taken prior to cooling and hydrate formation, b) 2 Hour 3D image taken after hydrate formation, c) 2 hour 3D image at 3.89 MPa, d) 2 hour 3D image at 3.82 MPa. The water signal reappears as hydrate dissociates.

4.2.2 Gas production through depressurization at constant pressure

No gas hydrate dissociation was observed at 4.24 MPa and pressure depletion was continued to 3.96 MPa. The pressure gradient and gas production at this point was low due to high hydrate saturation (61.7%) with subsequent low relative gas permeability. Only 9% of the CH_4 hydrate dissociated during the time the system was kept at 3.96 MPa, which is illustrated in Figure 4.6. When no further gas hydrate dissociation was observed, the pressure was reduced to 3.89 MPa. 20 hours through production at 3.89 MPa the gas production rate seemed to be leveling out; however, at 25 hours a sudden increase was observed in the production rate. Gas hydrate is a solid state material and will restrict fluid flow throughout the media. Almost 20% of the gas hydrate had dissociated at 25 hours, which apparently was sufficient to increase the relative permeability of CH_4. Production at 3.89 MPa was continued for approximately 70 hours. During that period, the dissociation reached a maximum after 80 hours, with a mole fraction of 0.4, but steadily decreased and equilibrated at 0.38 after 96 hours. At this point 47% of the hydrate had dissociated. The reduced hydrate saturation resulted in efficient recovery at 3.82 MPa, where the additional 53% gas hydrate was dissociated. Full recovery was achieved approximately 280 hours post hydrate formation.

Hydrate formation is an exothermic reaction, while hydrate dissociation is an endothermic reaction. Heat is required in an endothermic reaction, and gas production by pressure depletion will induce cooling of the hydrate reservoir. The rate of hydrate dissociation is therefore controlled by the conductive heat flow, where lack of conductivity may result in regained hydrate stability. If the reservoir is sufficiently cooled, free water may even turn into ice, thus complicating the production severely. At 3.89 MPa the curve did not equilibrate once maximum dissociation was reached, and the CH_4 loss could be explained by hydrate reformation due to lack of heat conductivity. Temperature readings at the core surface were provided by a single thermocouple and did not indicate any temperature below 3.8 ºC. Presence of a temperature gradient over the core is therefore the only possible explanation to support hydrate reformation. However, confirmation of such is not possible due to a single thermocouple providing temperature readings. Only small amounts of CH_4 were produced at 3.96 MPa, despite the fact that the gas hydrate was outside its stability region. At 4.24 MPa the system was still within the hydrate stability region, and the pressure drop to 3.96 MPa is not significant. It is therefore likely to assume that the CH_4 hydrate is within the metastable region at 3.96 MPa and the CH_4 hydrate is therefore more susceptible to minor PVT changes. A small temperature drop induced by the dissociation may provide temporary stability, thus altering the dissociation. These results are also presented by Husebø (2008), where an additional depressurization test was run using the same conditions as in this test. It is interesting to note that for 3.89 MPa the CH_4 production curve experienced the same drop in production from a maximum at approximately 0.4 (mole fraction) to a lower endpoint maximum. The reason for this is still unaccounted for, but due to the reproducibility of the result it would be interesting to run yet another test with additional thermocouples.

Gas production through depressurization induced hydrate dissociation may result in production of associated water (Chapter 1.4.1). This is one of the major problems with this production scenario. Water was detected in production lines post depressurization in this experiment, but due to limitations in the experimental setup there was no way to quantify the amount of produced water. Loss of geomechanical stability is another limitation with this production method. Bentheim is a consolidated sandstone not likely to be compacted or deformed, despite of large differential pressures over the core. This may not be the case for other porous rocks saturated with gas hydrates. Mallik has been subject to extensive research and several gas production tests have been performed at this site. Production from this field seems promising, however, problems with sand production have been reported (Numasawa et al., 2008). This is a frequent problem during production, and to simulate this in a future experimental production scenario it could be interesting to produce from gas hydrate formed in sand packs or other unconsolidated rocks.

Gas production through pressure depletion is considered an effective production method of gas hydrates. In this test, full recovery was achieved after a short period of time (approximately 280 hours). Depressurization induced gas production from CH_4 hydrates therefore provides promising results. Some associated water was experienced during production and is considered one of the major problems with this production method. Simulations of large scale production over a longer period of time reported a recovery of 54% from the gas hydrate itself, with additional production from free gas in the reservoir (Moridis et al., 2007). In a large scale reservoir CH_4 production from gas hydrate will evolve differently than compared to small experimental scale and providing a pressure drop over the whole reservoir is more challenging. However, especially Class 1G hydrate deposits with low supercooling in metastable hydrate region may be a promising production target for this

production scheme. The time frame for the simulation was 30 years, while the production in the experiment only lasted for approximately 280 hours.

4.3 Results from CO_2 Injection into Core with Open Fractures

CO_2 provides thermodynamically more stable gas hydrate than CH_4 at the experimental conditions used in this thesis (Chapter 1.4.2). Injection of CO_2 into established CH_4-hydrates will therefore induce an exchange process where CH_4 is released and made accessible for production, while CO_2 maintains the stability of the structure I hydrate. Currently, no reservoir scale production tests with CO_2 injection are known, but several experiments give support to the production method (Lee et al., 2003). Using a greenhouse gas for sequestration offers an attractive potential for CO_2 storage in addition to gas production. The thermodynamic stability of the gas hydrate is also increased, thus preventing possible massive hydrate dissociation with subsequent slope failure. Several CO_2 injection experiments have been conducted at the University of Bergen and at ConocoPhillips' Research Center in Bartlesville, looking at possibilities for CH_4 production through CO_2 sequestration. The results have generally been good, and total recovery has been estimated to 50-85% (Husebø, 2008). It is assumed that some of the limitation within this production method lies within kinetics and/or the diffusion rate of CO_2 through the established CH_4 hydrate. In this study, the contact area between CH_4 hydrate and CO_2 was effectively increased, and increased gas recovery may indicate limitations within diffusion rate. Two similar experiments were conducted on this matter and are presented in this chapter. However, the experimental work was not a part of this thesis, only the analysis.

4.3.1 Hydrate formation in a fractured core

Previous gas production from gas hydrates by injection of CO_2 have used either whole cores (Ersland, 2009) or single fractured cores (Graue et al., 2006b), where the fracture was kept open by a POM spacer. For this study, a Bentheim sandstone core was mechanically fractured twice in the longitudinal direction, separating the core into three different pieces (Figure 3.6). Each fracture was kept open by a POM spacer, and in addition cylindrical POM spacers were located at the two ends of the core. The purpose of the POM spacers is to provide efficient fluid flow through the core, while increasing the interface between CH_4 hydrate and CO_2 during CO_2 injection. Increased contact area between CH_4 hydrate and CO_2 may speed up the exchange process. The POM spacers also provided accumulation volume for the released CH_4 and were monitored *in situ* by MRI. MRI intensity is proportional to CH_4 concentration, and the data can be quantified to give information on the produced mole fraction. Through this experiment it will be possible to investigate to what extent diffusion of CO_2 limits the exchange rate.

4.3.2 Monitoring hydrate formation and the exchange process

CH_4 hydrates were formed in a 10 cm long whole Bentheim core, which was saturated to approximately 57% and assembled as described in Chapter 3.3.3. Hydrate formation was monitored by PVT data in conjunction with *in situ* MRI images. Figure 4.8 compares normalized inverted data from the MRI with normalized CH_4 consumption (material balance). The correlation between PVT data and MRI intensity from free water confirms the advantage of using MRI to monitor changes in hydrate saturation in the porous media, and also confirms the reliability of PVT data.

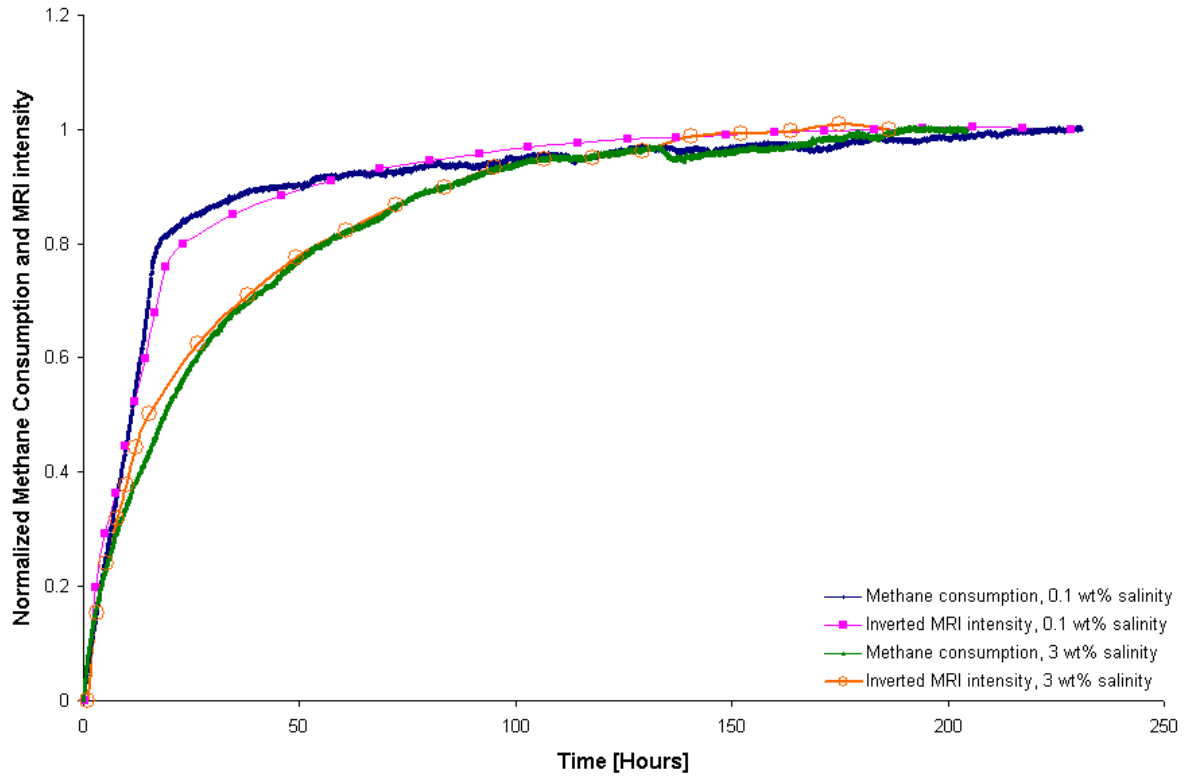

Figure 4.8 – Gas hydrate formation data from two different experiments using different brine salinity solutions on a fractured Bentheim core. Normalized CH_4 consumption data is corroborated by normalized inverted MRI intensities from free water.

4.3.3 CH_4 production during CO_2 injection

The CH_4 hydrate formation and CO_2 exchange process is visualized in Figure 4.9, and as expected the free water MRI intensity decreased as the sample was cooled and hydrate stable conditions were reached. At 0 hours the core is partially saturated with brine and pressurized to 8.37 MPa by CH_4 at room temperature (20 ºC). At 238 hours all the water was confirmed converted into CH_4 hydrate, and at 273 hours N_2 was flushed through the spacers to remove excess CH_4. CO_2 was then introduced to the system. The immediate result was loss of MRI signal because CO_2 contains no hydrogen and is therefore insensitive for magnetic resonance. CO_2 provides thermodynamically more stable gas hydrates and induces a micro scale CH_4 hydrate dissociation with subsequent stable CO_2 hydrate and free CH_4 gas that is accessible for production. This CH_4 mainly accumulated in the designated POM spacer. At 629 hours CH_4 had accumulated into the spacer due to the exchange process between the established CH_4 hydrate and the injected CO_2. At 645 hours CO_2 had been flushed through once more to remove produced CH_4 and at 957 hours additional produced CH_4 had accumulated in the spacer. Previous experiments within the group have shown a linear relationship between CH_4 concentration and MRI intensity (Appendix B6), thus, if compared to an image 100% saturated with CH_4 it is possible to quantify the molar fraction of CH_4 in the spacer. Substantial CH_4 production into the POM spacer was observed for both experiments. No intensity increase is observed from matrix, which indicates a direct conversion from CH_4 hydrate to CO_2 hydrate without detectable hydrate dissociation. Some small hydrate dissociation is likely to occur, but the general stability of the gas hydrate is maintained. The CH_4 accumulation in the spacer was significant; however, presence of a spacer does not guarantee accumulation specifically here. During the exchange, it is likely that CH_4 diffuse into the injection line. The injection line is connected to an “infinite” reservoir of CO_2 that

provides constant pressure and some CH_4 may actually diffuse into the pump cylinder. However, it is likely to assume that there will be a CH_4 gradient in the line and the mole fraction of CH_4 in the pump cylinder is therefore highly restricted. In addition, there is a temperature gradient in the line resulting in decreased gas density adjacent to the pumps. The CH_4 concentration gradient is not known and the exact amount of produced gas during the exchange process is therefore unknown. In addition, the free CH_4 present in the porous media prior to the CO_2 flush will contribute to increased recovery, thus compromising the actual recovery. In order to determine the actual CH_4 gradient several gas chromatography (GC) samples would have to be taken from different parts of the setup. This was not done and it is therefore not possible to quantify the amount of CH_4 diffused into the lines. Results acquired during the exchange process are therefore solely based on CH_4 accumulation in the spacer.

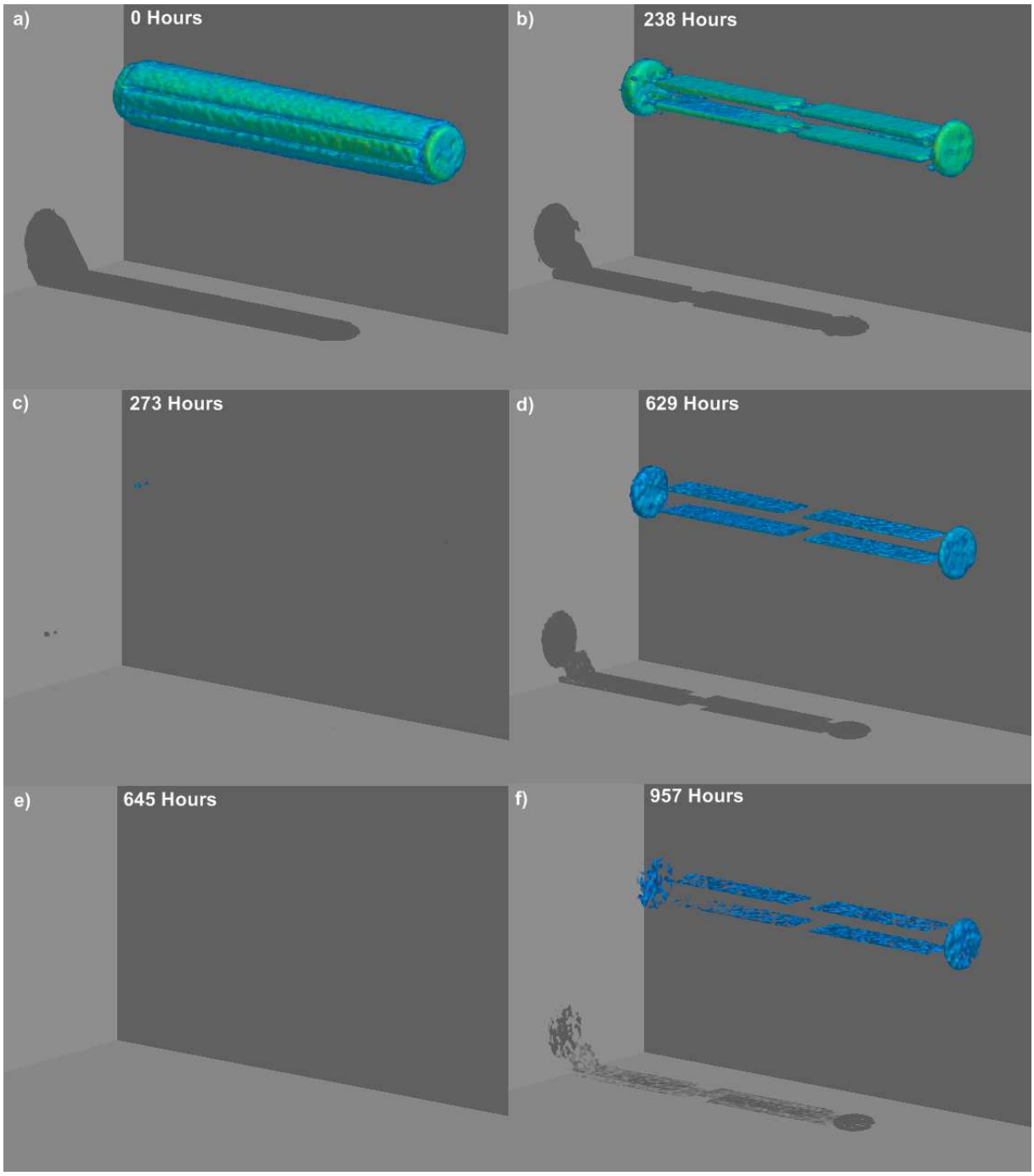

Figure 4.9 – Visualization of MRI signal from 0.1 wt% salinity test using T3D©Fortner Research, LLC: a) 9 hour 3D image prior to cooling and hydrate formation, where water and CH_4 was present at 8.37 MPa in the porous media and in the POM spacer, b) 9 hour 3D image after hydrate formation. The only visible signal left from the core is gas present in the spacers in the middle and at the end of the core, indicating that CH_4 hydrate had successfully been formed in the porous media, c) 9 hour 3D image post CO_2 flush, which should have removed all excess CH_4 from the spacers. Some signal is still visible from the end spacer, which may be some CH_4 left in the system or CH_4 produced during the time period of the image, d) 9 hour 3D image post CO_2 exchange with CH_4 hydrate resulting in produced CH_4 into the spacers, e) 9 hour 3D image post yet another CO_2 flush removing all produced CH_4 from the spacers, f) 9 hour 3D image showing more CH_4 produced during CO_2 exchange.

Figure 4.10 shows the development of CH_4 accumulation in the spacer. The intensity increase during the first hours is substantial, but the additional contribution decrease with time. This is due to decreasing chemical potential as CO_2 concentration is decreasing and CH_4 concentration is increasing. The effect of the first flush is more comprehensive than the second. The concentration of CH_4 hydrate is higher at the initial flush, which will make the flush more effective. During the second flush the CO_2 has to diffuse through established CO_2 hydrate in order to access the CH_4 hydrate. However, the effect of the second flush is significant as well, which may indicate high reactivity. It is therefore likely to assume that some CH_4 may have been released and displaced into the receiving pump cylinder during the CO_2 flush itself. If this is true, the mass balance in the system is not maintained, and the actual production recovery is higher than illustrated in Figure 4.10.

N_2 was injected prior to the CO_2 injection to remove excess CH_4. In Chapter 4.4 it will be established that N_2 alters the equilibrium of the CH_4 hydrate, thus resulting in preliminary CH_4 hydrate dissociation. Considering the effect of N_2, it is likely to assume that some CH_4 hydrate dissociated and free gas accumulated in the POM spacer before the CO_2 flush was initiated. CO_2 was then flushed through the system to remove N_2, but due to hydrate dissociation, some CH_4 is likely to have been displaced in this flush as well. The mass balance is therefore altered and the current moles of CH_4 in hydrates are less than initially. Mole fraction was used to determine the efficiency of the production method and due to less CH_4 available the recovery will never be 100%.

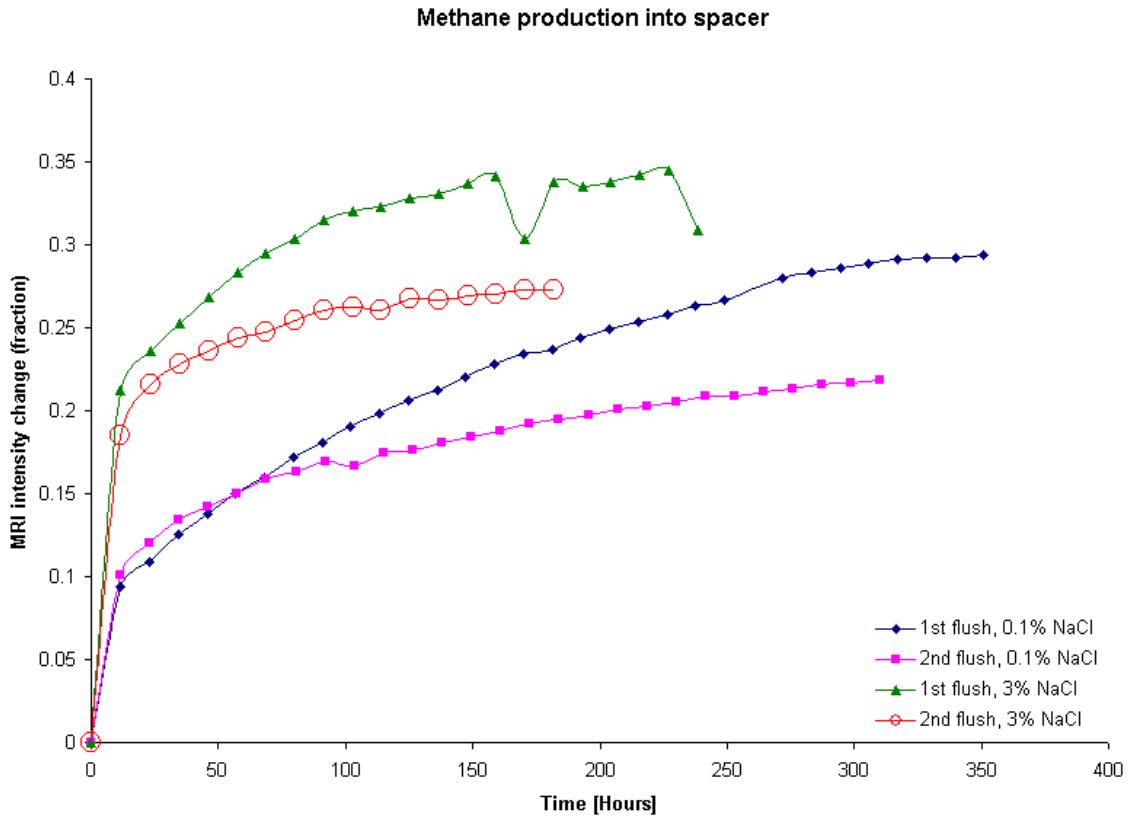

Figure 4.10 – CH_4 build-up in the POM spacer due to the exchange process with CO_2 resulting in increase of MRI intensity for the two experiments. The MRI intensity is an average from the longitudinal spacers, and is normalized to a spacer 100% filled with CH_4. The intensity increase during the first hours is substantial, but the rate slowly decreases. The first CO_2 flush results in higher intensity buildup, yet the second flush is very effective as well. The actual recovery is most likely higher but is not measureable due to diffusion into pores and lines. In addition some CH_4 may be produced during the CO_2 flush which is accumulated in a receiving cylinder and therefore not detected by the MRI.

Salinity impact on recovery

Figure 4.10 compares the result acquired for the two experiments, and it is evident that the recovery is higher for the high salinity (3 wt%) experiment. The salt affects the hydrate stability, where higher concentrations will result in more rapid recovery and higher total recovery due to the accelerated dissociation contribution from salt. This may indicate that some of the limitation with this production scheme lies within kinetics as well. Another explanation could also be that the fill fraction of hydrate was lower in this experiment due to the higher salinity and CO_2 could therefore move more freely in the core and benefit from diffusion in the aqueous solution. More free water will also increase the interface between CH_4 hydrate and CO_2. In Chapter 4.1 it was established that the salinity impact for 4 wt% NaCl and less was insignificant on fill fraction. In this study, 3 wt% was used and it is therefore questionable if this would affect the fill fraction. Considering these results and economic aspects in a future production scenario, it would be beneficial to produce from a high saline area where the salt itself would contribute to increasing the recovery. A thoroughly investigation on salinity impacts on CH_4 production during CO_2 sequestration is therefore considered highly interesting.

4.3.4 Comparison with previous single spacer CO_2 injection experiments

The main objective with these experiments was to investigate if an additional fracture and spacer would increase the exchange rate. A final recovery of 70%, when normalized to intensity of the spacer 100% filled with CH_4, has been reported in previous single spacer experiments (Ersland, 2008). The two double spacer experiments only offered 58% and 51% recovery when normalized to the intensity of a spacer 100% filled with CH_4 (Figure 4.11). However, the spacer volume in these two experiments are significantly larger, approximately twice the size of the spacer used in the single spacer experiment, and the total gas recovery must subsequently be corrected for the larger free volume in which CH_4 is produced. Increasing the interface between the CH_4 hydrate and CO_2 does therefore seem to affect the recovery of CH_4, and it is possible to conclude that diffusion is a limiting factor. These experiments indicate that increased contact area increases the gas recovery.

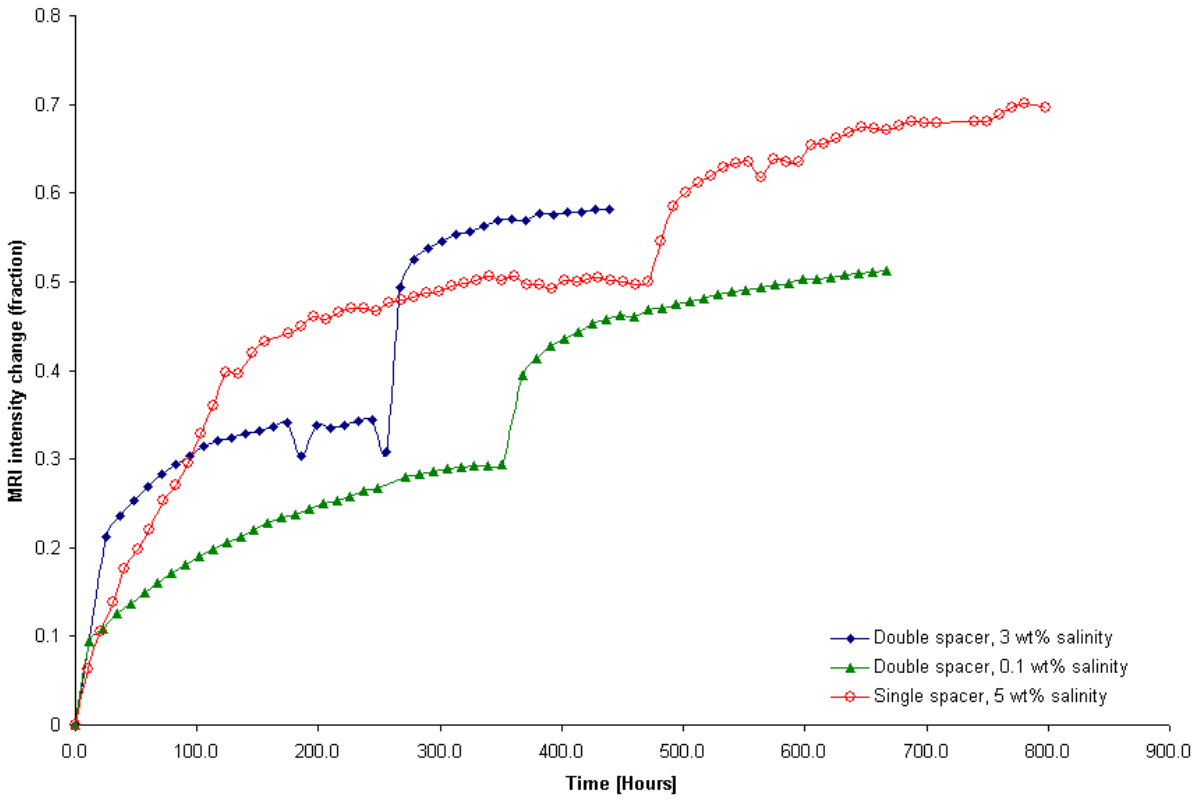

Figure 4.11 – CH_4 build-up in the POM spacer due to exchange process with CO_2, which results in increased MRI intensity. The MRI signal is average intensity from the spacer, normalized to a spacer 100% filled with CH_4. The figure includes data from two CO_2 flushes for each of the curves and compares results from the double spacer experiments with results from a previous single spacer experiment presented by Ersland (2008). These results are not normalized to the amount of CH_4 consumed during hydrate formation and are therefore not an estimate of total recovery. The spacer volume in the double spacer experiment is approximately twice the size of the accumulation volume in the single spacer and the recovery will thus be higher.

During the free water experiment (Chapter 4.4) it was discovered that N_2 does affect the existing CH_4 hydrate equilibrium, where higher N_2 concentrations alters the equilibrium more effectively. Using two spacers did not only increase the interface between the two phases, it also increased the CO_2 to CH_4 hydrate ratio. The existing hydrate equilibrium will therefore be altered more effectively. Ideally, the two spacers would constitute the same volume if only limitation in diffusion was to be investigated.

The observed recovery was 32% for the low salinity test (0.1 wt%) and 49% for the high salinity test (3 wt%) based on MRI intensity from the POM-spacer. However, the mole fraction considers the amount of CH_4 initially consumed during CH_4 hydrate formation. Due to dissociation by N_2 the actual amount of CH_4 is less, thus the actual recovery is higher. The results do not account for CH_4 diffused into lines, contribution from free CH_4 that may diffuse into the core, or CH_4 that has been produced during the CO_2 flush. Considering these uncertainties, it is difficult to make an accurate estimate on recovery. Previous experiments (Husebø, 2008) have concluded in a total recovery of 50-85%, which seems likely to apply here as well.

4.3.5 Comparison of depressurization and CO_2 data

A comparison of the two gas hydrate production schemes investigated in this study is presented in Figure 4.12. Depressurization induced gas production resulted in full recovery over a short period of time, as discussed in Chapter 4.2. The Bentheim sandstone core used for this experiment is supposed to be an analogue to conditions in a gas hydrate reservoir. However, due to the small size of the core, the entire core is forced below hydrate stable conditions during pressure depletion. This is not applicable on reservoir scale, where the pressure depletion mainly affects the area adjacent to the wellbore. It is therefore likely to assume that the recovery would not be as efficient on a larger scale. In addition, production of associated water was detected. CH_4 production through CO_2 injection showed promising results. The efficiency was not as high as for the pressure depletion, which is the main disadvantage with this production scheme. However, no hydrate dissociation was observed and the structural integrity of the sandstone was therefore maintained. This is not crucial for consolidated rocks like Bentheim, but for unconsolidated rocks it is important to maintain structural integrity during production. The thermodynamic stability of the gas hydrate will also be increased when CO_2 stabilizes structure I hydrates. To evaluate the two production schemes in a non-biased manner, more realistic pressure depletion conditions would have to be applied. Additionally, it would be beneficial to monitor the exchange process between CO_2 and CH_4 hydrate in a whole core, ideally on a larger scale than what a 10-14 cm long core provides. Experiments on a larger scale is desirable.

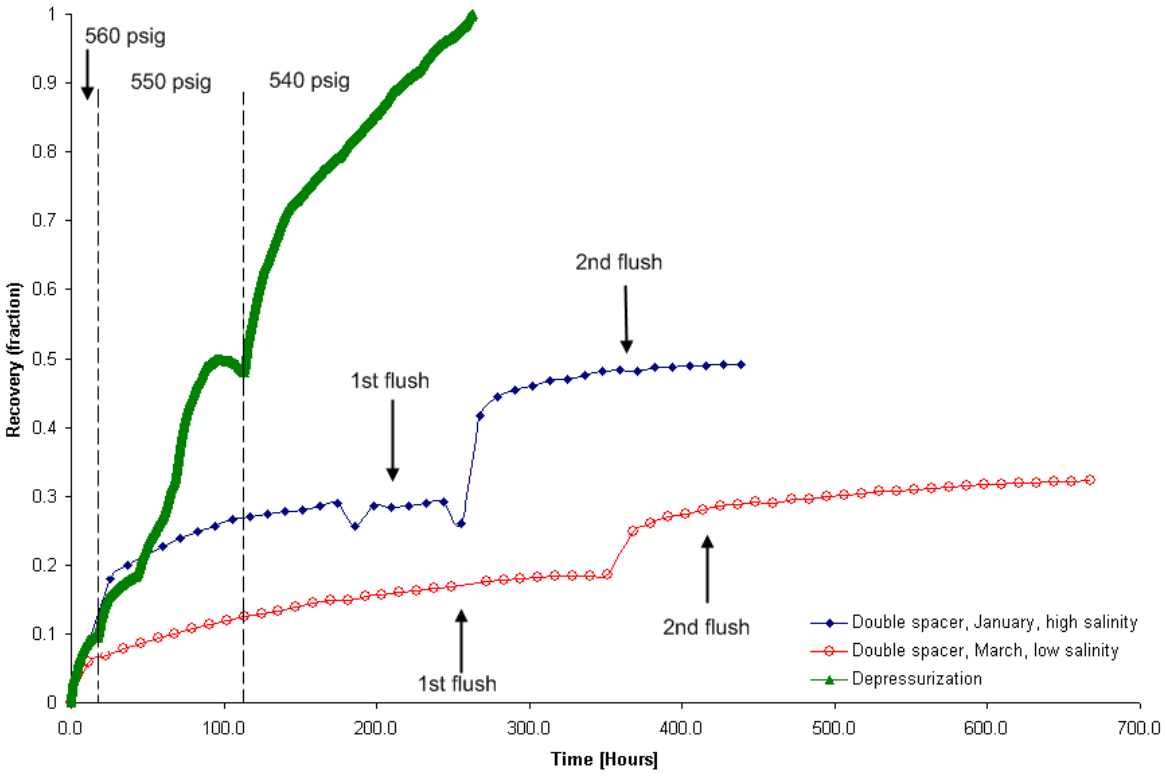

Figure 4.12 – Comparison of recovery results gained through depressurization and injection of CO_2 in double spacer. The figure clearly illustrates the efficiency of the depressurization experiment compared to the CO_2 sequestration. However, it is questionable if such a pressure drawdown is applicable on reservoir scale. It has also been mentioned that the total recovery through CO_2 sequestration is expected to be higher than illustrated in this figure.

4.3.6 Comparison with previous results

Lee et al. (2003) concluded that at least 64% CH_4 in a CH_4 hydrate reservoir should be theoretically recoverable through injection of CO_2. In structure I, the larger cages ($5^{12}6^2$) outnumber the smaller (5^{12}) by a factor of three, so three times as much gas may be stored in the larger cages. Additionally, the smaller cages in structure I are occupied to a smaller degree compared to the larger cages, so some 5^{12} cages may not be occupied by guest molecules. Major parts of the CH_4 is therefore bound to be stored in the larger cages ($5^{12}6^2$), where CO_2 is preferred when looking at both kinetics and equilibrium thermodynamics. CO_2 has a larger diameter than CH_4, which makes it hard for CO_2 to act as a guest molecule in the small cages. In fact, the molecular to cavity diameter ratio is 1.00 for CO_2, so the chances are low for swapping in these polyhedra and subsequently CO_2 swapping is limited to affect the larger cages. In later experiments Park et al. (2008) reported a possible recovery of 85%, which was achieved by using a binary mixture of N_2 and CO_2. While CO_2 was too large to occupy the smaller cages, N_2 proved thermodynamically more stable than CH_4 at the temperature and pressure conditions used in their experiments, and the increased recovery was explained by presence of N_2. It is worth noting that the paper never mentions how much gas the CH_4 hydrate was exposed to during the exchange process and it also fails to mention the size of the gas hydrate sample. This is critical, especially when considering how the alteration of the hydrate equilibrium in the free water experiment resulted in dissociation (Chapter 4.4). However, the paper does provide some interesting results that are worth further investigation.

Previous CO_2 sequestration experiments done in Bartlesville showed a total recovery of 50-85% (Husebø, 2008), which seems likely when compared to the experiments of Lee et al. (2003). In this study, it has been established that recovery was increased by using two spacers instead of one, thus increasing the contact area, and the total recovery is therefore expected to be in the upper region of this estimate.

4.3.7 Future development and improvement of the production scheme

Production of gas hydrates through CO_2 injection shows promising results, but compared to depressurization induced gas production the recovery is low. Limitations in the exchange process probably lie within both kinetics and diffusion, as indicated by these experiments. Measures should therefore be made to reduce these limitations and make the production scheme more effective. Lyon (2004) has suggested simultaneous injection of liquid CO_2 and SO_3 or HCl or other reagents, which easily dissolve in water and liquid CO_2. The injected solute will result in destabilization of CH_4 hydrate and consequent melting, leaving dissolved gas available for production while the interface between water and CO_2 has been increased and CO_2 hydrate formation will be initiated. McGrail et al. (2007) have suggested another production method with injection of a CO_2/water microemulsion. The results seem promising, however, CO_2 is injected at 25 ºC, which results in subsequent dissociation of CH_4 hydrate due to heat transfer, and there is no way to separate the effect of thermal injection from that of the micro emulsion. In experimental work presented in this thesis the injected CO_2 was partially cooled before contacting the core in order to investigate only the effect of the favorable thermodynamic stability offered by CO_2. Injection of heated CO_2 is one possible production scenario, but formation of CO_2 hydrates release sufficient heat to dissolve CH_4 hydrates. To validate the effect of the micro emulsion alone, it would have been interesting to see results where the injected micro emulsion was at reservoir temperature.

4.4 Production from Hydrate Reservoir with Free Water

In a hydrate reservoir, the gas hydrate will never completely saturate the pore system. The occurrence of gas hydrates are often divided into four different groups; 1) finely disseminated hydrate that may dissociate rapidly, 2) nodular hydrate of up to 5 cm bulk hydrate, 3) layered hydrates separated by thin layers of sediment, and 4) massive hydrates as thick as 3-4 m with 95% hydrate saturation (Sloan and Koh, 2008). The most usual occurrence of hydrate is as finely disseminated with subsequent low hydrate saturation, in some cases only a few percent, where the additional fluids present in the porous media will typically be water and different gases. In previous experiments, no excess water has been left in the porous medium after hydrate formation and the influence of excess water has therefore not been investigated. During hydrate formation, availability of guest molecules is most often the limiting factor. In a production scenario based on CO_2 sequestration, it is essential to be aware of what will happen to the free water surrounding the well bore once CO_2 is injected and how the gas permeability adjacent to the wellbore is affected. This experiment therefore aims at investigating how presence of CO_2 impacts a porous medium saturated with both CH_4 hydrate and free water. There was some free CH_4 left in the system as well at the initiation of CO_2 sequestration.

4.4.1 CH_4 hydrate formation

CH_4 hydrate was formed in a Bentheim core, and to provide excess water the hydrate formation was stopped prior to completion. The core had been saturated with 13.56 ml brine solution ($S_{w,i}$=50.9%), and with a CH_4 mole consumption of 0.00958 per ml of water and a total CH_4 mole consumption of 0.05891 during hydrate formation, the corresponding excess water prior N_2 injection was 7.4 ml (S_w=27.8%). The CH_4 hydrate formation is illustrated in Figure 4.13, comparing pump log data with MRI profile intensities.

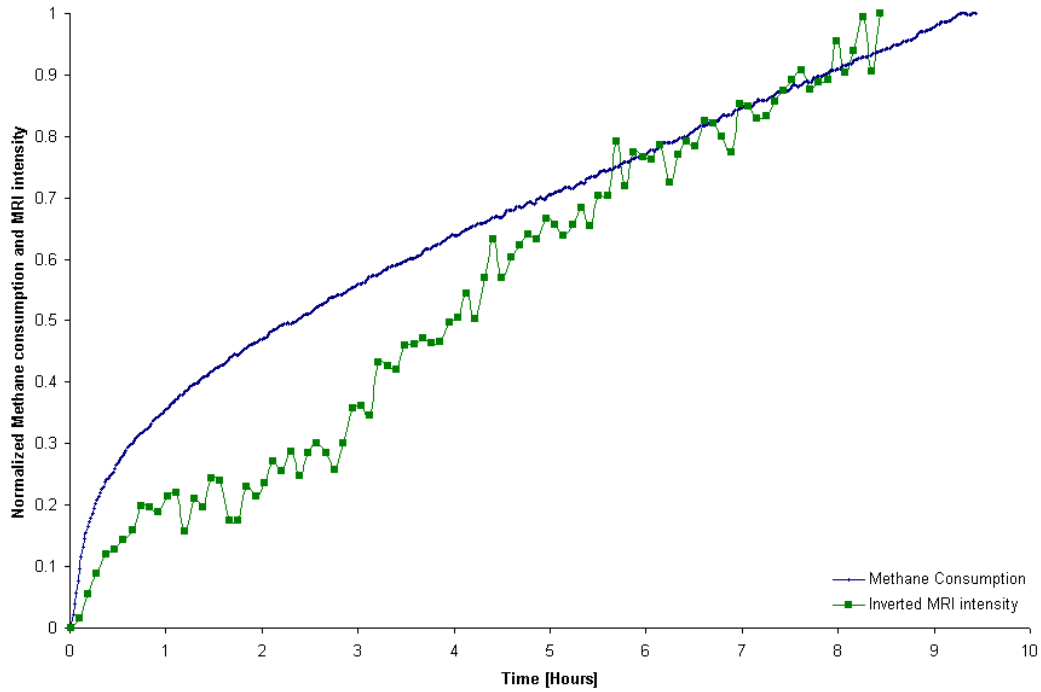

Figure 4.13 – Comparison between normalized injected CH_4 data from the pump logs and normalized inverted MRI intensity during hydrate formation. In this case 30 second profiles were taken every 5 minutes due to rapid hydrate formation. The SNR for these profiles is not too good, and the fluctuations of the curve illustrate the quality of the data, however, the trend is still clear.

Due to rapid hydrate formation, 30 second profiles were used to acquired MRI data. Subsequently, the SNR is a lot weaker than images taken over a longer period of time. This is reflected in the fluctuations of the MRI intensity in the figure, which indicates that the data is less reliable. However, the data clearly indicates hydrate formation and therefore corroborates the PVT data.

4.4.2 Intensity changes during the experiment

The presence of free water in the core and gas in the POM spacer was constantly monitored during the experiment by looking at intensity picked up by the MRI. The data from the MRI was converted into average intensity signals corrected for noise by using the ROI v.2.01 program. Figure 4.14 shows variations in averaged MRI intensities from the whole core at different times of the experiment. The first image at 0 hours was taken prior to hydrate formation, where both free water and free gas was present in the porous media, and the other intensity data are normalized to this intensity.

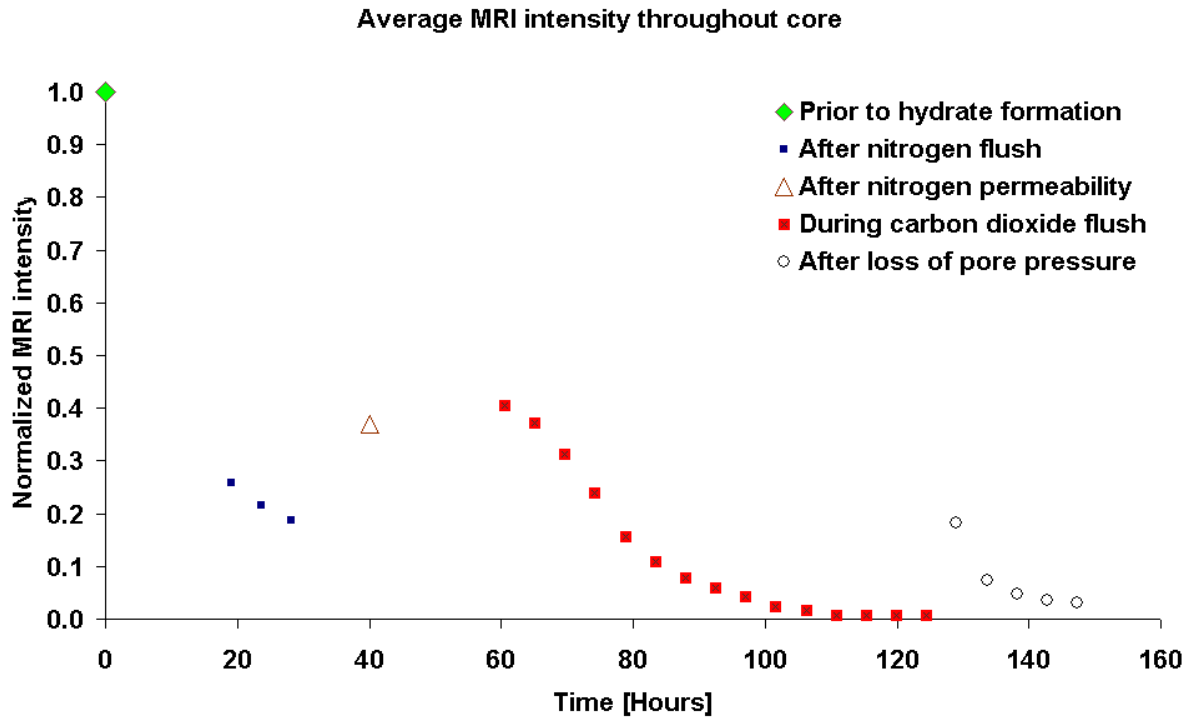

Figure 4.14 – Normalized MRI intensity for the whole core as a function of time. The image at 0 hours is a 9 hour 3D image with higher SNR compared to the remaining data points, which are 4 hour 3D images. Ideally all images should have had the same time span, but no 4 hour images were acquired prior to hydrate formation.

Average intensity variations over the whole core

Prior to this experiment, the common knowledge within the group had been that injection of N_2 into a CH_4 hydrate system would pose no risk to the existence of CH_4 hydrates because N_2 is not a stable hydrate former at the applied experimental conditions. However, Figure 4.14 leaves no doubt that N_2 affects the stability of the hydrate. 14.5 hours after the completion of the first 9 hour MRI image, N_2 was injected into the lines at both ends and into the spacer at the outlet end of the core to remove excess CH_4 from the system, thus limiting further hydrate growth. A pump connected to the outlet end of the core provided an "infinite" reservoir of N_2 by maintaining constant pressure at 8.37 MPa. Even 15 hours after this event, at 28 hours, the MRI intensity for the whole core shows no sign of dissociation. Gas permeability measurements at S_w=27.8% was initiated after 32 hours, where N_2 was injected at constant rate. Consequently, N_2 was not only introduced to the spacer but the whole core, thus increasing the interface between CH_4 hydrate and N_2. The next 4 hour 3D image taken after 40 hours clearly indicates rather substantial dissociation of CH_4-hydrate, as the normalized intensity is increased by approximately 0.2 over a very short period of time. Calculations were conducted with CSMGem (Sloan and Koh, 2008) and accordingly, presence of N_2 will result in dissociation of hydrate. The extent of hydrate dissociation is dependent on the moles of N_2 present. The system was at equilibrium as long as only CH_4 and CH_4 hydrate was present. However, once another gas is introduced the equilibrium is altered and may result in dissociation of the gas hydrate if the N_2 concentration is sufficiently high. During the permeability measurements 42.7 ml of N_2 (at 8.37 MPa and 4 ºC) were injected, equivalent to 1.6 pore volumes, which was allowed to destabilize the existing CH_4 hydrate. The experimental data acquired through this experiment along with the calculated data leave no doubt that N_2 does alter the CH_4 hydrate equilibrium.

After 56 hours, injection of CO_2 was initiated at constant rate of 0.00833 ml/min. As expected, sequestration of CO_2 resulted in a loss of MRI intensity as the free water was converted into gas hydrates (Figure 4.15). It is likely to assume that an exchange process between CH_4 hydrates and CO_2 took place as well during the flush; however, gas samples for GC were not acquired and it is therefore not possible to evaluate the exchanged volume. After one pore volume of CO_2 had been flushed through the core permeability measurements were conducted by injecting CO_2 at very low rate. After approximately 125 hours pore pressure was lost and a substantial amount of gas leaked out, resulting in dissociation of some hydrate. This was confirmed by the 4 hour 3D image completed at 129 hours (Figure 4.14), showing a sudden intensity increase. However, the system was yet again pressurized with CO_2, which converted the water back to gas hydrate. Figure 4.15 visualizes the growth sequence by showing a selection of four 3D images taken at various times throughout the experiment.

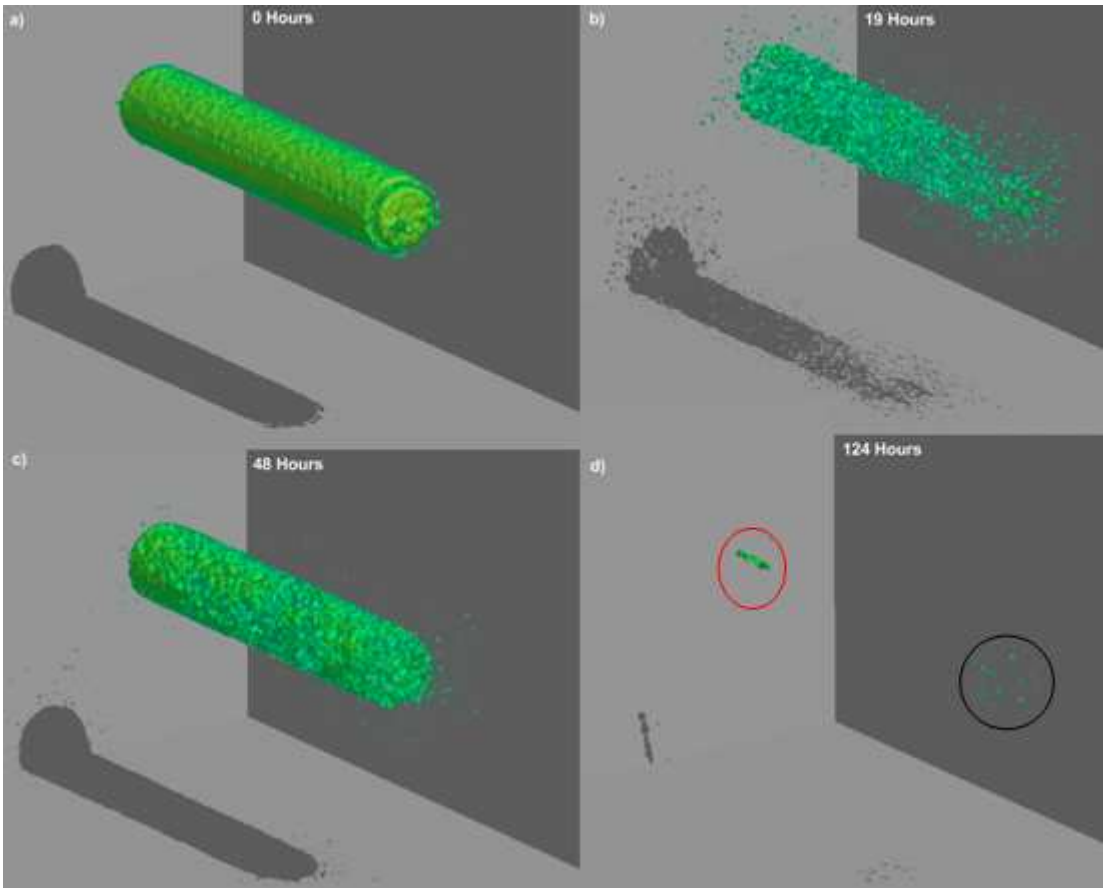

Figure 4.15 – Visualization of hydrate formation using T3D: a) 9 hour 3D image taken prior to cooling and hydrate formation, b) 4 hour 3D image taken after the first N_2 flush that removed excess CH_4 from the lines, c) 9 hour 3D image taken after N_2 was flushed through the core, resulting in dissociation of some of the gas hydrate with subsequent intensity increase due to more free water, d) 4 hour 3D image taken after CO_2 hydrate formation. The only signal left at this time was some water present at the inlet end of the core (marked by the red circle) and some produced CH_4 in the spacer located at the outlet (marked by the dark blue circle). In order to visualize the CH_4 accumulation in the spacer, which was confirmed by the ROI, the threshold of the T3D images had to be adjusted to allow higher noise ratio. That is why there is a lot of noise in the images, especially in b).

Intensity variations along the length of the core

While Figure 4.14 was looking at average intensity over the whole core, Figure 4.16 visualizes variations in the MRI intensity along the length of the core during the time span that N_2 was present in the system. During the first three images (after 19, 24 and 28 hours) in Figure 4.16, N_2 was mainly present in the lines at both ends and in the spacer due to the N_2 flush. At this time, N_2 had not been flushed through the core, and limited diffusion rate prevented N_2 from accessing the middle part of the core. During this period, an overall decrease in MRI intensity was observed in Figure 4.14, which seems to correlate with Figure 4.16 when considering the loss of MRI signal from the middle of the core due to continued hydrate formation. N_2 had not been flushed through the core and CH_4 was therefore still present in major parts of the core. It is likely to assume that the CH_4 concentration was at its highest in the middle of the core, thus making continued hydrate formation possible. CH_4 was most likely present in the end parts of the core as well, but due to alteration of the equilibrium, detectable hydrate formation did not occur here. It is likely that some small scale dissociation took place at both ends, but with simultaneous small scale hydrate formation by excess water and CH_4 the dissociation was not detectable. At 32 hours, three permeability measurements were initiated, injecting a total of 42.7 ml of N_2 (at 8.37 MPa and 4 ºC) through the core. By injecting N_2 at constant rate throughout the core, excess CH_4 was displaced and the interface between N_2 and CH_4 hydrate was increased. The next 3D image completed at 40 hours revealed rather substantial dissociation, mainly close to the inlet and outlet end of the core, where the availability of the N_2 was higher. At the middle of the core the hydrate dissociation was less extensive, probably due to lower N_2 concentration. It is likely to assume that the free CH_4 concentration was higher here, thus temporary equilibrium may be established faster than at the ends of the core, which may have limited the negative effect of N_2.

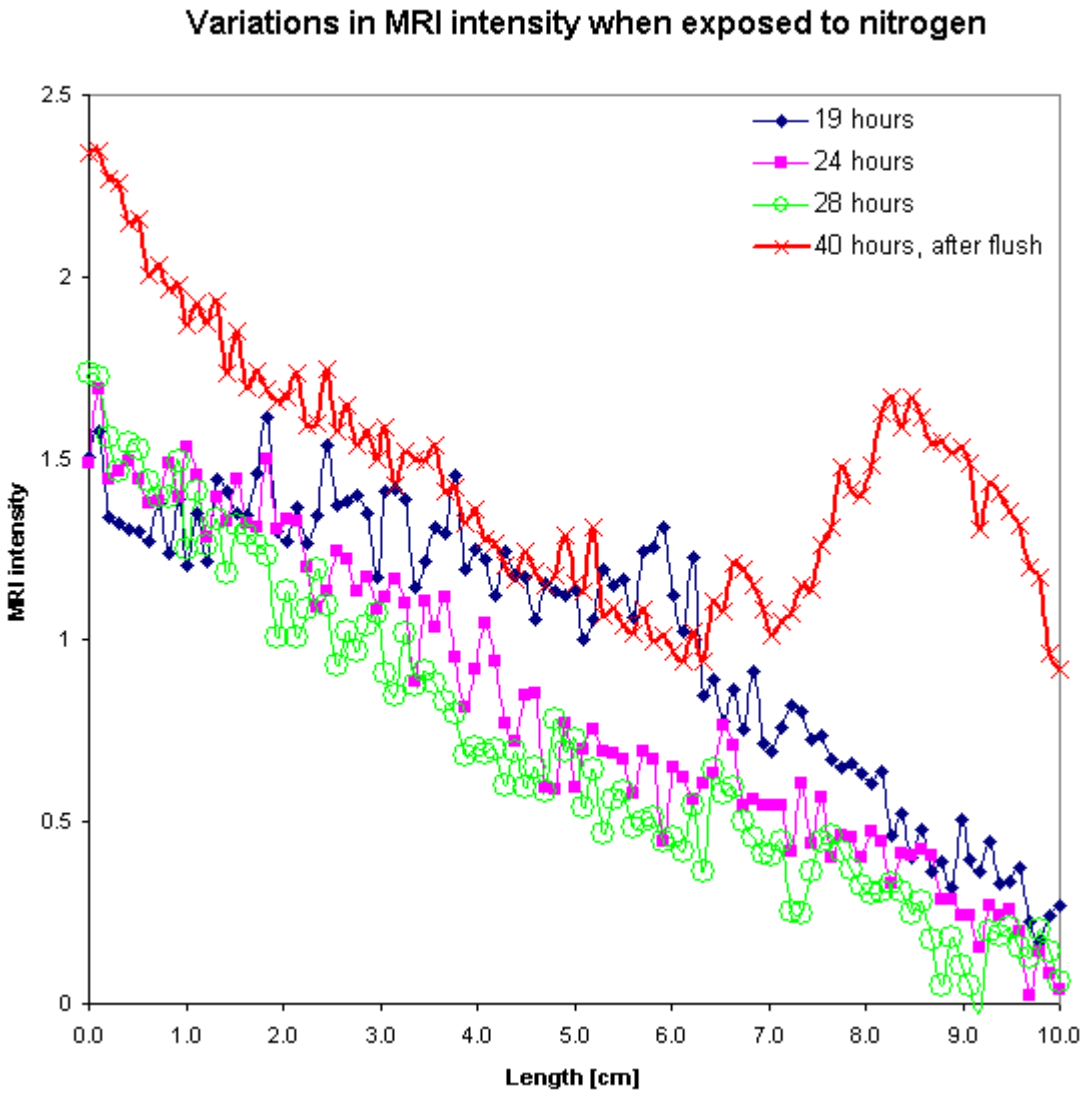

Figure 4.16 – MRI intensity variations over the core length normalized by the average intensity from the image completed at 19 hours. The first image at 19 hours shows a rather inhomogeneous distribution of gas hydrate where the saturation of such is higher at the outlet of the core. At 14.5 hours N_2 was introduced to the system and was used to maintain pressure. No substantial MRI intensity changes occurred within the next 9 hours, however, at 32 hours the first N_2 permeability measurement was conducted by injecting N_2 through the core at constant rate. This exposed more of the CH_4 hydrate to N_2, resulting in the substantial dissociation observed at 40 hours.

Saturation distribution

Another interesting point from Figure 4.16 is the inhomogeneous distribution of CH_4 hydrates. The MRI intensity is far higher to the left side, indicating presence of more free water. This is visible from Figure 4.15 b) as well and it therefore seems likely to assume inhomogeneous growth of hydrate. In Figure 4.17 MRI intensity is also displayed, but here the inhomogeneous distribution of the signal is not very well detected, probably due to low SNR in the 1D profiles. A plausible reason for the inhomogeneous hydrate growth will be further discussed in Chapter 4.4.3.

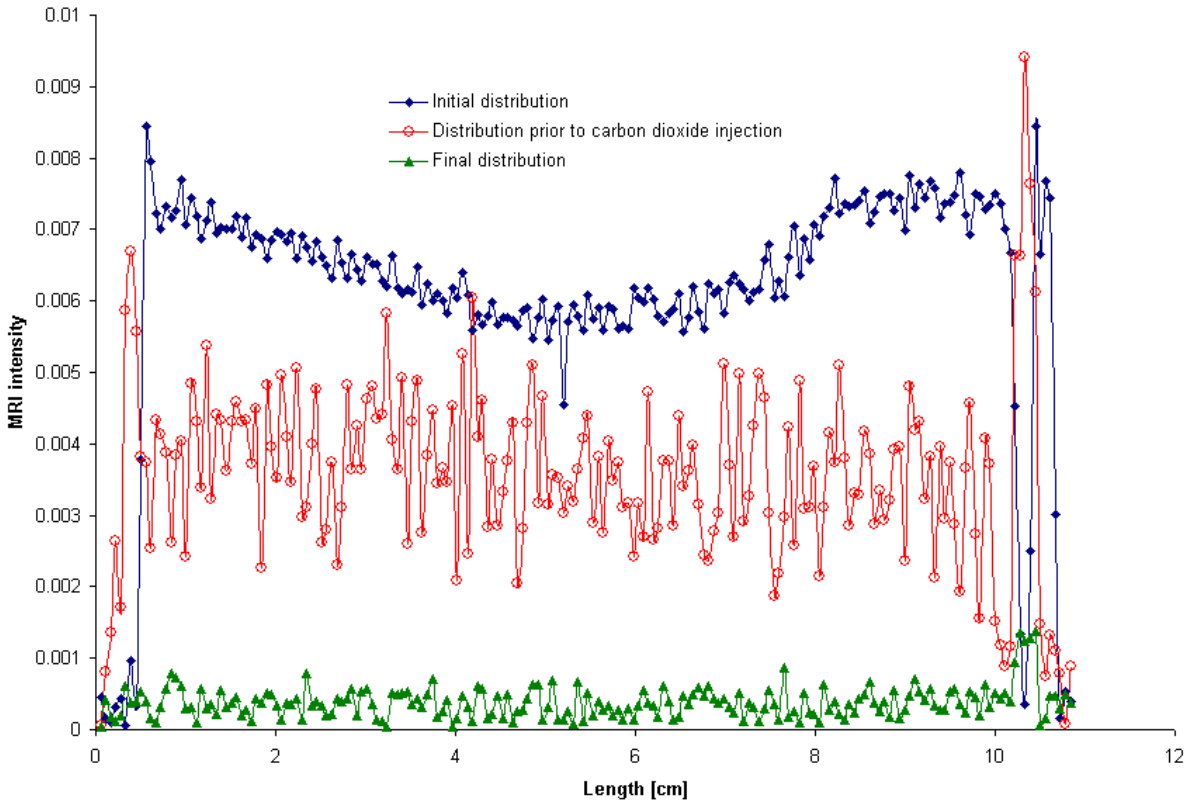

Figure 4.17 – 1D MRI profiles displaying intensity changes over the core. The blue points show the initial water distribution, and it is easily seen that the saturation is higher at the ends of the core. The intensity steadily decreased as hydrate was formed. SNR in the profiles is very low, which is reflected in the fluctuating signal.

Intensity variations observed in the spacer

At the producing end of the core, a POM spacer was mounted to enable accumulation of produced CH_4 during the exchange process with CO_2. This process did not occur until the very end of the test, but changes in MRI intensity in the spacer throughout the whole experiment is shown in Figure 4.18. At 0 hours, the spacer was filled with CH_4, resulting in high intensity. After the N_2 flush, the intensity started out low but increased as some CH_4 diffused into the spacer, most likely as a result of free gas diffusion and some CH_4 hydrate dissociation induced by the N_2. After the N_2 permeability measurements, CH_4 was displaced from the spacer, resulting in low intensity (40 hours). At the initiation of the CO_2 flush the intensity was back to approximately the same level as before the N_2 permeability measurements, indicating further hydrate dissociation, but decreased steadily as CO_2 was injected. At the very end of the test, between 129 and 147 hours, CO_2 was providing constant pressure from the inlet of the core and the valve at the outlet end was shut in to prevent CO_2 from flushing through the core, thus allowing released CH_4 to accumulate in the spacer. During this period the intensity was steadily increasing, indicating an exchange process between the CO_2 gas and the CH_4 hydrate, where swapping of the gases resulted in CO_2 hydrate and free CH_4 gas that diffused into the spacer and resulted in increased MRI intensity. Ideally, the exchange process would have been allowed to progress over a longer period of time, however, the effect of the exchange process has been confirmed in previous experiments and was never the main objective of this experiment.

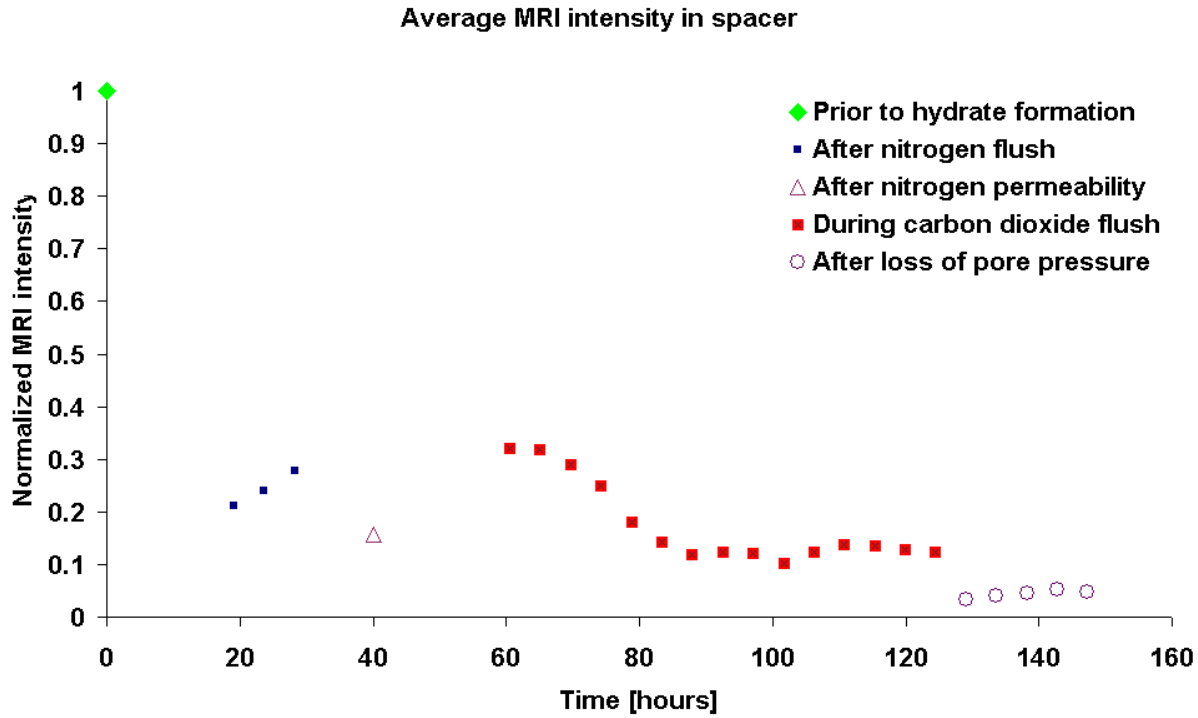

Figure 4.18 – Normalized MRI intensity in the POM spacer as a function of time. Presence of CH_4 in the spacer results in increased MRI intensity. The first image is a 9 hour 3D image which has higher SNR compared to the remaining data points (4 hour 3D images). Ideally they would all have the same SNR because they are normalized to each other. The figure illustrates the loss or gain of intensity in the spacer during the various stages of the experiment.

4.4.3 Relative permeability measurements

To be able to produce gas from gas hydrates, it is essential to confirm flow capacity through the porous media saturated with gas hydrates. One of the main purposes of this experiment was to investigate progression of permeability during hydrate formation, and to achieve this a differential pressure transducer was measuring the differential pressure while different gases were injected at constant rate over a short period of time. This was done both with some excess water still present in the core and after all the water had converted into hydrate. Ideally, an in line gas chromatograph should have been used to make sure that the gas obtained at the outlet end of the core equaled the gas at the inlet end. This was not done for this experiment, so there is no way to assure that the injected gas does not turn in to hydrates during the injection or mix with another gas to compromise the assumed gas viscosity. However, N_2 is not known to form hydrates at the experimental conditions, but it will influence the amount of free water present, as discussed in the previous section. CO_2 will form hydrate at this pressure, but was only used for permeability measurements after all the free water had converted into hydrate and would therefore not compromise the pressure measurements by forming gas hydrate during injection. The results from the permeability measurements are presented in Table 4.1.

Table 4.1 – Permeability measurements using N_2 and CO_2 at different flow rates.

	Permeability measurements			
	With excess water		Without excess water	
Rate [m^3/s]	3.3E-07	8.3E-07	1.3E-09	1.3E-09
Pressure [Pa]	62742.5	125485.0	79979.4	68947.8
Hydrate saturation	~0.32	~0.32	0.63	0.63
Water saturation	~0.28[g]	~0.28[g]	0	0
Permeability [mD]	2.3±0.1[h]	2.9±0.1	0.040±0.002	0.046±0.002

Two publications have agreed on grain diameter for Bentheim sandstone between 50 and 500-550 μm (Klein and Reuschlé, 2003, Schutjens et al., 1995), and even for the higher grain diameter Reynolds number for these rates does not exceed 10[i]. Consequently, no consideration of the inertia resistance factor was needed, and Darcy's law was applied because the flow was considered within the Darcy flow regime. Usually when gas permeability is measured, high rates are needed to cause noticeable differential pressure over the core. In this experiment, however, the flow capacity throughout the experiment was limited, which restricted the injection rate during permeability measurements. Reynolds number is proportional to the flow rate and consequently low rates impacts the Reynolds number and causes it to be less than 10. Higher permeability values were expected, as permeability measurements with higher values, ranging between 1 and 25 mD, have been presented in previous publications (Ersland et al., 2008, Stevens et al., 2007). The permeability presented in this thesis would definitely restrict the feasibility of production

[g] Due to presence of N_2 with subsequent hydrate dissociation the actual S_w was probably higher.
[h] Uncertainties were calculated based on equation (4.1) and uncertainties provided by manufacturer.
[i] For CO_2 a density of 951.045 kg/m^3 was used based on calculations, which resulted in a Reynolds number of $6.16*10^{-3}$ for the higher grain diameter, and the flow was well within Darcian flow regime. For N_2 calculations suggested a density of 101.794 kg/m^3, which resulted in Reynolds number 2.29 for the higher grain size. However, at current PVT conditions the N_2 is within supercritical state and this value is by no means the absolute value. It is still assumed that the flow was not in the Forchheimer flow regime.

from gas hydrates for high hydrate concentration and low free water concentration, but the previously reported values may provide sufficient production conditions.

Presence of water in lines

After assembling and saturating the core it was mounted inside the MRI and a profile was run. The profile showed some presence of water in the lines, which was redistributed during the pressurization process. Most of the water was displaced into the core, but a low intensity signal could still be observed from the lines, indicating presence of some water. Figure 4.15d) clearly shows some signal from the inlet end of the core (marked by the red circle) at the end of the experiment. In Figure 4.19 this is more easily observed, and water presence can clearly be detected in the red circles at the left end of the core.

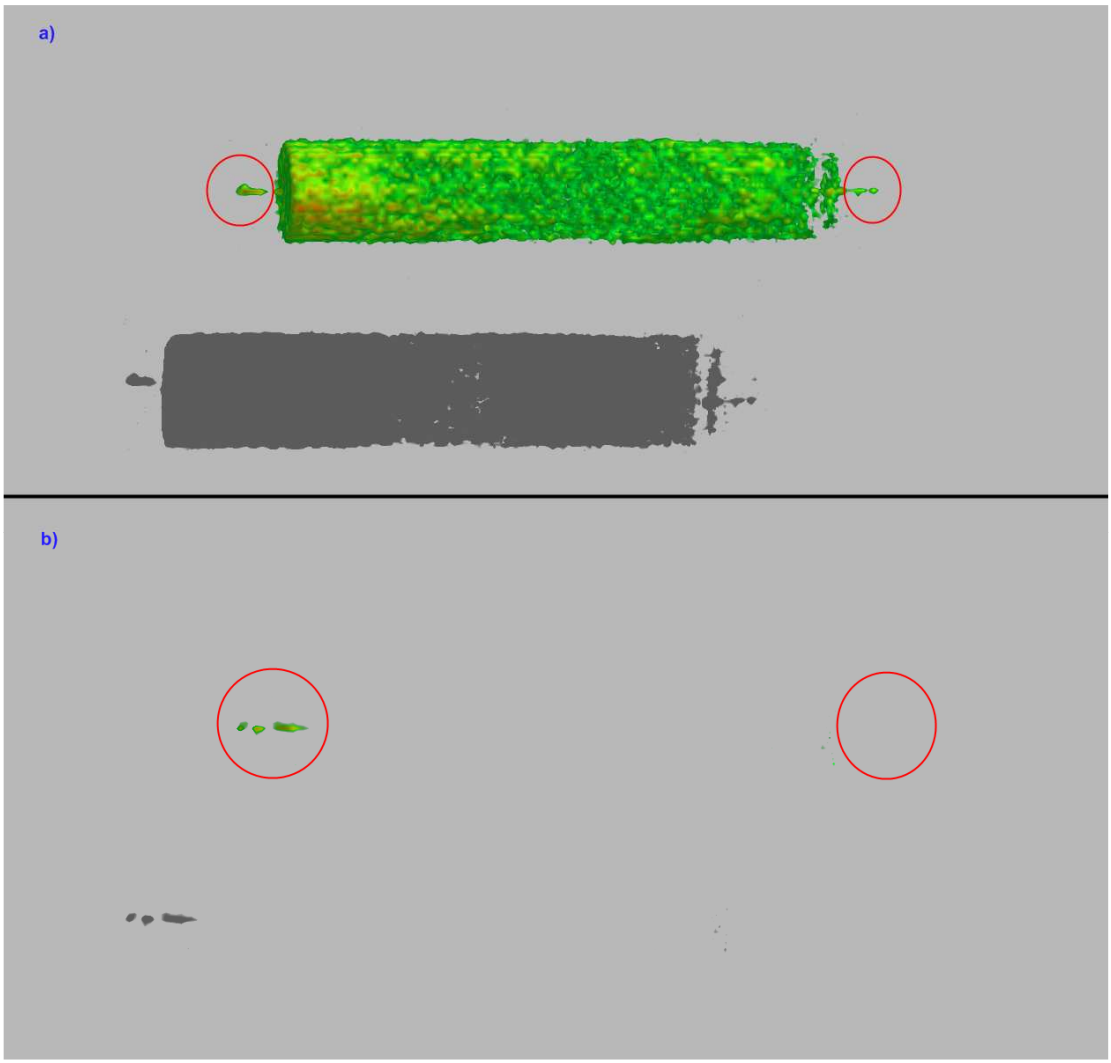

Figure 4.19 – Presence of water in lines during and after hydrate formation. In a) hydrate formation is progressing, and in b) the formation has stopped. In b) the water has been redistributed compared to the above picture, and the discontinuity may be a result of gas injection and subsequent hydrate formation in the lines.

As mentioned in Chapter 4.4.2 the distribution of CH_4 hydrate was inhomogeneous, even though CH_4 was injected from both ends. This may also provide support to the theory of hydrate formation in the left line. Presence of a hydrate plug would effectively lower the CH_4 delivery to the left end of the core, thus constraining hydrate formation. During permeability measurements it is likely that presence of gas hydrate in the line constricted the gas flow, and when higher flow rates were used the differential pressure diverged. The flow rate was very limited, and it was not possible to make measurements with multiple higher flow rates, thus the foundation for the inertia resistance factor β was limited.

4.4.4 Dissociation of hydrate by injection of Fluorinert

During the first experiment, a small imperfection in the Teflon shrink tubing resulted in confining liquid (Fluorinert FC-40) leaking into the porous sample. Despite the leakage of confining liquid pressure was not lost, on the contrary, pore pressure was actually increased to 10.44 MPa, and no temperature changes were reported. However, once Fluorinert contacted the hydrate it resulted in massive dissociation, and the original objective of the test was not fulfilled. According to the manufacturer 3M™, Fluorinert FC-40 consists of perfluoro compounds, primarily compounds with 12 carbons, and is not considered to react with any material because it is chemically stable (3M, 2009). Because the hydrate stability was not altered through temperature or pressure change, the only alternative left was for Fluorinert to act as a hydrate inhibitor. Considering the fact that Fluorinert is non-toxic and non-reactive this was found intriguing and very interesting, and Fluorinert was therefore injected at the end of the last test to see if the dissociation could be reproduced. This time no dissociation occurred, and the reason for the previous dissociation is still unknown.

4.5 Designing and Building new Experimental Setups

4.5.1 Challenges during designing and building

The already existing experimental setup was modified and in addition two new experimental setups were designed and built as a part of this thesis. This was done in order to improve the existing setup and to provide additional experimental setups for new master students and further gas hydrate investigation. The two new setups were based on cooling mechanisms described in other papers (Seol et al., 2006). Several challenges were encountered during the process, most of which were related to the pumps provided for the new setups. Three Isco D-series pumps were available and intended for these experimental setups, however, these lacked logging possibilities. To resolve this, programming in Labview was initiated. Several data files were acquired from ConocoPhillips and a program was developed based on these. The final program made it possible to control the pumps from a computer and to log pressure and volume data over time.

In the first setup the core holder was totally submerged in circulating antifreeze and due to large reserves of circulating antifreeze no temperature gradient was observed over the core. In the new experimental setups the antifreeze is constricted to flow in a cooling jacket, and the amount of surrounding antifreeze is limited. It is therefore likely that there exist a temperature gradient over the core, but it is yet to be established.

4.5.2 Testing of the new experimental setups

One of the main concerns of these experimental setups was if their conductive heat transport was able to provide low and stable temperatures. This was tested on several occasions, and by reducing the temperature of the Thermo Neslab RTE-17 refrigerated bath to between 2-3 ºC the core temperature was maintained constant at 4.0 ± 0.1 ºC. In order to confirm that the setups were fully functional experiments were run on these setups. This was done at the very end of the work included in this thesis, and the results from these tests are therefore not included. Setup III with the resistivity core holder is shown in Figure 4.20.

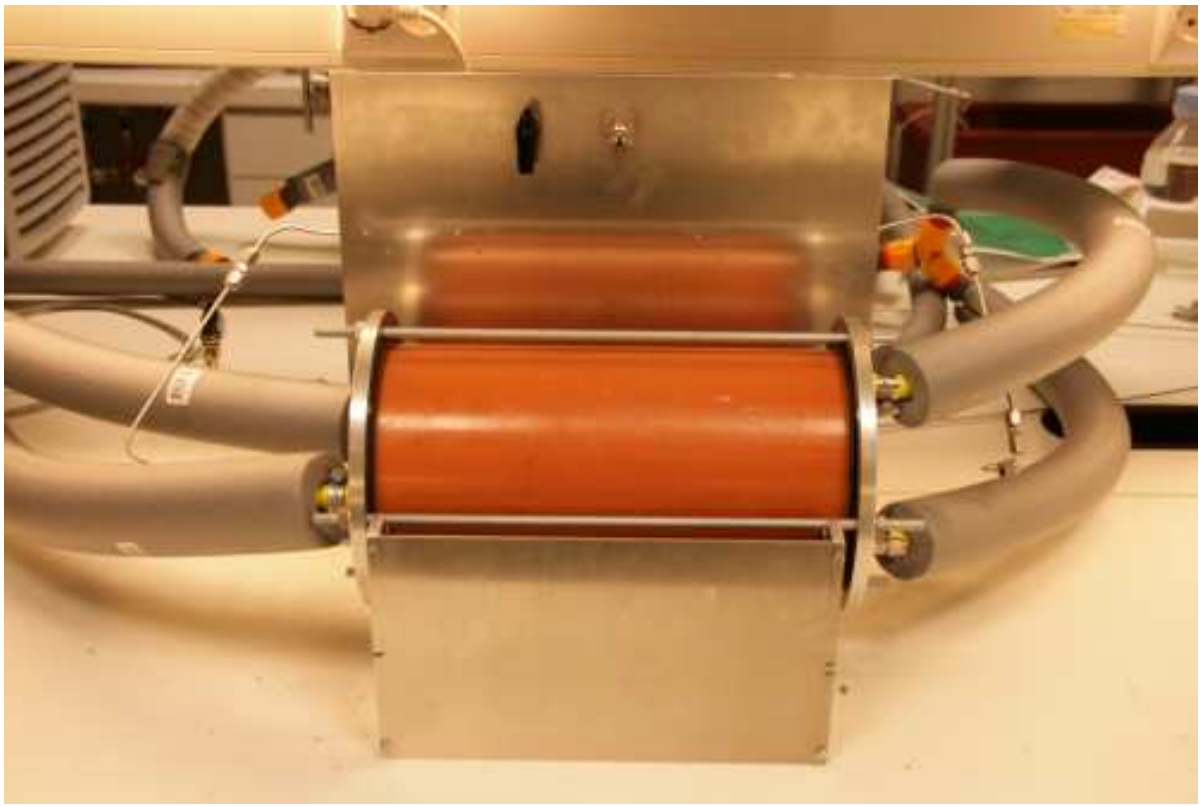

Figure 4.20 – Experimental setup with resistivity core holder. The first setup that was built (Appendix B2) used a regular Temco core holder where the cooling jacket only covered parts of the length of the core holder. The resistivity core holder was shorter, and a new design was therefore applied to provide sufficient cooling, where the cooling jacket covered the whole length of the core.

4.6 Uncertainties

During the experiments conducted in this thesis several uncertainties have to be considered. Errors often differ by several orders of magnitude; leaving some insignificant while others can not be ignored. Some uncertainties are exact, while others are results of conditions that can not be controlled, and estimates of these uncertainties are therefore very approximate. Exact uncertainties include measurements of weight and length, where the uncertainty for each apparatus is stated by the manufacturer. The uncertainty e.g. for the slide caliper used to measure length and diameter of the core, is stated as 0.02 mm. However, inhomogeneities in the core results in errors far higher than that of the slide caliper. It is therefore important to be conscious when considering uncertainties. The exact uncertainties stated by the manufacturer are often insignificant when compared to the experimental uncertainties.

4.6.1 Uncertainties applying for all experimental setups

High pressure systems were used in this study, and considering the low viscosity of gas this is what affects the uncertainty the most. At high pressures, even small imperfections in the experimental setup will result in leaks that make it hard to determine the exact amount of CH_4 that has contributed to hydrate growth. Leaks are inevitable, and it is therefore crucial to get a correct estimate on the leakage rate. At the University of Bergen this is especially critical, as the experimental data are acquired only as PVT data from pump logs and the calculations are based on conservation of mass. In order to correct for leaks, the CH_4 delivery logs from the Quizix pumps are used, looking at CH_4 delivery pre and post hydrate formation and comparing these (Figure 4.21). Due to temperature fluctuations at the University of Bergen, these data are taken over a 24 hour period to accommodate temperature fluctuations, which affect gas density and subsequent gas delivery. However, the leakage rate may alternate during the time span of the experiment and in such cases it is impossible to correct for errors. In these experiments the leakage rate was measured both before and after hydrate formation, and did not seem to change significantly. The leakage rate varied from 0.0001 ml/h to 0.05 ml/h in the different experiments, but seemed to remain constant during each experiment. This leak is a small for such a high pressure system pressurized with gas. The gas leakage estimate has generally been good, as confirmed in experiments where PVT data has been corroborated by *in situ* MRI images.

Differences from core to core are bound to occur, even though Bentheim is considered a homogeneous rock. The initial water saturation and consequent hydrate growth pattern will be affected by differences in pore structure and pore throats. The CH_4 gradients throughout the hydrate may also be affected by differences in saturation, which will affect the hydrate growth pattern. Ideally, the same sample should have been used for all experiments after comprehensive cleaning to minimize the variables. With reduced variables it would have been easier to make definite conclusions

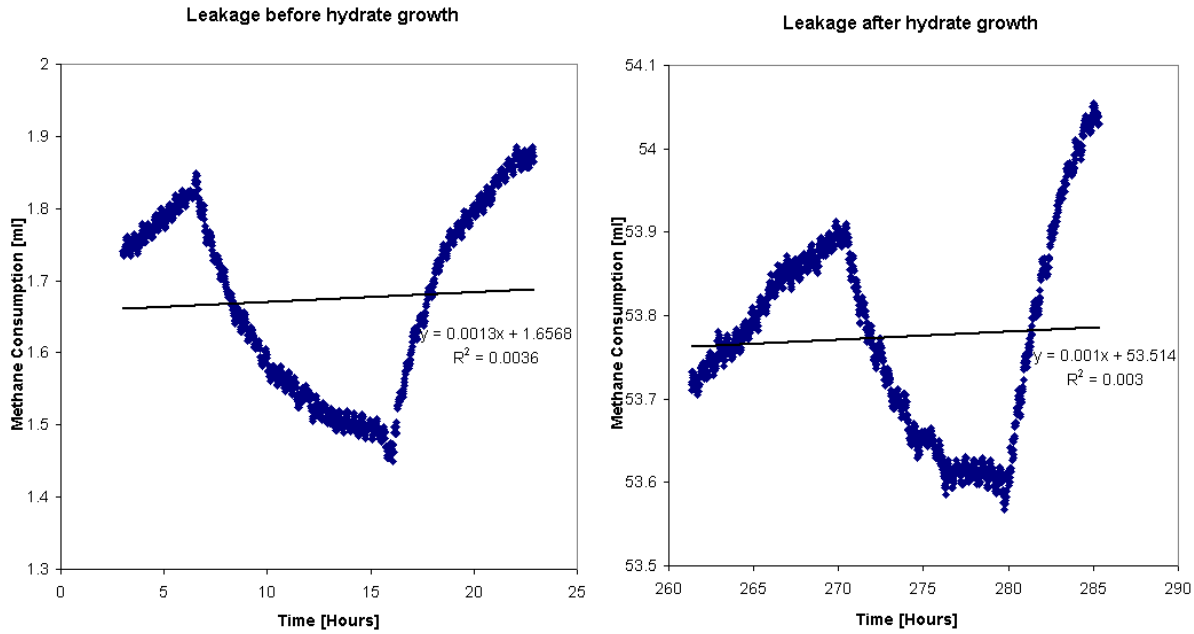

Figure 4.21 – Comparison of CH_4 flux pre and post hydrate formation. Due to temperature fluctuations, data points for 24 hour periods are used, which form the foundation for estimating average leakage flux. The fluxes in this figure seem to correlate with a rate of 0.0013 ml CH_4 per hour prior to hydrate formation and 0.001 ml CH_4 per hour post hydrate formation.

4.6.2 Specific uncertainties during salinity experiments

Temperature fluctuation is another factor that contributes to uncertainties, due to the PVT sensitivity of gas. At ConocoPhillips Research Center in Bartlesville a Thermo Scientific NESLAB HX recirculating chiller was maintaining constant room temperature 24/7. In Bergen the laboratory was not equipped with such a chiller, and the laboratory is located in a room with several windows, leaving the lab more exposed to outside temperature fluctuations. The gas density is very sensitive to temperature changes, where reduced temperature increases the gas density. The CH_4 pumps are set to maintain constant system pressure of 8.37 MPa, and when gas density increases, the volume of the system has to be decreased to maintain the pore pressure. The piston movement, with subsequent displacement of CH_4 from the pump cylinder, results in additional CH_4 delivery from the pumps. Over time, this will cause fluctuations in the CH_4 consumption graph. This cycle is illustrated in Figure 4.22, where the 24 hour periods seem to align with the local maximum values of the curve. Another limitation in Bergen is the lack of imaging possibilities, where there are no means for measuring hydrate distribution throughout the core. However, the PVT data has been corroborated by MRI on several occasions. It can therefore be concluded that PVT data is useful when determining hydrate growth.

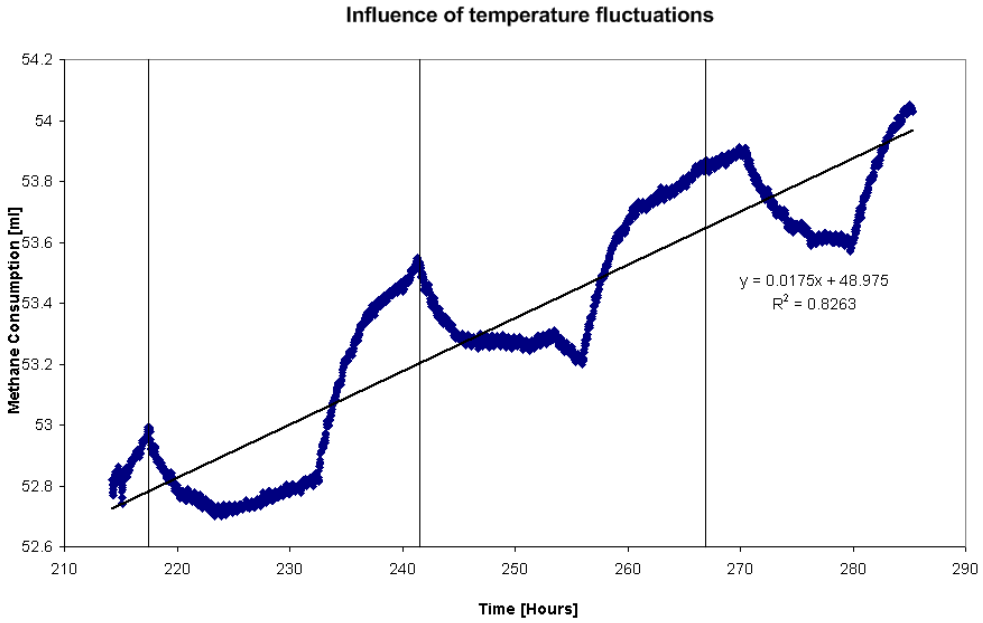

Figure 4.22 – CH_4 delivery log over a 70 hour period. The room temperature is affected by variations in outside temperature, resulting in fluctuations in the CH_4 delivery log. The vertical lines represents a specific time (15:51). The 24 hour period seem to align with the peaks, but the last peak is somewhat off. Outside temperature variations from day to day was not recorded, so it is hard to say what shifted the peak. It seems likely that the last day was colder than the previous one, resulting in shifting of the peak, but without outside temperature logs it is impossible to draw any conclusions.

In order to get an estimate on the fill fraction several calculations were performed. Uncertainties are related to the assumption of total conversion of water into hydrates, the leakage rate that was applied and also the fact that previous experiments have concluded in only 90% cage filling (Ersland, 2009), which means that on average only 7.2 cavities are formed per 46 water molecules. The fill fraction uncertainty was calculated using

$$\Delta f(x_1, x_2, x_3) = \sqrt{\left(\frac{\partial f}{\partial x_1}\right)^2 (\Delta x_1)^2 + \left(\frac{\partial f}{\partial x_2}\right)^2 (\Delta x_2)^2 + \left(\frac{\partial f}{\partial x_3}\right)^2 (\Delta x_3)^2}\,, \qquad (4.1)$$

and the uncertainties are presented along with the fill fraction values in Appendix B5. Where applicable, this equation was used to make an estimate on the absolute error in other experiments as well.

4.6.3 Specific uncertainties during depressurization experiment

Data from the MRI were compared to the CH_4 consumption curve, and the correlation between the two curves was very good, indicating that the uncertainty throughout hydrate growth was limited. As mentioned in Chapter 4.2.1, confining pressure was lost for a short period of time; however, no leak was detected during this period. The test was therefore not assumed compromised. Small uncertainties in the MRI can occur, but it is calibrated for each run and the uncertainties are considered rather insignificant. The magnetization of the MRI is dependent on temperature, where fluctuations in the room temperature will affect the experienced magnetization. However, the room chiller provides constant temperature, and no temperature fluctuations therefore affect the MRI. During depressurization 100% of the CH_4 was recovered. During experimental work several uncertainties are encountered and no experimental value presented in this work will therefore be an exact value. However, the Quizix pumps used during the experiment are high precision pumps, where the delivered and received volumes are considered exact values. No uncertainty estimate will be made on the recovery.

4.6.4 Specific uncertainties during double spacer experiment

The experimental data during the exchange process were acquired by the MRI, and the accuracy of the MRI is therefore crucial for the result. It has already been established that the certainty of the MRI is satisfactory and uncertainty from the MRI is therefore considered insignificant compared to others. The main uncertainties were mentioned in Chapter 4.3 and include alteration of existing equilibrium once N_2 was introduced to the system, free CH_4 that diffuses and accumulates in the spacer and contributes to increased MRI intensity, and diffusion of produced CH_4 into the porous media and injection lines. These represent the major uncertainties in this experiment and due to the magnitude of these uncertainties and lack of monitoring possibilities no uncertainty estimate will be made. Previous single spacer experiments have estimated 50-85% recovery (Husebø, 2008, Ersland, 2008). It is likely that the results acquired in the double spacer test are located in this recovery span as well, but it was confirmed that the recovery using two spacers was higher than for a single spacer. It is therefore likely that the recovery in these experiments is located in the upper region of the estimate.

4.6.5 Specific uncertainties during free water experiment

During this experiment N_2 was injected in relation with permeability measurements. Presence of N_2 resulted in hydrate dissociation, as discussed in Chapter 4.4.2. The main purpose of this experiment was not to investigate the exchange process between CO_2 and CH_4 hydrate, and the associated dissociation was therefore not that relevant. The main purpose was to examine progression of permeability during hydrate formation, and an estimate on the uncertainty was established using Equation (4.1). Due to CH_4 hydrate dissociation during permeability measurements, the corresponding water saturation is unknown and only an estimate. The flow capacity of the core was expected to be at least two orders of magnitude higher, but was most likely limited due to hydrate plugging. The relative permeability is therefore mainly affected by experimental uncertainties, which exceed the calculated uncertainty.

Chapter 5

Conclusions and Future Work

Natural gas hydrates are distributed in numerous locations worldwide and represent a yet untapped energy resource. Current technical hurdles include accurate assessment of the location of gas hydrate deposits and preliminary effective production methods that provide adequate economic incentives for further development of production technology.

CH_4 hydrates have been successfully formed on several occasions in this study to investigate processes involved during CH_4 hydrate formation and CH_4 production from CH_4 hydrates. Through these studies PVT data was used to corroborate the value of *in situ* MRI monitoring, where MRI intensity was proportional to concentrations of both CH_4 and water. MRI was used to monitor hydrate progression in all experiments except for the salinity experiments.

Salinity impacts on induction time and hydrate growth pattern has been investigated through six different experiments, looking at the effect of salinities ranging between 1 wt% and 10 wt%. The fill fraction results show clear dependency on the salinity of the accessible brine, where higher salinities restricted the hydrate growth. The induction time was significantly affected by increased salinity, where higher salinity resulted in increased induction time. Salt alters the thermodynamic stability of hydrate, and at sufficient concentration further growth is inhibited. CSMGem calculated this value to 14 wt%, and the experimental results were compared with the calculated values. Most of the experimental data was within ±7% of the theoretical expected values. Continued work should include studies of how differences in saturation and initial brine distribution influence hydrate growth.

CH_4 production was implemented through depressurization, and full recovery was achieved after a short period of time (280 hours). The gas permeability was limited until 20% of the gas hydrate had dissociated, after which the CH_4 production rate increased. The current hydrate saturation at that point was approximately 50%. Some associated free water was produced, which is one of the major disadvantages with this production method. Additionally, there is the loss of structural integrity in cases where gas hydrates provide stability to the sediment. No pressure gradient is present in this experiment; however, in a reservoir a pressure gradient would be present. This is an up-scaling issue, and it would therefore be beneficial to further investigate this production scheme on a larger scale to observe how pressure and production evolve with time. During the period the system was maintained at 3.96 MPa the system was outside hydrate stability region, and in theory hydrate dissociation and subsequent gas production should have been higher. Limited production is explained by progression of a temperature gradient. Future depressurization studies should investigate if production at 3.96 MPa continues once the conductive heat flow has heated the core back to 4.0 ^{o}C. In correlation with this test, it would be interesting to add multiple thermocouples at different locations on the core to investigate if a temperature gradient evolves during dissociation. Substantial sand production has been reported at Mallik (Numasawa et al., 2008), and to study this in a future depressurization test hydrates should be formed in unconsolidated sand packs.

Increased contact area between CH_4 hydrate and CO_2 may contribute to increased recovery over a shorter period of time, as indicated by the results from CO_2 injection into a core with two longitudinal fractures. CH_4 production during CO_2 injection was high, and no hydrate dissociation was detected by the MRI. It is therefore assumed that CO_2 maintained the stability of structure I hydrate, and the stability of the sedimentary rock was not compromised. The thermodynamic stability of the hydrate is increased with CO_2 as a guest molecule, and an additional benefit is sequestration of a green house gas. The observed recovery increase could also be a result of increased CO_2/CH_4 hydrate volume ratio, and in a future experiment it would therefore be interesting to investigate what impact two longitudinal fractures would have on the exchange process if the accumulation volume of the two spacers equaled the volume of a single spacer. Another discovery was the fact that the higher salinity experiment provided faster and higher recovery than the low salinity experiment. Salt is a hydrate inhibitor and alters the thermodynamic stability of the hydrate deposit. In addition, increased salinity impacts fill fraction at sufficiently high concentration with subsequent increased amount of free water. This may serve as transport channels for CO_2 and CH_4 (Liu and Flemings, 2006, Kvamme, 2006). Further research on this matter should be conducted to evaluate the implications salinity have on gas production from hydrates. This may help to establish the economic feasibility of different gas hydrate deposits. Currently, depressurization tests using different salinities have been initiated at the University of Bergen to investigate salinity impacts on depressurization induced CH_4 production. Future research should also focus on further development of production by CO_2 injection, where simultaneous injection with other solvents or gases may increase the production potential.

In this study, CO_2 sequestration into a core saturated with hydrate and free water was conducted to investigate how CO_2 will impact free water close to a wellbore. CO_2 hydrate formed and a small scale exchange between already established CH_4 hydrate and CO_2 was detected, as expected. Permeability measurements revealed limited flow capacity over the core, however, these results may have been compromised by presence of hydrate plugs in the injection line, and the validity of the results can therefore be questioned. Future experiments should investigate the progression of permeability for different hydrate saturations. This is essential in order to determine the economic feasibility of gas production from hydrates. A resistivity setup has been designed and built in this thesis, which will make it possible to determine how permeability correlates to resistivity, and a study on this matter is about to be initiated. The resistivity well also provides an additional manner to monitor hydrate growth. Production from high-saturated gas hydrate accumulations and hydrate deposits adjacent to gas reservoirs are considered the most economically feasible production targets. The permeability is expected to be limited when gas hydrate saturation is high, and future experiments should investigate production potential for different permeabilities and possible methods for manipulation of permeability.

In this thesis hydrate properties and production schemes have been investigated on a relatively small scale, where the total core volume never exceeded 300 cm^3. To acquire more representative data it would be beneficial to upscale the experimental work. A new pressure vessel will be acquired shortly, which will be able to provide experimental conditions for larger cores. Continued experimental work would also benefit from implementation of experimental data into a simulator.

References

3M *"Fluorinert FC-40 Material Safety Data Sheet"*. 2009

BALDWIN, B. A., MORADI-ARAGHI, A. & STEVENS, J. C. *"Monitoring hydrate formation and dissociation in sandstone and bulk with magnetic resonance imaging"*. Magnetic Resonance Imaging, **21** (9): 1061-1069.(2003)

BIN, D. *"Effect of Methane on the Global Climate Change"*. SPE Annual Technical Conference and Exhibition, Anaheim, CA, USA, November 11-14, 2007

BLOCH, F. *"Nuclear Induction"*. Physical Review, **70** (7-8): 460-474.(1946)

BOSWELL, R. & COLLETT, T. S. *"The Gas Hydrate Resource Pyramid"*. Fire in the ice, NETL Fall Newsletter, 5-7.(2006)

BRYN, P., BERG, K., FORSBERG, C. F., SOLHEIM, A. & KVALSTAD, T. J. *"Explaining the Storegga Slide"*. Marine and Petroleum Geology, **22** 11-19.(2005)

CARROL, J. "*Natural Gas Hydrates"*, Burlington, Elsevier Science, 2003

CHAPLIN, M. *"Water structure and science"*. http://www.lsbu.ac.uk/water/index2.html 2008

CIRCONE, S., KIRBY, S. & STERN, L. A. *"Direct Measurement of Methane Hydrate Composition along the Hydrate Equilibrium Boundary"*. The Journal of Physical Chemistry, **109** (19): 9468-9475.(2005)

CLENNELL, M. B., HOVLAND, M., BOOTH, J. S., HENRY, P. & WINTERS, W. J. *"Formation of natural gas hydrates in marine sediments*
1. Conceptual model of gas hydrate growth conditioned by host sediment properties". Journal of Geophysical Research, **104** (B10): 22,985-23,003.(1999)

COATES, G. R., XIAO, L. & PRAMMER, M. G. "*NMR Logging - Principles & applications"*, Texas, Halliburton Energy Services, 1999

DAVIDSON, D. W. "*Water - A Comprehensive Treatise: Clathrate Hydrates"*, Water - A Comprehensive Treatise, New York, Plenum Press, 1973

DICKENS, G. R., O'NEIL, J. R., DAVID, K. R. & R.M., O. *"Dissociation of Oceanic Methane Hydrate as a Cause of the Carbon Isotope Excursion at the End of the Paleocene"*. Paleoceanography, **10** (6): 965-971.(1995)

DURHAM, W. B., KIRBY, S. H., STERN, L. A. & ZHANG, W. *"The strength and rheology of methane clathrate hydrate"*. Journal of geophysical research, **108** (B4): 2003)

EBINUMA, T. *"Method for dumping and disposing of carbon dioxide gas and apparatus therefor"*. Japan, 1993

EIA, E. I. A. *"International Energy Outlook 2008"*. http://www.eia.doe.gov/oiaf/ieo/world.html 2008

EISENBERG, D. & KAUZMANN, W. "*The Structure and Properties of Water"*, Oxford, Oxford University Press, 1969

ERSLAND, G. *"Studies of flow mechanisms and hydrate phase transitions in fractured rocks"*. Department of Physics and Technology, University of Bergen, PhD Thesis, 2008

ERSLAND, G., Personal communication (2009)

ERSLAND, G., HUSEBØ, J., GRAUE, A., KVAMME, B., BALDWIN, B. A., HOWARD, J. J. & STEVENS, J. *"Measurements of Gas Permeability and Non-Darcy Flow in Gas-Water-Hydrate Systems"*. 6th International Conference on Gas Hydrates, Vancouver, BC, Canada, July 6-10, 2008

ETHERIDGE, D. M., STEELE, L. P., FRANCEY, R. J. & LANGENFELDS, R. L. *"Atmospheric methane between 1000 A.D. and present: Evidence of antropogenic emissions and climatic variability"*. Journal of Geophysical Research, **103** (D13): 15,979-15,993.(1998)

FRANKS, F. "*Water: A Comprehensive Treatise"*, New York, Plenum Press, 1972

GOEL, N. *"In situ methane hydrate dissociation with carbon dioxide sequestration: Current knowledge and issues"*. Journal of Petroleum Science and Engineering, **51** (3-4): 169-184.(2006)

GRACE, J., COLLETT, T. S., COLWELL, F. S., ENGLEZOS, P., JONES, E., MANSELL, R., MEEKISON, J. P., OMMER, R., POOLADI-DARVISH, M., RIEDEL, M., RIPMEESTER, J. A., SHIPP, C. & WILLOUGHBY, E. "*Energy from gas hydrates: Assessing the opportunities & challenges for Canada"*, 2008

GRAUE, A., Personal communication (2009)

GRAUE, A., KVAMME, B., BALDWIN, B. A., STEVENS, J., HOWARD, J. J., ASPENES, E., ERSLAND, G. & HUSEBØ, J. *"Environmentally Friendly CO2 Storage in Hydrate Reservoirs Benefits from Associated Spontaneous Methane Production"*. Offshore Technology Conference, Houston, Texas, USA, May 1-4, 2006a

GRAUE, A., KVAMME, B., BALDWIN, B. A., STEVENS, J., HOWARD, J. J., ASPENES, E., ERSLAND, G. & HUSEBØ, J. *"MRI Visualization of Spontaneous Methane Production From Hydrates in Sandstone Core Plugs When Exposed to CO2"*. Offshore Technology Conference, Houston, May 1-4, 2006b

GUNN, D. A., NELDER, L. M., ROCHELLE, C. A., BATEMAN, K., JACKSON, P. D., LOVELL, M. A., HOBBS, P. R. N., LONG, D., REES, J. G., SCHULTHEISS, P., ROBERTS, J. & FRANCIS, T. *"Towards improved ground models for slope instability evaluations through better characterization of sediment-hosted gas-hydrates"*. Terra Nova, **14** (6): 443-451.(2002)

HAHN, E. L. *"Spin Echoes"*. Physical Review, **80** (4): 580-594.(1950)

HAMMERSCHMIDT, G. G. *"Formation of Gas Hydrates in Natural Gas Transmission Lines"*. Industrial & Engineering Chemistry, **26** (8): 851-855.(1934)

HANSEN, J. *"Defusing the global warming time bomb"*. Scientific American, 2004

HASHEMI, R. H. & BRADLEY, J. W. R. "*MRI the basics"*, Baltimore, Williams & Wilkins, 1997

HESTER, K. *"Probing Hydrate Stability and Structural Characterization of both Natural and Synthetic Clathrate Hydrates"*. Colorado School of Mines, PhD Thesis, 2007

HESTER, K., Hydrate structures - Personal Communication (2009)

HESTER, K. & BREWER, P. G. *"Clathrate Hydrates in Nature"*. Annual Reviews of Marine Science, **1** 303-327.(2009)

HUANG, H. & AYOUB, J. *"Applicability of Forchheimer Equation for Non-Darcy Flow in Porous Media"*. SPE Journal, **13** (1): 112-122.(2008)

HUSEBØ, J. *"Monitoring depressurization and CO2-CH4 exchange production scenarios for natural gas hydrates"*. Department of Physics and Technology, University of Bergen, PhD Thesis, 2008

HUSEBØ, J., Personal communication (2009)

HUSEBØ, J., ERSLAND, G., KVAMME, B., GRAUE, A. & STEVENS, J. *"The effect of brine salinity on fill fraction and formation pattern of methane hydrates in sandstone"*. International Conference on Gas Hydrates, Vancouver, Canada, July 6-10, 2008a

HUSEBØ, J., GRAUE, A., KVAMME, B., STEVENS, J., HOWARD, J. J. & BALDWIN, B. A. *"Experimental investigation of methane release from hydrate formation in sandstone through both hydrate dissociation and CO2 sequestration"*. 6th International Conference on Gas Hydrates, Vancouver, Canada, July 6-10, 2008b

HUSEBØ, J., KVAMME, B. & GRAUE, A. *"In-Situ Hydrate Formation and Reformation Kinetics Measured by Magnetic Resonance Imaging"*. WSEAS Transactions on Systems and Control, **2** (1): 59-66.(2007)

IPCC *"IPCC FOURTH ASSESSMENT REPORT: CLIMATE CHANGE 2007"*. http://www.ipcc.ch/ipccreports/assessments-reports.htm 2007

JADHAWAR, P., YANG, J., JADHAWAR, J. & TOHIDI, B. *"Preliminary Experimental Investigation on Replacing Methane in Hydrate Structure with Carbon Dioxide in Porous Media"*. Fifth International conference on Gas Hydrates, Trondheim, Norway, June 13-16, 2005

JEFFREY, G. A. *"Hydrate Inclusion Compounds"*. Journal of Inclusion Phenomena, **1** 211-222.(1984)

KATZ, M. E., PAK, D. K., DICKENS, G. R. & MILLER, G. K. *"The Source and Fate of Massive Carbon Input During the Latest Paleocene Thermal Maximum"*. Science, **286** 1531-1533.(1999)

KENNETT, J. P., HILL, T. M. & BEHL, R. J. *"Methane Hydrates in Quaternary Climate Change"*. 5th International Conference on Gas Hydrates, Trondheim, Norway, June 12-16, 2005

KLEIN, E. & REUSCHLÉ, T. *"A Model for the Mechanical Behaviour of Bentheim Sandstone in the Brittle Regime"*. Pure and Applied Geophysics, **160** (5): 833-849.(2003)

KLEINBERG, R. L., FLAUM, C., GRIFFIN, D. D., BREWER, P. G., MALBY, G. E., PELTZER, E. T. & YESINOWSKI, J. P. *"Deep Sea NMR: Methane Hydrate Growth Habit in Porous Media and its Relationship to Hydraulic Permeability, Deposit Accumulation, and Submarine Slope Stability"*. Journal of Geophysical Research B, 2003)

KOH, C. A. *"Towards a fundamental understanding of natural gas hydrates"*. Chemical Society Reviews, **31** 157-167.(2002)

KVAMME, B. *"A Unified Nucleation Theory for the Kinetics of Hydrate Formation"*. Annals of the New York Academy of Sciences, **912** 496-501.(2000)

KVAMME, B. *"Initiation and growth of hydrate"*. 4th International Conference on Natural Gas Hydrate, Yokohama, Japan, May 23-26, 2002a

KVAMME, B. *"Kinetics of Hydrate Formation from Nucleation Theory"*. International Journal of Offshore and Polar Engineering, **12** (4): 2002b)

KVAMME, B. *"Kinetics of hydrate formation in porous media"*. The History of Convergent and Passive Margins in the Polar Realm, Québec, September 18, 2006

KVAMME, B., Personal communication (2009)

KVENVOLDEN, K. A. *"Methane Hydrate - a major reservoir of carbon in the shallow geosphere?"*. Chemical Geology, **71** 41-51.(1988)

KVENVOLDEN, K. A. & ROGERS, B. W. *"Gaia's breath--global methane exhalations"*. Marine and Petroleum Geology, **22** (4): 579-590.(2005)

LEDERHOS, J. P., LONG, J. P., SUM, A., CHRISTIANSEN, R. L. & SLOAN, E. D. *"Effective kinetic inhibitors for natural gas hydrates"*. Chemical Engineering Science, **51** (8): 1221-1229.(1995)

LEE, H., SEO, Y., SEO, Y.-T., MOUDRAKOVSKI, I. L. & RIPMEESTER, J. A. *"Recovering Methane from Solid Methane Hydrate with Carbon Dioxide"*. Angewandte Chemie, **115** (41): 5202-5205.(2003)

LELIEVELD, J., CRUTZEN, P. J. & DENTENER, F. J. *"Changing concentration, lifetime and climate forcing of atmospheric methane"*. Tellus B, **50** (2): 128-150.(1998)

LIEN, J. R. "*PTEK211 Grunnleggende reservoarfyskk (Kjeneranalyse og logging)"*, Bergen, Universitetet i Bergen - Institutt for fysikk og teknologi, 2004

LIU, X. & FLEMINGS, P. B. *"Passing gas through the hydrate stability zone at southern Hydrate Ridge, offshore Oregon"*. Earth and Planetary Science Letters, **241** (1-2): 211-226.(2006)

LIU, Y., ZHANG, W., LIU, Y. & REN, S. *"Experimental Characterisation and modelling of acoustic and electrical resistance in hydrate bearing sediments"*. 6th International Conference on Gas Hydrates, Vancouver, BC, Canada, July 6-10, 2008

LONG, J. P. *"Gas Hydrate Formation Mechanism and Its Kinetic Inhibition"*. Colorado School of Mines, PhD Thesis, 1994

LONG, J. P. & SLOAN, E. D. *"Hydrates in the ocean and evidence for the location of hydrate formation"*. International Journal of Thermophysics, **17** (1): 1-13.(1996)

LU, H., SEO, Y., LEE, J., MOUDRAKOVSKI, I., RIPMEESTER, J. A., CHAPMAN, N. R., COFFIN, R. B., GARDNER, G. & POHLMAN, J. *"Complex gas hydrate from the Cascadia margin"*. Nature, **445** 303-306.(2007)

LYON, R. K. *"Catalyst allowing conversion of natural gas hydrate and liquid CO2 to CO2 hydrate and natural gas"*. USA, 2004

MAKOGON, Y. F. "*Hydrates of Hydrocarbons",* Tulsa, Oklahoma, PennWell Books, 1997

MAKOGON, Y. F., MAKOGON, T. Y. & HOLDITCH, S. A. *"Gas Hydrate Formation and Dissociation with Thermodynamic and Kinetic Inhibitors"*. SPE annual Technical Conference and Exhibition, Houston, Texas, USA, October 3-6, 1999

MCGRAIL, B. P., SCHAEF, H. T., WHITE, M. D., ZHU, T., KULKARNI, A. S., HUNTER, R. B., PATIL, S. L., OWEN, A. T. & MARTIN, P. F. (2007) *Using Carbon Dioxide to Enhance Recovery of Methane from Gas Hydrate Reservoirs: Final Summary Report*. IN ENERGY, U. S. D. O. (Ed.). Pacific Northwest National Laboratory.

MORIDIS, G. J., COLLETT, T. S., BOSWELL, R., KURIHARA, M., REAGAN, M. T., KOH, C. & SLOAN, E. D. *"Toward Production From Gas Hydrates: Current Status, Assessment of Resources, and Model-Based Evaluation of Technology and Potential"*. SPE Unconventional Reservoirs Conference, Keystone, Colorado, USA, February 10-12, 2008

MORIDIS, G. J. & KOWALSKY, M. *"Depressurization-induced gas production from class 1 and class 2 hydrate deposits"*. Proceedings, TOUGH Symposium, Berkeley, CA, USA, May 15-17, 2006

MORIDIS, G. J., KOWALSKY, M. B. & PRUESS, K. *"Depressurization-Induced Gas Production From Class 1 Hydrate Deposits"*. SPE Reservoir Evaluation & Engineering, **10** (5): 458-481.(2007)

MORIDIS, G. J. & SLOAN, E. D. *"Gas production potential of disperse low-saturation hydrate accumulations in oceanic sediments"*. Energy Conversion and Management, **48** (6): 1834-1849.(2007)

MULLIN, J. W. "*Crystallization",* 3rd. Oxford, UK, Butterworth-Heinmann, 1993

MURRAY, D. R., KLEINBERG, R. L., SINHA, B. K., FUKUHARA, M., OSAWA, O., ENDO, T. & NAMIKAWA, T. *"Saturation, Acoustic Properties, Growth Habit, and State of Stress of a Gas Hydrate Reservoir from Well Logs"*. Petrophysics, **47** (2): 129-137.(2006)

NING, F., JIANG, G. & ZHANG, L. *"Comprehensive utilization of geothermal and solar energy to exploit gas hydrates buried in oceanic sediments"*. 6th International Conference on Gas Hydrates, Vancouver, BC, Canada, 2008

NUMASAWA, M., YAMAMOTO, K., YASUDA, M., FUJII, T., FUJII, K., DALLIMORE, S. R., WRIGHT, J. F., NIXON, F. M., IMASATO, Y., CHO, B., IKEGAMI, T., SUGIYAMA, H., MIZUTA, T., KURIHARA, M. & MASUDA, Y. *"Objectives and Operation Overview of the 2007 JOGMEC/NRCan/AURORA Mallik 2L-38 Gas Hydrate Production Test"*. 6th International Conference on Gas Hydrates, Vancouver, BC, Canada, July 6-10, 2008

OHGAKI, K., TAKANO, K., SANGAWA, H., MATSUBARA, T. & NAKANO, S. *"Methane exploitation by carbon dioxide from gas hydrates -phase equilibria for*

CO2-CH4 mixed hydrate system-". Journal of chemical engineering of Japan, **29** (3): 478-483.(1996)

OTA, M., MOROHASHI, K., ABE, Y., WATANABE, M., SMITH, J. R. L. & INOMATA, H. *"Replacement of CH4 in the hydrate by use of liquid CO2"*. Energy Conversion and Management, **46** (11-12): 1680-1691.(2005)

PARK, Y., CHA, M., CHA, J. H., SHIN, K., LEE, H., PARK, K. P., HUH, D. G., LEE, H. Y., KIM, S. J. & LEE, J. *"Swapping Carbon Dioxide for Complex Gas Hydrate Structures"*. ICGH 2008, Vancouver, BC, Canada, 2008

PHALE, H. A., ZHU, T., WHITE, M. D. & MCGRAIL, B. P. *"Simulation study on injection of CO2-Microemulsion for Methane Recovery From Gas-Hydrate Reservoirs"*. SPE Gas Technology Symposium, Calgary, Alberta, Canada, 2006

PHILLIPSMEDICALSYSTEMS "*Basic Principles of MR Imaging"*, 1984

PURCELL, E. M. *"Resonance Absorption by Nuclear Magnetic Moments in a Solid"*. Physical Review, **69** (1-2): 37-38.(1946)

RIPMEESTER, J. A. *"Hydrate Research-From correlations to a knowledge-based discipline"*. Annals of the New York Academy of Sciences, **912** 16.(2000)

RIPMEESTER, J. A., TSE, J. S., RATCLIFFE, C. I. & POWELL, B. M. *"A new clathrate hydrate structure"*. Nature, (325): 135-136.(1987)

SCHUTJENS, P. M. T. M., HAUSENBLAS, M., DIJKSHOORN, M. & VAN MUNSTER, J. G. *"The Influence of Intergranular Microcracks on the Petrophysical Properties of Sandstone — Experiments to Quantify effects of core damage"*. International Symposium of the Society of Core Analysts, San Fransisco, September 12-14, 1995

SELLEY, R. C. "*Elements of Petroleum Geology"*, Second. London, Academic Press, 1998

SEOL, Y., KNEAFSEY, T. J., TOMUTSA, L. & MORIDIS, G. J. *"Preliminary Relative Permeability Estimates of Methane Hydrate-bearing sand"*. TOUGH Symposium, Lawrence Berkeley National Laboratory, Berkeley, California, USA, May 15-17, 2006

SLOAN, E. D. *"Natural Gas Hydrates"*. Journal of Petroleum Technology, **43** (12): 1414-1417.(1991)

SLOAN, E. D. *"Fundamental principles and applications of natural gas hydrates"*. Nature, **426** 353-363.(2003)

SLOAN, E. D. & KOH, C. A. "*Clathrate Hydrates of Natural Gases"*, 3rd edition. Boca Raton, CRC Press, 2008

STEVENS, J. C., BALDWIN, B. A., GRAUE, A., ERSLAND, G., HUSEBØ, J. & HOWARD, J. J. *"Measurements of Hydrate Formation in Sandstone"*. International Symposium of the Society of Core Analysts, Calgary, Canada, 2007

STILLINGER, F. H. & RAHMAN, A. *"Improved simulation of liquid water by molecular dynamics"*. The Journal of Chemical Physics, **60** (4): 1545-1557.(1974)

TAYLOR, C. J., MILLER, K. T., KOH, C. A. & SLOAN JR, E. D. *"Macroscopic investigation of hydrate film growth at the hydrocarbon/water interface"*. Chemical Engineering Science, **62** (23): 6524-6533.(2007)

THOMAS, C. P. *"Methane Hydrate: Major Energy Source for the Future or Wishful Thinking"*. SPE Annual Technical Conference and Exhibiton, New Orleans, Louisiana, September 30-October 3, 2001

TRAVESSET, A. *"The Many Phases of Ice"*. http://www.physics.iastate.edu/staff/travesset/phasesofice.doc 2008

TRÉHU, A. M., BOHRMANN, G., TACK, F. R., TORRES, M. E. & COLWELL, F. S. (2003) *Proceedings of the Ocean Drilling Program, Initial Reports*.

VLAARDINGERBROEK, M. T. & DEN BOER, J. A. "*Magnetic Resonance Imaging"*, Berlin, Springer-Verlag, 1996

YAMAMOTO, K. & DALLIMORE, S. R. *"Aurora-JOGMEC-MRCan Mallik 2006-2008 Gas Hydrate Research Project Progress"*. National Energy Technology Laboratory, 2008

ZHOU, Y., CASTALDI, M. J. & YEGULALP, T. M. *"Experimental Investigation of Methane Gas Production from Methane Hydrate"*. Industrial & Engineering Chemistry Research, **48** (6): 3142-3149.(2009)

ZUMDAHL, S. S. "*Chemical principles"*, 5td edition. Boston, Houghton Mifflin Company, 2005

Part III

Attachments

Nomenclature

ΔG	=	Gibbs free energy
σ	=	surface tension
r_c	=	critical radius
x	=	mole fraction
μ	=	chemical potential
v_m	=	molar volume
R	=	the ideal gas constant
T	=	temperature
f	=	fugacity
P^{eq}	=	equilibrium pressure
ϕ	=	porosity
V_p	=	pore volume
V_b	=	bulk volume
Q	=	total flow
K	=	permeability
A	=	areal
μ	=	viscosity
ΔP	=	pressure difference
L	=	length
$\vec{q}$	=	flow rate vector
k_{eff}	=	effective permeability
k_r	=	relative permeability
R_e	=	Reynolds number
ρ	=	density
v	=	specific discharge (rate per area)
d_p	=	grain diameter of the porous medium
∇P	=	pressure gradient
β	=	inertia resistance factor
k_{app}	=	apparent permeability
$\vec{\mu}$	=	magnetic dipole moment
γ	=	gyromagnetic ratio
$\vec{J}$	=	angular momentum
$\vec{\tau}$	=	torque
$\vec{B}$	=	magnetic field
$\vec{M}$	=	magnetization
U	=	potential energy
ΔE	=	energy difference
h	=	Planck's constant
$\hbar$	=	Planck's constant divided by 2π
f_L	=	the Larmor frequency
ϖ_L	=	angular frequency

Appendix A: Supplementary tables and figures for Part I

Appendix A1: Summary of guest molecules and their molecular to cavity diameter ratio (Sloan and Koh, 2008).

		Molecular and cavity diameter ratio			
Guest Hydrate Former		**Structure I**		**Structure II**	
Molecule	**Diameter (Å)**	5^{12}	$5^{12}6^2$	5^{12}	$5^{12}6^4$
He	2.28	0.447	0.389	0.454	0.342
H_2	2.72	0.533	0.464	0.542	0.408
Ne	2.97	0.582	0.507	0.592	0.446
Ar	3.8	0.745	0.648	0.757	0.571
Kr	4.0	0.784	0.683	0.797	0.601
N_2	4.1	0.804	0.700	0.817	0.616
O_2	4.2	0.824	0.818	0.837	0.631
CH_4	4.36	0.855	0.744	0.868	0.655
Xe	4.58	0.898	0.782	0.912	0.687
H_2S	4.58	0.898	0.782	0.912	0.687
CO_2	5.12	1.00	0.834	1.02	0.769
C_2H_6	5.5	1.08	0.939	1.10	0.826
c-C_3H_6	5.8	1.14	0.990	1.16	0.871
$(CH_2)_3O^2$	6.1	1.20	1.04	1.22	0.916
C_3H_8	6.28	1.23	1.07	1.25	0.943
i-C_4H_{10}	6.5	1.27	1.11	1.29	0.976
n-C_4H_{10}	7.1	1.39	1.21	1.41	1.07

Appendix A2: Summary of estimates made on CH_4 contained in *in situ* gas hydrates.

Estimates of *In Situ* Methane Hydrates

Year	CH_4 amount 10^{15} m^3 STP	Citations
1973	3053	Trofimuk et al.
1977	1135	Trofimuk et al.
1982	1573	Cherskiy et al.
1981	120	Trofimuk et al.
1981	301	McIver
1974/1981	15	Makogon
1982	15	Trofimuk et al.
1988	40	Kvenvolden and Claypool
1988	20	Kvenvolden
1990	20	MacDonald
1994	26.4	Gornitz and Fung
1995	45.4	Harvey and Huang
1995	1	Ginsburg and Soloviev
1996	6.8	Holbrook et al.
1997	15	Makogon
2002	0.2	Soloviev
2004	2.5	Milkov
2005	120	Klauda and Sandler

Appendix B: Supplementary tables and figures for Part II

Appendix B1: Summary of properties for cores used during experiments in this thesis.

Core	Weight [g]	Length [cm]	Width [cm]	saturation	Salinity [wt%]
H15	441.92	10.26	5.16	0.51	2.0
H16	438.62	10.22	5.16	0.51	8.0
H17	427.19	10.22	5.15	0.49	2.0
H18	433.14	10.20	5.15	0.46	4.0
H19	426.57	10.20	5.15	0.41	10.0
H20	421.43	9.82	5.17	0.59	1.0
HDP1[j]	596.72	14.02	5.18	0.49	0.1
BH-3P-01 A[k]	56.37	10.08	1.13	0.57	3.0
BH-3P-01 B	78.98	10.10	1.06	0.57	3.0
BH-3P-01 C	53.76	10.07	1.10	0.57	3.0
BH-3P-01 A	56.31	10.08	1.13	0.57	0.1
BH-3P-01 B	78.91	10.10	1.06	0.58	0.1
BH-3P-01 C	53.70	10.07	1.10	0.57	0.1
BHW01[l]	218.38	9.95	3.74	0.52	0.1
BHW08	218.16	10.00	3.73	0.51	0.1

[j] Whole core used for depressurization test.
[k] Core fractured into three pieces, A, B and C. Used for double spacer experiment. The core was cleaned after the first experiment and used once more for the second experiment.
[l] Whole cores used for experiment with excess water.

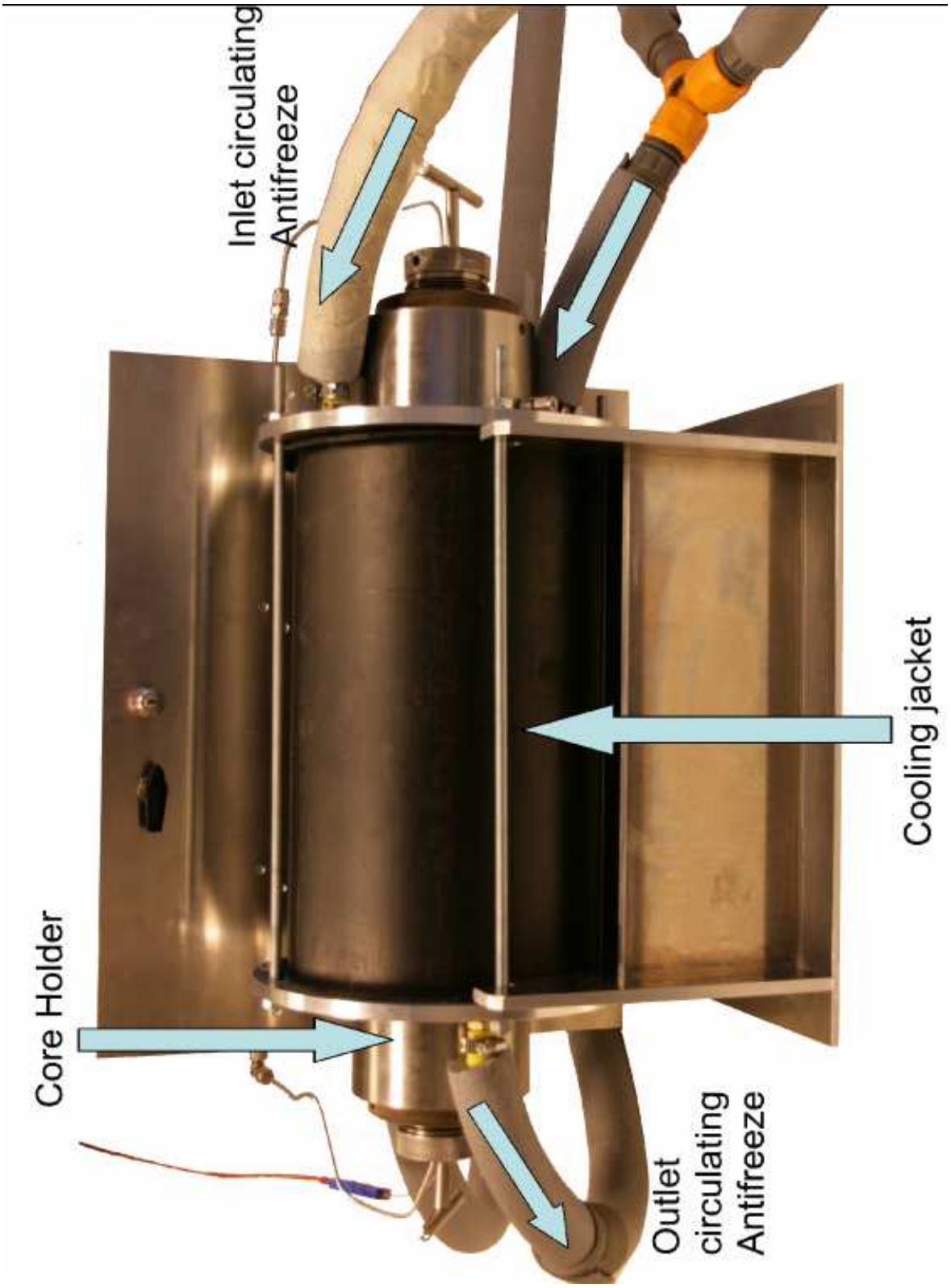

Appendix B2 – New experimental setup designed and built during this thesis.

Appendix B3 – Illustration of tube in tube where Fluorinert is circulating in the inner tube, and antifreeze is circulating in the outer PVC tube and maintaining low temperature of Fluorinert.

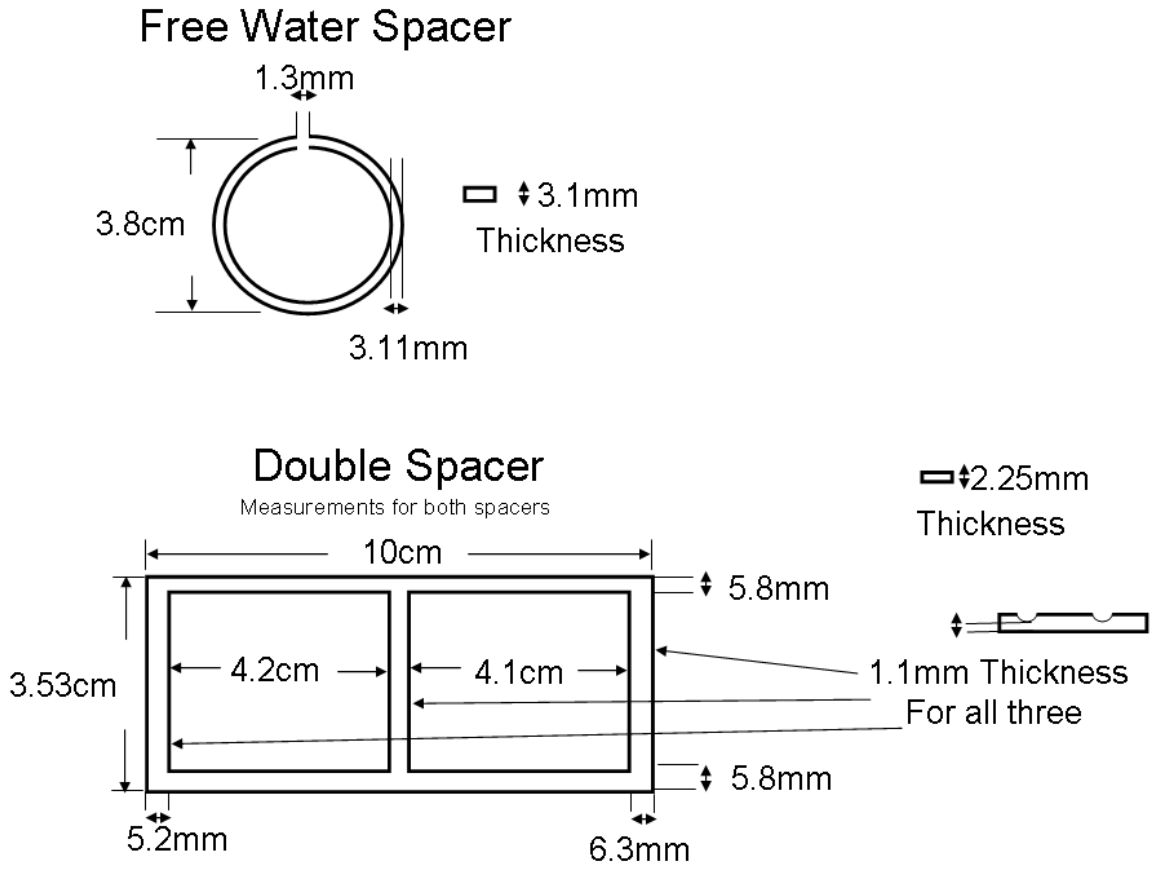

Appendix B4 – POM spacer volumes.

Appendix B5: Details on cores used during salinity experiments.

Core	CH_4 injected during hydrate formation [ml]	Expansion of hydrate [ml]	CH_4 in hydrate [mol]	Amount of brine [g]	Amount of water in hydrate [mol]	Estimated Fill Fraction	Uncertainty
H15	41.74	6.32	0.192	24.81	1.35	0.82	0.09
H16	21.69	6.33	0.113	26.2	1.34	0.49	0.06
H17	48.16	6.63	0.218	26.01	1.41	0.89	0.10
H18	37.32	5.83	0.172	23.34	1.24	0.8	0.09
H19	16.45	5.46	0.089	26.92	1.34	0.38	0.12
H20	49.93	7.18	0.228	27.91	1.53	0.85	0.10

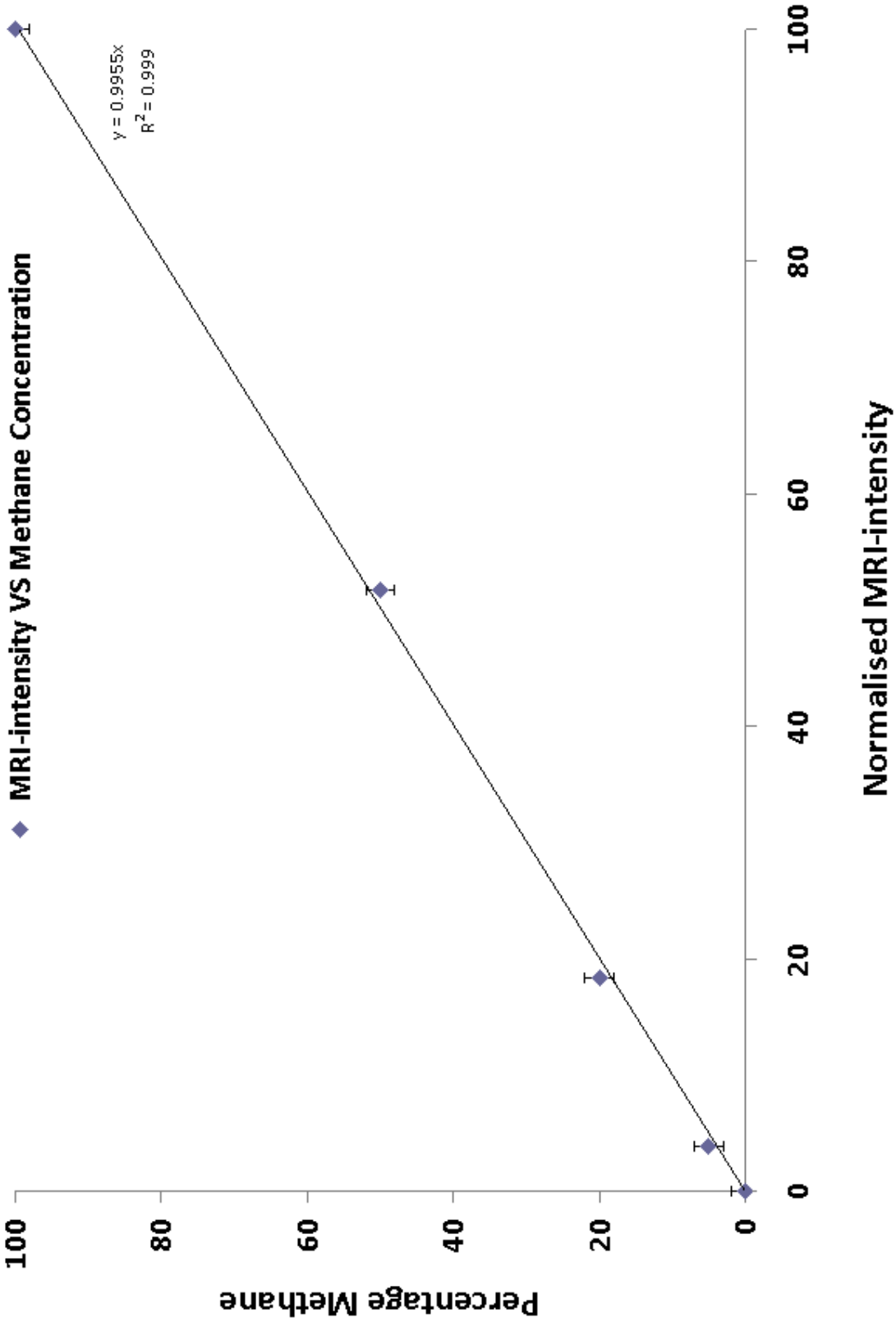

Appendix B6 – Linear relationship between MRI intensity and CH_4 concentration (Ersland, 2009).